博士論文

Development of Higher Order Particle Discretization Scheme for analysis of cracking phenomena

(亀裂解析のための高次粒子離散化手法の開発)

A DISSERTATION
SUBMITTED TO THE DEPARTMENT OF CIVIL ENGINEERING
OF THE GRADUATE SCHOOL OF ENGINEERING,
UNIVERSITY OF TOKYO
IN PARTIAL FULFILLMENT OF THE REQUIREMENTS
FOR THE DEGREE OF
DOCTOR OF PHILOSOPHY

Mahendra Kumar Pal
(ﾏﾍﾝﾄﾞﾗ ｸﾏｰﾙ ﾊﾟｰﾙ)

September, 2015

Development of higher order Particle Discretization Scheme for analysis of cracking phenomena

Mahendra Kumar Pal

September 3, 2015

Acknowledgement

First and foremost, I would like to thank to almighty God for his gift to me in form of intelligence and ability to think. He conferred the wisdom to me for succeeding in my life.

I would like to express my sincere and deep gratitude to Prof. Lalith Wijerathne and Prof. Muneo Hori, an institution of learning, whose expertise and passion in academia brought constant intellectual and critical discussion to my research. This provided a thought provoking environment that allowed this dissertation to come into existence.

Moreover, I would like to convey my special thanks to my supervisor Prof. Lalith Wijerathne for his relentless work, a truly mentoring example worth of my deepest admiration. I cannot repay the valuable time that he had devoted to me during this research work. It was indeed a fantastic, fruitful and unforgettable experience of my life.

It gives me an immense pleasure to thank Prof. Tsuyoshi Ichimura, Prof. Seizo Tanaka and Prof. Hiromichi Nagao for their guidance, teaching and help throughout my studies. I would like to express my sincere gratitude to my doctorate committee members, Prof. Lalith Wijerathne, Prof. Shinobu Yoshimura, Prof. Muneo Hori, Prof. Tsuyoshi Ichimura, and Prof. Kohei Nagai, whose brilliant comments, suggestions and criticism provided guidance and challenges to this research.

I would like to thank JICA for awarding me with JICA-Friendship scholarship and providing me the necessary fund and support to accomplish my research work; and the Alma mater IIT Hyderabad, Prof. KVLS and Prof. A. Rajagopal for their support and recommendations in obtaining this scholarship. I admire the efforts of my JICA coordinators for their parental love and care.

I am grateful and thankful to my fellow lab members and friends whose continuous support has motivated me to keep moving forward. I extend my gratitude especially to Gustavo, Ryoichiro Agata, Kohei Fujita, Stephen Jacob, Mohd. Nabeel, Supun Chamara, Leo Aguilar, Ireshika Karunarathna and all others.

I owe a great deal of appreciation to my parents for gifting me this life. Their moral teachings and love have always aided me in developing my personality. I cannot forget to thank my sweet sister; Priyanka to whom, I owe everything. I would like to extend my appreciation to Manjiri R Kulkarni, Kalpana Nautiyal Vyas, Rajesh Vyas, Madhuri Chauhan and Ambika Kondiram Dudhate for being part of a family away from family. I

extend my sincere thanks to Tuba Zahra and Shanthanu R. Menon for their stupidities and craziness. Nevertheless, I admire their helping nature.

Finally, I am thankful to my university the University of Tokyo, and prestigious institute, Earthquake Research Institute (ERI) for dispensing support and all other things, I needed for my research work.

Abstract

In this thesis, higher order extension of Particle Discretization Scheme (PDS) and its implementation in FEM framework are considered, with the aim of simulating cracking phenomena in brittle elastic solids. The main advantages of original PDS-FEM, proposed by Hori *et. al.*, are its numerically efficient failure treatment, ability to reproduce crack branching without any special treatments and modeling the effects of material heterogeneities. On the contrary, most of existing FEM approaches involve complex treatments for modeling these phenomena. However, the original implementation of PDS-FEM has first order accuracy. The main objectives of this thesis are to increase the order of accuracy, implement a suitable failure treatment and application to simulate cracking phenomena in brittle solids.

A unique property of PDS is the usage of conjugate tessellations to approximate functions and their derivatives, respectively. In the original formulation, characteristic functions of Voronoi and Delaunay tessellations,$\{\phi^{\alpha}(\boldsymbol{x})\}$ and $\left\{\psi^{\beta}(\boldsymbol{x})\right\}$, are used for approximating functions and derivatives, respectively, leading to constant variation of the approximated fields within each tessellation element. In the higher order extension of PDS, the fields within each tessellation element is approximated as local function expansion, and the field over the whole domain is approximated as the union of these local function expansions. Though, any suitable set of base functions can be used in local expansions, polynomial bases are used in this study; motivated by Taylor and Maclaurin series. As an example, a function $f(\boldsymbol{x})$ and its derivative $g(\boldsymbol{x})$ are approximated as $f^{d}(\boldsymbol{x}) = \left(\sum_{(\alpha,n)} f^{\alpha n} P^{\alpha n}\right)$and $\mathrm{g}^{d}(\boldsymbol{x}) = \left(\sum_{(\beta,m)} \boldsymbol{g}^{\beta m} Q^{\beta m}\right)$, where $P^{\alpha n} = \{1, \boldsymbol{x} - \boldsymbol{x}^{\alpha}, \ldots\}\, \phi^{\alpha}(\boldsymbol{x})$ and $Q^{\beta m} = \left\{1, \boldsymbol{x} - \boldsymbol{x}^{\beta}, \ldots\right\} \psi^{\beta}(\boldsymbol{x})$ are the local polynomial bases with the respective tessellation element as their support. The use of local polynomial expansions, whose support are confined to respective tessellation elements, to approximate a function gives rise to the particle nature of this discretization scheme and produces numerous discontinuities in $f^{d}(\boldsymbol{x})$. It is to smoothly connect those discontinuous local polynomial expansions and define a bounded approximation for the derivatives, the conjugate tessellation: $\{\Psi^{\beta}\}$, is used for approximating the derivatives. The numerous discontinuities in $f^{d}(\boldsymbol{x})$ along Voronoi boundaries are utilized by PDS-FEM to numerically efficiently model discontinuities or cracks in solving boundary value problems.

The above mentioned formulation (hereafter, refereed as *formulation-A*) doesn't guarantee that approximation scheme will necessarily satisfy the fundamental requirement; $\nabla \times \boldsymbol{g}^d = 0$, which is called the curl free condition, hereafter. Another formulation, based on the curl free constraint is also proposed and referred as *formulation-B*. In formulation-B, functions are approximated just as in formulation-A, while the derivative approximations are redefined such that the curl-free condition is always satisfied. Formulation-B performs better in function approximation, but same is not translated while solving BVP.

The higher order PDS is implemented in FEM framework and tools for simulating cracks in brittle elastic solids are developed. The developed codes are designed such that arbitrary sets of polynomials can be used in approximating functions and derivatives. Further, the codes are enhanced with distributed parallel computing extensions so that large scale models can be simulated. The developed codes for higher order PDS-FEM are validated and verified with different benchmark problems, and the patch tests are also conducted. It is demonstrated that compatible higher order convergence rate can be obtained; second order accuracy in the displacement field is attained with the polynomial bases up to the first order both in 2D and 3D. Furthermore, problem associated with imposing essential boundary conditions is discussed and demonstrated that the choice polynomial order for approximating derivatives to be one order higher than that of function mitigates the need of specifying derivatives as essential boundary conditions. Both the formulation-A and B are validated using benchmark tests and demonstrated that both formulation-A and B have $p+1$-order convergence rate for function and derivatives, when using p^{th} and $(p+1)^{th}$ order polynomial bases for approximating functions and derivatives, respectively. Further, both the formulation-A and B exhibit nearly the same accuracy. Formulation-B doesn't offer any additional improvement in results in analyzing the BVPs.

In order to validate the modeling of brittle cracks, standard benchmark problems are considered; mode-I crack in 2D and penny shaped crack in 3D subjected to far-field tensile loading. It is shown that the both the displacement and stress fields are in good agreement with analytic solution except the near neighborhood of the crack tips. Point of inflection is an important factor, which decides the nature of approximated function. Hence, sensible selection of inflection point is suggested and investigated with several numerical experiments. Selection of mid point of broken edge of Delaunay triangle encapsulating crack-tip as inflection point in place of center of gravity rectifies the above mentioned problem. Obtained results are in good agreements with analytic solution but a slight shift in stress singularity is observed. Seeking the improvement in results, problem is re-analyzed with curl free formulation. But, curl free formulation doesn't enhance result anymore. Even, it doesn't offer traction free surface. Further, J-integral calculation is done. It is shown that error in J-integral calculation disappears at the rate of 1.7, which is 1.0 in case of 0^{th}order PDS-FEM.

It is shown that even the proposed higher order extensions of PDS-FEM can also offer a simple and numerically efficient crack treatment, just as the original 0th-order PDS-FEM.

The proposed crack treatment, which involves judicious selection of point of inflection, the verification tests conducted with standard mode-I crack problem indicate it produces higher accuracy and convergence rate of J-integral, compared to those of 0th-order PDS-FEM. Further, the formulation-A is superior in modeling cracks; formulation-A has higher and sustained convergence rate of J-integral compared to formulation-B. On top of that, crack surfaces produced by formulation-A are nearly traction free, while those with both formulation-B and 0th-order PDS-FEM have notable surface traction. Because of the superior performance in modeling cracks, the formulation-A is chosen as the higher order PDS-FEM. When it comes to crack modeling, improved accuracy in crack tip stress field and surface traction are the main improvement in higher order PDS-FEM compared to 0th-order. Irrespective of the crack configuration, higher order PDS-FEM reproduces a nearly traction free crack surface. Such salient feature of proposed numerical scheme, categorized it into the list of numerically efficient methods.

Contents

Acknowledgement **1**

Abstract **3**

1 Introduction **1**
1.1 Motivation 1
1.2 Thesis structure 3

2 Literature Review **4**
2.1 Review 4
2.2 Observation from literature review 7
2.3 Objectives of the current work 7

3 Higher order Particle Discretization Scheme (PDS) **9**
3.1 0th-order PDS 9
3.2 Higher order extension of PDS 10
3.2.1 *Formulation-A* 10
3.2.2 *Formulation-B* : ensuring $\boldsymbol{\nabla} \times \boldsymbol{\nabla} f^d = \mathbf{0}$ 12
3.3 Numerical examples 14
3.4 A possible interpretation 16
3.5 Comparison with Taylor series expansion 19

4 Implementation of PDS in FEM framework **20**
4.1 Target boundary value problem: infinitesimal deformation of linear elastic continuum 20
4.2 Formulation of higher order PDS-FEM 21
4.2.1 *Higher order PDS-FEM with the formulation-A* 21
4.2.2 *Higher order PDS-FEM with the formulation*-B; with $\boldsymbol{\nabla} \times \boldsymbol{\nabla}(u_i^d) = 0$ 23
4.3 Modeling crack in PDS-FEM 24
4.3.1 In *formulation-A* 25

4.3.2 In *formulation-B* 26

5 Imposing essential boundary conditions **27**
5.1 Introduction 27
5.2 Problem statement 30
5.2.1 Weak formulation 30
5.3 Treatment to enforce essential boundary conditions 31
5.3.1 Specifying the all coefficients of approximation on boundary 31
5.3.2 Consistency condition 32
5.3.3 Increasing the order of polynomial bases used for derivative approximation 33
5.4 Conclusion 34

6 Linear elastic stress analysis of solid **36**
6.1 Infinite domain with circular cavity 36
6.1.1 Setting boundary condition 37
6.1.2 Results with artificially set boundary conditions 39
6.1.3 Comparison of two formulations: weak stress concentration 43
6.2 Uniformly pressured thick hollow cylinder 45
6.2.1 Results and discussions 46
6.3 Conclusion 46

7 Stress analysis of fracture mechanics **48**
7.1 Mode-I problem: Infinite domain with finite crack 48
7.2 Branched crack problem 54
7.3 Arch shape crack 57
7.4 Penny shaped crack in 3D 57
7.5 Conclusion 62

8 Concluding Remarks **66**
8.1 Summary and conclusion 66
8.2 Future work 67

A Explicit expressions **69**
A.1 Strain displacement relations *(formulation-A)* 69
A.1.1 Matrix form for $\epsilon_{ij}^{\beta n}$ 70
A.2 Weak form of the equilibrium equation 71
A.2.1 Matrix form of the weak form of the equilibrium equation 71
A.3 Strain displacement relations (*formulation-B*) 72

B Integration Scheme **73**

C Motivation for 1O/2O PDS **76**

D Patch test **79**
D.1 Patch Test 79
D.1.1 Patch test as verification tool 79
D.1.2 Patches 79
D.1.2.1 Rigid body mode Patch test 80
D.1.2.2 Constant strain mode Patch test 81
D.2 Conclusion 83

E Analytic expression for Mode-I crack **86**

Bibliography **90**

List of Tables

3.1 Convergence rate of approximation (function , the derivative) for function $f(x) = \frac{x}{\sqrt{10x+x^3}}$. Here, $ord(P^\alpha)$and $ord(Q^\beta)$ are the highest order of polynomial of basis set, respectively. 14

5.1 Convergence rate of solution function and derivative with different combination of bases of approximation scheme. Here, $ord(P^\alpha)$is highest order of polynomial bases for approximating the function while, $ord(Q^\beta)$is same for derivative. 34

6.1 Convergence rate of solution function and derivative with different combination of bases of approximation scheme. Here, $ord(P^\alpha)$ is highest order of polynomial bases for approximating the function while, $ord(Q^\beta)$ is same for derivative. 41

D.1 Patch teat summary: Displacement value at patch node 84

D.2 Patch test summary: Strain value at patch node 85

List of Figures

3.1 Set of basis functions, $P^{\alpha n}$ used for approximating function in 2-dimension. Here $(a,\, b)$ is point of inflection. 12
3.2 Solution space spanned by curl-free formulation of higher order PDS is subset of that of formulation in [48]. 14
3.3 Approximation of function. 15
3.4 Approximation of derivative. 15
3.5 Convergence of function $f(x) = Sin(x)$ approximation with $0^{th}-$order and 1st-order PDS. 15
3.6 Plots of 1st-order PDS approximation of function $f(x, y) = \sin(xy/40)$ and the derivative $\frac{\partial f(x,y)}{\partial x}$ 17
3.7 Comparison of convergence rates with *formulation-A* and *B* 18
3.8 Explanation of function and derivative approximation 18

4.1 Modeling a crack passing through a Delaunay element; (a) existing discontinuities in the displacement field approximated with PDS, (b) modeling a crack by dropping contribution from infinitesimally thin neighborhood of Voronoi boundary to be broken. 25

5.1 Boundary Voronoi and its Delaunay, with boundary edge is parallel to (a) vertical axis (b) horizontal axis} 29
5.2 Solution function and its derivative by specifying all the terms of polynomial along boundary. Here, Analytical solution is shown in blue color, while red color curve denotes the solution from higher order PDS-FEM. . . 31
5.3 Solution function and its derivative with consistency equation (see Eq. 5.13) . Here, Analytical solution is shown in blue color, while red color curve denotes the solution from higher order PDS-FEM. 32
5.4 Solution function and its derivative with basis $P^{\alpha n} = \{1, (x - x^{\alpha})\}$ and $Q^{\beta n} = \{1, (x - x^{\beta}), (x - x^{\beta})^2\}$. Analytical solution is shown in blue color, while red color curve denotes the solution from higher order PDS-FEM. . . 34

6.1 A plate with circular hole subjected to far field $\sigma_0 = 10$ MPa. Lower straight edge is subjected to symmetric boundary conditions. 37
6.2 Result from PDS-FEM 1st order without any special treatment to boundary conditions (a) Stress σ_{xx} Distribution (b) Comparison of result with analytical solution along section AB 38
6.3 Surface plot of displacement and stress fields obtained with first order PDS-FEM. The color indicates the scale of vertical axis. 40
6.4 Comparison of stress in x-direction, σ_{xx} from (a) 0-th order PDS-FEM (b)1st order PDS-FEM 41
6.5 Comparison of stress, σ_{xx} with analytical solution along the width of plate (AB section) 42
6.6 Displacement and stress fields with 1st-order PDS-FEM with *formulation-B*. 43
6.7 σ_{xx} obtained with curl-free HO-PDS-FEM, along the section A-B. 44
6.8 Difference of $\boldsymbol{u}$ and σ_{xx} from 1st-order PDS-FEM *formulations A* and *B*, in the vicinity of the stress concentration. 44
6.9 Rate of convergence (a) displacement (b) strain , setting the boundary conditions with *methodology-A and B* 45
6.10 Thick hollow cylinder applied with uniform internal and external pressure . 46
6.11 (a) Displacement, u_r in radial direction 47
6.12 (a) ϵ_{rr} (b) Convergence rate of displacement with 1st order PDS-FEM based on *formulation-A* 47

7.1 Setting of the mode-I problem. $a = 0.25$ 49
7.2 Distribution of σ_{yy} in the vicinity of the crack tip at the right end. Note that blue color indicates compression. 50
7.3 σ_{yy} along a section passing through the upper crack surface, in the right half of the crack. 51
7.4 Point-wise convergence of stress σ_{yy} for mode-I crack problem 52
7.5 Crack tip element 52
7.6 Distribution of σ_{yy} in the vicinity of the crack tip at the right end. blue color indicates compression. 53
7.7 Comaprison of σ_{yy} of analytic and PDS-FEM solutions, along right half of the crack length. 55
7.8 Convergence rates of J-integral for the mode-I crack problem. 56
7.9 Crack problems: A plate with dimensions 5×10 unit, fixed at bottom end and applied displacement at top edge 56
7.10 Distribution of σ_{yy} in the vicinity of crack surfaces. 1st-order PDS-FEM with formulation-A perform better in modeling traction free crack surfaces. 58

7.11 Comparison of stress obtained from 0th order PDS-FEM and 1st order PDS-FEM along OC 59
7.12 Distribution of σ_{yy} in the vicinity of crack surfaces. 1st-order PDS-FEM with formulation-A perform better in modeling traction free crack surfaces. 60
7.13 Comparison of calculated traction (a) Along the crack surface (b) Normal to the crack surface 61
7.14 A penny shape crack problem 62
7.15 Stress σ_{zz} distribution obtained with 0th and 1st order PDS-FEM. 63
7.16 Traction normal to the crack surface 64
7.17 Traction along the crack surface 65

B.1 $\phi(x, y) = 1 - H(n_y(y - y_0) + n_x(x - x_0))$ 74

D.1 An element patch attached to a patch node, herein labelled as i 80
D.2 Procured results with displacement setting $u(x, y) = 0.1$ and $v(x, y) = 0$. 81
D.3 Displacement and strain with BCs $u(x, y) = 0.0$ and $v(x, y) = 0.1$ 81
D.4 Displacement and strain results obtained by setting the BCs as $u(x, y) = x$ and $v(x, y) = 0.0$ 82
D.5 Displacement and strain with boundary condition setting $u(x, y) = 0.0$ and $v(x, y) = y$ 82

Chapter 1

Introduction

1.1 Motivation

Cracking of solid is a common phenomenon which leads to failure. Nature of these cracks is complex and very sensitive to the small changes in many factors such as material properties, pre-existing microscopic cracks and flaws, loading, geometry of solid and etc. Crack propagation mainly depends upon the stress singularity at the tip, which direct crack propagation by creating new crack surfaces. Also, crack surfaces are complicated, as they kink or branch in bulk body. The minor variation in above mentioned factors govern the nature of nature of stress state at crack-tip, causing the bending and branching of cracks. However, these factors have negligible influences in ordinary deformation problems. To analyze such sensitive problems, construction of probability distribution function (PDF) of crack path is needed. Probabilistic studies are usually based on statistical data or Monte-Carlo simulation with efficient technique to model the crack in 3-dimensional problems.

There are number of numerical methods to simulate the cracking phenomena, out of which, the recent advancements are element free Galerkin method, extended finite element method (XFEM), generalized finite element method (GFEM), Discontinuous Galerkin Method, etc. These recent advancements have surely increased the capabilities of simulating cracking phenomena. But at the same time, these advancements have introduced numerical treatments which are computationally expensive and complex in implementation, making those unsuitable for the fore-mentioned probabilistic studies required in analyzing cracking phenomena. Some of the disadvantages in these numerical methods are: the need of tracking crack front in 3D; need of special treatment for modeling crack branching; difficulties in modeling the presence and the effects of minor heterogeneities, etc.

Particle Discretization Scheme-Finite Element Method (PDS-FEM) is an efficient numerical scheme to simulate cracking phenomena, compared to the other FEM based recent advancements. It uses Particle Discretization Scheme (PDS) to approximate functions and the derivatives. PDS uses two conjugate domain tessellations, one of which are used for

approximating functions and other for approximating their derivatives. Basically, PDS uses Voronoi and Delaunay pair to approximate functions and derivatives, respectively. In original PDS, functions are approximated with the characteristic functions of Voronoi elements, and those approximations consists of discontinuities along edges of Voronoi elements due to the use of characteristic functions. It is to define bounded derivatives, PDS uses characteristic function of Delaunay tessellation to approximate derivatives. Implementation of PDS in FEM framework to solve Boundary Value Problems (BVPs) is called as PDS-FEM.It is rigorously proved that PDS-FEM, when applied to solve BVP of linear elasticity, has the identical stiffness matrix with linear FEM. The advantage of PDS-FEM is that it provides a numerically efficient treatment for modeling cracks, utilizing the discontinuities in the approximated displacement field. Also, it is demonstrated that the crack tip stress field modeled with PDS-FEM is as accurate as the linear FEM. In addition it does not require any special treatments to track the crack fronts, to model crack branching and produce the crack bending, kinking and branching due to the effect of minor heterogeneity in materials. These features and the numerically efficient crack treatment make PDS-FEM an ideal tool for probabilistic studies of crack propagation phenomena. Several experimental observations of 3D crack propagation has been reproduced with PDS-FEM such as quasi-static, dynamic, dynamic at ultra high strain rates and in non-linear materials problems.

One limitation of the original PDS and PDS-FEM are those only have first order accuracy. It surely is desirable to have higher order accuracy for obvious reasons. The major objectives of this thesis are to develop higher order extension of PDS, implementation of higher order PDS-FEM with numerical efficient failure treatment and verification. Instead of the characteristic functions of tessellation elements used in original PDS, the higher order PDS uses set of polynomial basis, whose support is confined to the respective tessellation element, to approximate functions and its derivatives. As an example, in higher order PDS, a given function within the domain of a Voronoi element is approximated as a linear combination of a set of polynomials basis whose support is confined to the Voronoi element, and the function over the whole domain of analysis is approximated as summation of approximations over each Voronoi. Similarly, the derivatives are approximated with Delaunay tessellation. Just as in original PDS, higher order approximate of a function also consists of discontinuities along Voronoi boundaries, and it is to define bounded derivatives that PDS uses Delaunay tessellation. As it is shown solving several benchmark problems, the higher order extension produces higher accuracy and higher convergence rates. The higher order PDS-FEM also provide a numerically efficient failure treatment, and the analysis of mode-I crack problems indicates significant improvement in accuracy and convergence rates of J-integral and the crack surfaces passing through Delaunay element to be nearly traction free. The latter is a notable improvement compared with original PDS-FEM.

1.2 Thesis structure

This thesis is divided into 8 (eight) chapters with several Appendices and begins with motivation chapter as opening chapter. 2nd chapter briefly overviews the positive and negatives features of readily available conventional numerical schemes. The novel concept of higher order PDS is introduced in the third chapter of the thesis followed by it's implementation in FEM framework in succeeding chapter. Both chapters talk about the curl free and non-curl free formulation. Fifth chapter emphasis on problems and its solution in imposing essential boundary conditions. Further, it defines a criterion to select the most suitable basis function to solve any boundary value problem (BVP). Stress analysis of solids without crack is depicted in chapter six, while the chapter seven talks about the modeling of crack and stress analysis of fracture problem. Final chapter includes some concluding remarks and few ideas for future improvement and application of developed numerical scheme.

Chapter 2

Literature Review

2.1 Review

Function approximation by polynomial with least square mapping technique is a natural choice but it does not guarantee to reproduce the point value at any given point of domain. Extensive investigations done by McLain [1], Gordon *et. al.* [2], Barhhill [3], and Lancaster *et. al.* [4, 5, 6] show that least squares approximations can be extended to produce interpolatable approximations. Lancaster and Salkauskas [6] has pioneered in Moving Least Square Methods (MLS) and further enhanced it to produce an interpolant. Initially, the usage of MLS was limited to function approximation and surface generation only but, later it has been extended to solve various partial differential equations and boundary value problems in elasticity [7, 8, 9]. MLS has its own charm in many interdisciplinary researches. For example, Liew *et. al.* [7, 8] have implemented MLS into the differential quadrature method and called it as MLSDQ. They have investigated different properties of MLSDQ such as size of support, completeness of basis function and node-irregularity on numerical accuracy. Because of its advantages, MLS is further used as approximation scheme in the development of meshfree methods [9]. The weight functions, used in the proposed MLSDQ are computed with the help of basis function of MLS and their partial derivatives, which are empirical and do not entertain analytic mechanics researchers.

Taylor series fulfill the requirement of a differentiable approximation solution requested in computational mechanics and this make it a popular tool over MLS. Taylor series method has been explored and studied by several authors for solving ordinary differential equations (ODEs) and differential algebraic equations (DAEs) [10, 11, 12, 13, 14, 15, 16]. In single variable function, Taylor series coefficients can be easily obtained by differentiating the analytic function. Such as, initial value problem where, only time is an independent variable. In case of multi-variable function, partial differentiations are required and many algorithm has been proposed to calculate it efficiently [14]. Therefore, applicability of such proposal is limited to the solution of initial value problem, whereas explicit expression to

derive partial derivative w.r.t. space for boundary value solution can not be obtained easily. Hence some advance and differentiable kind of interpolatory approximations are needed. G.Groza and N. Pop [17] have proposed Newton interpolation series which convert the governing equation into system of algebraic equations. Converting the differential equation into integral equation and making use of operational matrix of integration to eliminate the tedious integration operations to get the system of system of algebraic equation is another alternative demonstrated in References [12, 15, 16]. In-spite of accurate interpolatary approximation polynomial, rigorous and illustrative analysis tool is lacking.

When it comes to solve boundary value problems in solid mechanics, Finite Element Method (FEM) is the dominant numerical method. FEM is based on variational principle, and uses piecewise polynomials to approximate an unknown field. The expansion of application domain of FEM, especially in mechanics, is quite wide. However, still it needs improvements for solving some specific problems like crack propagation. In the early 2000s, enhancement by enriching of basis functions with inclusion of special function seeking the accurate solution of fracture problem has attracted research community of applied mechanics and subsequently, many new schemes were proposed such as Discrete Element Method (DEM) [18], adaptive refinement based on force configuration [19], mesh-free methods [20],and eXtended Finite Element Method (XFEM) [21, 22]. Although their sophisticated numerical treatments comes with high numerical overhead and complex implementation, accuracy of crack-tip stress field is improved drastically. Remarkable feature of these enhancement is abandonment of mesh dependency. However, concrete criterion to choose generalized additional shape function for any problem is very resilient as it is problem specific decision. Mesh-less methods require the tracking and modeling of crack-surface, which are accomplished with level-set functions and Heaviside function, respectively. Analytic functions are then further included into approximating basis function to accurately reproduce the stress singularity, end up with hefty computational cost. Inclusion of enrichment function can be restricted to a very specific zone in order to reduce the computational cost but it requires blending elements to smooth-en the solution in transition zone, developed between enriched element and ordinary elements. Currently, the requirement of blending element is also eliminated.

Optimal convergence of standard XFEM is depended on several factors such as integration rule [23], radius of branch enrichment [23, 24], and imposing Dirichlet boundary conditions [25]. Laborde *et. al.* [23] have suggested that suitable enrichment functions shall be considered in approximation polynomial in order to obtain the optimal convergence. Various factors, which are responsible for lowering the convergence rate such as numerical integration scheme and suitable enrichment function have been studied by Laborde *et al*. Further, some more improvement such as modification in enriched domain and special concern on transition between enriched zone and other domain using partition of unity or non-conformal methods are investigated and discussed. Moes *et. al.* [25] have identified the techniques to impose Dirichlet boundary condition with help of Lagrange multipliers

and as result they have succeeded in preserving the convergence rate. Since conventional way to enforce boundary conditions does not keep the convergence rate intact, which is a notable enhancement.

Particle based numerical methods have been another popular and widely used tool in solid mechanics and fluid mechanics. A salient feature of particle methods is that large deformations and damage can be easily simulated, which make them more powerful tool for failure modeling. However, damage of material is very sensitive to the local minor heterogeneities. On the top of this, loading configuration plays a vital role in propagation of cracks. Hence, it becomes more important to perform probabilistic analysis of crack-path variability instead of deterministic analysis. Probabilistic study is based on statistical model [29] or Monte-Carlo simulation [30]. To achieve a converged solution, a large number of simulations are needed, which results into high computational cost. In the era of high performance computing (HPC), computational cost may not be an influential factor but probabilistic study requires an efficient and accurate numerical analysis tool.

Particle based numerical schemes such as smooth particle method (SPH)[26], element free Galerkin method (EFGM)[31], reproducing kernel particle method (RKPM)[32] are efficient methods for failure analysis. Accuracy of these methods is improved by introducing some additional nodes in domain, where more refinement (*h-adaptivity*) is needed. However, these methods are not capable of incorporating the Poison's effect and encounter problems in enforcing the essential boundary conditions as well.

Approximation scheme for particle methods do not have strict interpolatory properties that means in general they are not equal to particle value of the dependent variable along the boundary points. Hence imposing essential boundary condition is not straightforward unlike in FEM. Different approaches have been proposed to give discourse to the issues related to imposing essential BCs. Lagrange multiplier, proposed by Belystchko *et. al.* [31] leads to non-positive definite stiffness matrix and such matrices are not desired by conjugate gradient method. Therefore, this scheme can not be adopted as trivial solution rather it demands for further investigations. Campbell [34] has addressed this issue by reconsidering the original kernal integral estimate and used the residual term obtained via integration by parts. Another scheme named Image particle method, proposed by Takeda *et.al.* [35], satisfies the no-slip boundary condition and concept was further extended to curved boundary by Morris *et.al.* [36]. Libersky *et.al.* [37, 38] has revisited the problem and addressed it using symmetric reflecting surface boundary using the Ghost particles. In order to stimulate the Ghost particle concept, Randles *et.al.* [39, 40] have proposed new definition of boundary and define the communication of boundary value of dependent variable from boundary to internal points. According to the new definition, a surface away from conventional boundary particle by one half of the local smoothing length is considered as boundary. However, enforcing the essential boundary is still a major concerned and debatable topic in particle methods. In nutshell, particle methods and finite element method have their own positive and negative features in solving elasticity problems.

Conventional FEM endures many difficulties in solving the fluid-structure interaction (FSI) such as presence of convective terms, in-compressibility constraints in fluid equations, tracking of free surface of fluid and many others. As it is known that principle of stationary action has a ability to enhance the numerical scheme to address above mentioned problems. A method, which uses Lagrange functional satisfying the governing equation of solid and fluid domain, can illustrate the interaction of contacting domains, is called Particle Finite Element Method [PFEM] [41, 42, 43]. PFEM assumes mesh nodes in fluid and solid domain as particles, which are free to move independently .In this method nodes of finite element mesh are observed as moving particle by tracing the movement of individual particles. As method has easily eliminated the convective terms but difficulty is transferred in tracking the movement of moving the mesh nodes. Furthermore, in case of complex and large scale problem, methodology request for re-meshing along the time solution. Hence, some innovative approach is needed for efficient re-meshing technique as well as algorithm to trace the movement of mesh nodes (particles).

Considering the merits of finite element methods and particle methods, particle discretization scheme (PDS)[44, 45, 46, 47] has been proposed and further extended to higher order [48, 49] by elevating the order of polynomial of basis function used for approximation. PDS is based on local polynomial expansion about the mother points of domain tessellation. Smoothness of polynomial expansion can not be ensured simultaneously and therefore, conjugate domain is used to approximate/discretize derivative of the function. These displacement discontinuities along Voronoi boundaries i.e.$\partial\phi^{\alpha}$'s are utilized in introducing the crack in domain and as a result PDS-FEM turns into an efficient and illustrative numerical technique to model strong discontinuities. Moreover, author is intended to explore the possibilities and consequences of local polynomial expansion in solving the BVP.

2.2 Observation from literature review

Ease in simulation of propagating crack and computationally efficient probabilistic studies of crack-path variability are appealing research interest. And therefore, Development of computational efficient numerical scheme braced with rigorous mathematics is contemporary priority among the research community. Furthermore, improvement in inherent accuracy of conventional methods with lower order approximating polynomial is needed to be addressed. In addition to this, extra additional work is required to address the issue in context of imposing essential boundary conditions exclusively for particle based methods.

2.3 Objectives of the current work

The current thesis has following major objectives to be fulfilled

- Development of higher order particle discretization scheme by introducing the higher order polynomial for approximating the function and its derivative
- Implementation of developed higher order PDS in FEM framework to solve the boundary value problem
- Efficient simulation of the brittle crack in 3-Dimensional domain

Chapter 3

Higher order Particle Discretization Scheme (PDS)

This chapter opens with a brief introduction of original PDS proposed by Hori *et. al.*[44, 45], which is referred as 0th-order PDS, and presents the higher order extension of PDS in details. Specifically, two possible higher order extensions of PDS are presented. One is natural extension which does not strictly satisfy the fundamental condition $\boldsymbol{\nabla} \times \boldsymbol{\nabla} f^d = 0$, and the other strictly satisfying this curl-free condition; $f^d(\boldsymbol{x})(\approx f(\boldsymbol{x}))$ is the higher order PDS approximation of the function $f(\boldsymbol{x})$. One would expect that the curl-free extension to perform better and have attractive mathematical properties, since the function space it uses to approximate guarantees to satisfy the fundamental property $\boldsymbol{\nabla} \times \boldsymbol{\nabla} f^d = 0$, while function space of its counterpart does not. However, as it is demonstrated, both these extensions produce nearly the same accuracy and convergence rates.

3.1 0th-order PDS

A unique property of PDS is the usage of conjugate tessellations to approximate functions and their derivatives, respectively. In the original formulation, non-overlapping characteristic functions, $\phi^\alpha(\boldsymbol{x})$ and $\psi^\beta(\boldsymbol{x})$ of Voronoi tessellation $\{\Phi^\alpha\}$ and Delaunay tessellations $\{\Psi^\beta\}$ are used for approximating functions and derivatives, respectively, leading to constant variation of the approximated fields within each tessellation element. Stating the same in mathematical language, approximation of 0^{th}order PDS is expressed as follows

$$f(\boldsymbol{x}) \approx f^d(\boldsymbol{x}) = \sum_{\alpha=1}^{N^\alpha} f^\alpha \phi^\alpha$$
$$(\boldsymbol{\nabla} f)_i \approx g_j^d(\boldsymbol{x}) = \sum_{\beta=1}^{N^\beta} g_i^\beta \psi^\beta$$

Here, the characteristics function of Voronoi tessellation is defined as follows:

$$\phi^{\alpha}(\boldsymbol{x}) = \begin{cases} 1 & \text{if } \boldsymbol{x} \in \Omega^{\alpha} \\ 0 & \text{if } \boldsymbol{x} \notin \Omega^{\alpha} \end{cases} \tag{3.1}$$

Similarly, characteristic function of Delaunay tessellation, ψ^{β} is defined.

The set of coefficients $\{f^{\alpha}\}$s' and $\left\{g_i^{\beta}\right\}$s' are calculated by minimizing the error $E^f = \int (f - f^d)^2 dv$ and $E^g = \int (\boldsymbol{\nabla} f^d - \boldsymbol{g}^{\beta})^2 dv$, respectively. It results into following explicit expressions.

$$f^{\alpha} = \frac{1}{\Phi^{\alpha}} \int_{\Phi^{\alpha}} f(\boldsymbol{x}) dv$$
$$g_i^{\beta} = \frac{1}{\Psi^{\beta}} \sum_{\alpha} f^{\alpha} \int_{\Psi^{\beta}} \phi^{\alpha}{}_{,i}\, dv$$

where, $\Phi^{\alpha}$and Ψ^{β}stand for volume of Voronoi and Delaunay block.

The above mentioned formulation is referred as 0th order PDS in this thesis.

3.2 Higher order extension of PDS

In the above presented original proposal of PDS, by minimizing a certain error, a representative constant value is calculated to approximate a function within each Voronoi element, and function over the whole domain is approximated as the union of those. The same hold for the derivative, while Delaunay elements are used instead of Voronoi. In higher order PDS, instead of one constant value, the function within a Voronoi element is approximated as a polynomial series whose support is limited to the respective Voronoi element. The union of all those polynomial series defines the higher order PDS's approximate for a function. The same applies for derivatives, with Delaunay elements. In this sense, the constant representative value within each Voronoi or Delaunay element in original PDS can be considered as constant term in polynomial expansion used in higher order PDS. Hence the original version of PDS is referred here as 0th-order PDS.

The rest of this subsection presents the two formulations of higher order PDS; one which does not guarantee to satisfy $\boldsymbol{\nabla} \times \boldsymbol{\nabla} f^d = 0$, and the one which guarantee to satisfy this curl-free condition. Hereafter, the formulation which does not satisfy $\boldsymbol{\nabla} \times \boldsymbol{\nabla} f^d = 0$ is referred as *formulation-A* and the other which guarantee to satisfy this curl-free condition as *formulation-B*.

3.2.1 *Formulation-A*

Let f be a target function defined over an analysis domain Ω. The conjugate Voronoi and Delaunay tessellations, $\{\Phi^{\alpha}\}$ and $\{\Psi^{\beta}\}$, for this Ω is considered. $\boldsymbol{y}^{\alpha}$ denotes the mother

point of Voronoi tessellation, while $\boldsymbol{z}^{\beta}$ denotes the center of gravity of Delaunay tessellation . The characteristic function of Φ^{α} and Ψ^{β}, are denoted by ϕ^{α} and ψ^{β} respectively. The higher order PDS's approximation of function $f^{d}(\boldsymbol{x}) \approx f(\boldsymbol{x})$, is defined as

$$\begin{aligned} f(\boldsymbol{x}) \simeq f^{d}(\boldsymbol{x}) &= \sum_{\alpha=1}^{N^{\alpha}} \left(\sum_{n=0}^{|P^{\alpha}|} f^{\alpha n} P^{n} \phi^{\alpha}(\boldsymbol{x}) \right) \\ &= \sum_{\alpha=1}^{N^{\alpha}} \sum_{n=0}^{|P^{\alpha}|} f^{\alpha n} P^{\alpha n}, \end{aligned} \tag{3.2}$$

while the approximations for derivatives, $g_{i}^{d}(\boldsymbol{x})$, are defined as

$$\begin{aligned} \boldsymbol{\nabla}_{,i} f(\boldsymbol{x}) \simeq g_{i}^{d}(\boldsymbol{x}) &= \sum_{\beta=1}^{N^{\beta}} \left(\sum_{m=0}^{|Q^{\beta}|} g_{i}^{\beta m} Q^{m} \psi^{\beta}(\boldsymbol{x}) \right) \\ &= \sum_{\beta=1}^{N^{\beta}} \sum_{m=0}^{|Q^{\beta}|} g_{i}^{\beta m} Q^{\beta m}. \end{aligned} \tag{3.3}$$

Here,

$$P^{\alpha n} \in P^{\alpha} = \{1, (\boldsymbol{x} - \boldsymbol{y}^{\alpha}), \ldots, (\boldsymbol{x} - \boldsymbol{y}^{\alpha})^{r}, \ldots\ldots\} \, \phi^{\alpha}(\boldsymbol{x}) \tag{3.4}$$

and

$$Q^{\beta m} \in Q^{\beta} = \left\{1, (\boldsymbol{x} - \boldsymbol{z}^{\beta}), \ldots, (\boldsymbol{x} - \boldsymbol{z}^{\beta})^{r}, \ldots\ldots\right\} \psi^{\beta}(\boldsymbol{x}). \tag{3.5}$$

N^{α} is total number of Voronoi tessellations and N^{β} is total number of Delaunay tessellations.As an exampleexample, in 2D, PDS can use any combination of the bases tabulated in 3.1 as elements of P^{α}..

The unknown coefficients $f^{\alpha n}$ are determined by minimizing the error, which results in the following linear system of equation,

$$\sum_{m}^{|P^{\alpha}|} I^{\alpha n m} f^{\alpha m} = \int_{\Phi^{\alpha}} P^{\alpha n} f(\boldsymbol{x}) dv. \tag{3.6}$$

Similarly, the unknown coefficients $g_{i}^{\beta n}$'s are determined by minimizing

$$E^{g} = \int \left(\boldsymbol{g}^{d}(\boldsymbol{x}) - \boldsymbol{\nabla} f^{d}(\boldsymbol{x}) \right)^{2} dv,$$

$n=0$			1			
$n=1$		$(x-a)^1$		$(y-b)^1$		
$n=2$	$(x-a)^2$	$(x-a)^1$	$(y-b)^1$	$(y-b)^2$		
$n=3$	$(x-a)^3$	$(x-a)^2$	$(y-b)^1$	$(x-a)^1$	$(y-b)^2$	$(y-b)^3$

Figure 3.1: Set of basis functions, $P^{\alpha n}$ used for approximating function in 2-dimension. Here $(a,\, b)$ is point of inflection.

where $||(.)||^2$ denotes the norm of a vector $(.)$, which results in the following system of equation,

$$\sum_{m}^{|Q^\beta|} I^{\beta nm} g_i^{\beta m} = \sum_{n'}^{|P^\alpha|} f^{\alpha n'} \int_{\Psi^\beta} Q^{\beta n} P^{\alpha n'}{}_{,i}\; dv. \tag{3.7}$$

Here,

$$I^{\alpha nm} = \int_{\Phi^\alpha} P^{\alpha n} P^{\alpha m} dv$$

and

$$I^{\beta nm} = \int_{\Psi^\beta} Q^{\beta n} Q^{\beta m} dv \tag{3.8}$$

As is seen, it is straightforward to include the higher order polynomials in the original PDS that uses the characteristic functions as the basis functions. From now on, we call this PDS as higher order PDS. Indeed, Eq.(3.2) or (3.3) gives an expression of this higher order PDS, just by including higher order polynomials in $\{P^\alpha\}$.

Obviously, the basis functions included in P^α and Q^β, do not have to be polynomials. P^α and Q^β can contain any function provided certain basic requirements specified by Eq. 3.6 and Eq. 3.7 are satisfied: elements in P^α must have bounded derivatives at any point $\boldsymbol{x} \in \Phi^\alpha \cap \Psi^\beta$, for $\Phi^\alpha \cap \Psi^\beta \neq \emptyset$; $\int_{\Phi^\alpha} P^{\alpha n} dv$ should be bounded, etc. However, we prefer polynomial bases in higher order PDS.

3.2.2 *Formulation-B* : ensuring $\boldsymbol{\nabla} \times \boldsymbol{\nabla} f^d = \mathbf{0}$

The *formulation-A* does not always guaranteed to satisfy the fundamental conditions $\boldsymbol{\nabla} \times \boldsymbol{\nabla} f^d = \mathbf{0}$, except for special choices of the base polynomial sets P^β, though the function being approximated $f(\boldsymbol{x})$ always satisfies $\boldsymbol{\nabla} \times \boldsymbol{\nabla} f = \mathbf{0}$. This is one possible limitation of the higher order formulation of PDS presented in previous section and [48]. It is of

interest to consider alternative formulations of PDS which guarantees to satisfy this curl-free condition, and explore its advantages and disadvantages.

The only difference in curl-free formulation is the way derivatives are approximated. In the curl-free implementation, the given trial function $f(\boldsymbol{x})$ is approximated exactly in the same manner as in the *formulation-A* (see Eq. 3.6) An approximation for the derivative which always satisfy the curl-free condition is defined as $\tilde{g}_i^{\psi}(\boldsymbol{x}) \equiv \left(\boldsymbol{\nabla} f^{\psi}\right)_i$, where f^{ψ} is an approximation of f defined over the tessellation $\{\Psi^{\beta}\}$ as

$$f(\boldsymbol{x}) \simeq f^{\psi}(\boldsymbol{x}) = \sum_{\beta}^{N^{\beta}} \sum_{n}^{|Q^{\beta}|} \tilde{f}^{\beta n} \bar{Q}^{\beta n}. \tag{3.9}$$

Minimizing the error $\tilde{E} = \int_{\Psi} \left(\boldsymbol{\nabla} f^{\psi} - \boldsymbol{\nabla} f^{\phi}\right)^2 dv$, the unknown coefficients $\tilde{f}^{\beta n}$'s can be expressed in terms of $f^{\alpha n}$'s as $\tilde{f}^{\beta m} = A^{\beta m \alpha n} f^{\alpha n}$, where

$$A^{\beta m \alpha n} = \left[\sum_{j} \int_{\Psi^{\beta}} \bar{Q}_{,j}{}^{\beta m} \bar{Q}_{,j}{}^{\beta r} dv\right]^{-1} \left[\sum_{i} \int_{\Psi^{\beta} \cap \Phi^{\alpha}} \bar{Q}_{,i}{}^{\beta r} P_{,i}^{\alpha n}\, dv\right] \tag{3.10}$$

With the aid of the above expression, the approximated derivative of the curl-free formulation of PDS, $\tilde{g}_i^{\psi}(\boldsymbol{x}) \approx (\boldsymbol{\nabla} f)_i$, can be expressed as $\tilde{g}_i^{\psi}(\boldsymbol{x}) = \left(\boldsymbol{\nabla} f^{\psi}\right)_i = \sum_{\beta} \tilde{g}_i^{\beta}$, where

$$\tilde{g}_i^{\beta}(\boldsymbol{x}) \;=\; \sum_{\alpha}^{N^{\alpha}} \sum_{m}^{|Q^{\beta}|} \sum_{n}^{|P^{\alpha}|} A^{\beta m \alpha n} f^{\alpha n} \bar{Q}_{,i}^{\beta m} \tag{3.11}$$

It can be readily prove that the above definition of approximate gradient always satisfy the curl-free condition (i.e. $\boldsymbol{\nabla} \times \tilde{g}_i^{\psi} = \mathbf{0}$). as mentioned above, PDS defined with Eq. 3.9 and 3.11 are referred as the *curl-free PDS* or *formulation-B*, in this thesis.

Some possible advantages of this curl-free formulation, in solving boundary value problems, are; increase in accuracy, faster convergence with iterative linear system solvers, relaxing the need of higher order derivatives as boundary conditions, etc. However, the satisfaction of curl-free condition is not essential since the space spanned by solution of PDS satisfying this curl-free condition is a subset of the space spanned by the solution of PDS *formulation-A* presented in previous section and [48] (see Fig. 3.2). PDS-FEM based on both these formulations are used to solve various benchmark problems comprise of stress concentration and singularities in linear elasticity and the merits of the two formulations are discussed in chapters 6, and 7.

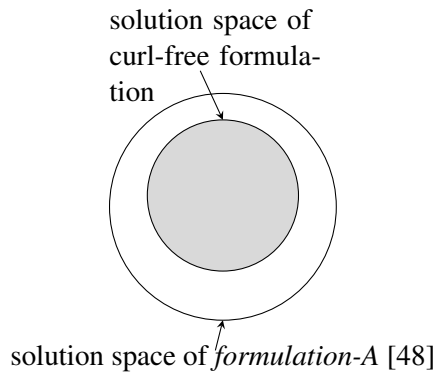

Figure 3.2: Solution space spanned by curl-free formulation of higher order PDS is subset of that of formulation in [48].

		$ord(Q^\beta)$			
		2	**3**	**4**	**5**
$ord(P^\alpha)$	**2**	(2, 2)	(2, 2)	(2, 2)	(2, 2)
	3		(3, 3)	(3, 3)	(3, 3)
	4			(4, 4)	(4, 4)
	5				(5, 5)

Table 3.1: Convergence rate of approximation (function , the derivative) for function $f(x) = \frac{x}{\sqrt{10x+x^3}}$. Here, $ord(P^\alpha)$and $ord(Q^\beta)$ are the highest order of polynomial of basis set, respectively.

3.3 Numerical examples

Comparison of 0th and higher order PDS It is of interest to investigate the rate of convergence of the PDS approximation of derivatives, $g^d_{,i}$, which is computed by using the discretized function, f^d; see Eq. (3.7). In one-dimensional setting, two examples, a smooth function of $\sin x$ and a singular function of $x/\sqrt{10x + x^3}$, are picked up for this investigation. Figure. 3.3 and 3.4 demonstrate the approximation of singular function and the derivative with $0^{th}-$order and 1st-order PDS, where a significant improvement in approximation can be easily observed. Figure 3.5 compares the convergence rate of $0^{th}-$order and 1st-order PDS. As is seen, the 1st-order PDS has higher accuracy and higher convergence rate. Further, convergence rate of the approximated function and derivative for the function $f(x) = x/\sqrt{10x + x^3}$, with different combinations of polynomial bases are shown in Table 3.1. As is seen, the convergence rates increase with the increasing order of polynomial bases included in P^α and Q^β, and best to use equal order polynomial bases both for P^α and Q^β.

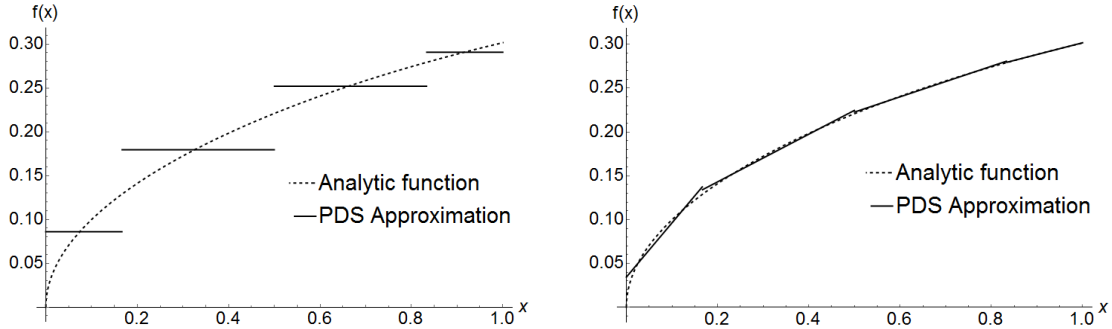

(a) 0th-order (b) 1st-order

Figure 3.3: Approximation of function.

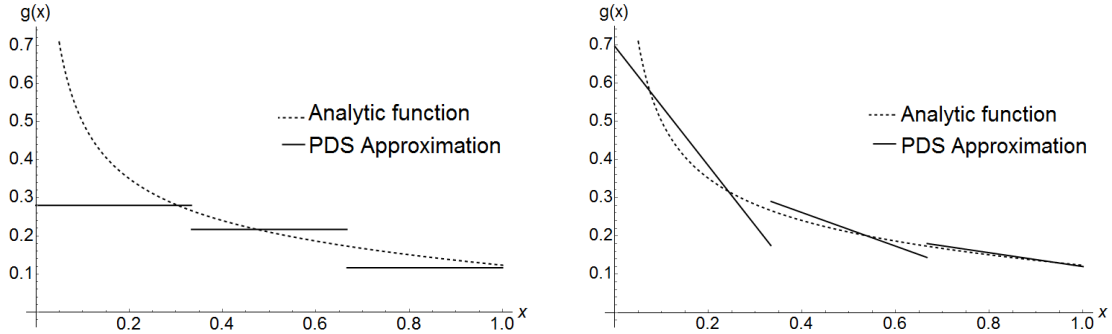

(a) 0th-order (b) 1st-order

Figure 3.4: Approximation of derivative.

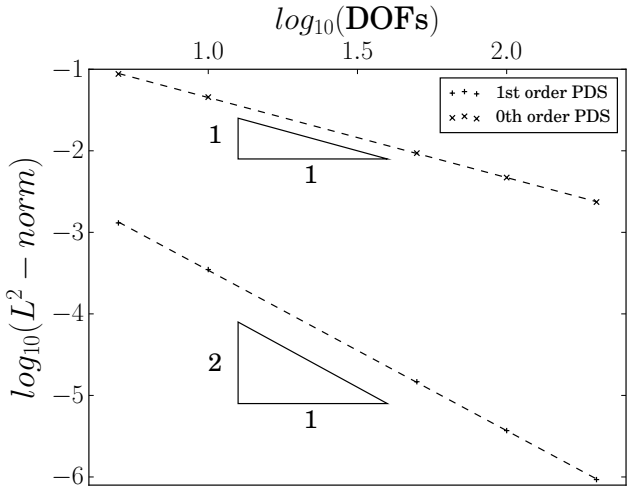

Figure 3.5: Convergence of function $f(x) = Sin(x)$ approximation with $0^{th}-$order and 1st-order PDS.

Comparison of *formulation-A* and *formulation-B* A 2-Dimensional function $f(x, y) = \sin(xy/40)$ is considered as target function to perform a comparative analysis of *formulation-A* and *B*. Figure 3.6 shows the approximated function and it's derivative in x-direction. The inherent discontinues along the tessellation boundaries can be easily seen in all the cases. These discontinuities are utilized in modeling the cracks in solid domains. Further convergence rate analysis of both formulation has been accomplished and procured results are shown in Fig. 3.7. Errors in approximation of function with both formulation are exactly the same, as it must be. In the case of derivative, the error in approximation with *formulation-B* is slightly lower than that of *formulation-A*, and both have the same rate of convergence. It can be concluded that curl free formulation (i.e. *formulation-B*) performs slightly better than *formulation-A* in approximating the derivative. Thought the improvement in approximating functions and their derivatives is negligible, what improvement formulation-B would bring in solving boundary value problem is the important question.

3.4 A possible interpretation

PDS is a approximation scheme which use non-overlapping support functions, described as characteristics function so that discontinuity of functions are naturally expressed. In a mathematical viewpoint, allowing discontinuity in a discretized function could be accepted if Taylor series expansion is considered. A smooth function allows Taylor series expansion, but when the expansion is taken at two neighboring points, the two expanded polynomials are not smoothly connected and discontinuity appears.

A union of local polynomial expansions which are taken at a set of points could be regarded a discretization of a smooth function. The connection of neighboring expansion is a key point for this union. Higher order PDS uses derivatives of the function; polynomials in neighboring Voronoi blocks share derivative in polynomial form in a common Delaunay block. Fig. 3.8 shows illustrated the approximation of function and calculation of derivative using Voronoi and Delaunay tessellation.

Union of local polynomial expansions is a key characteristic of higher order PDS, which differentiates it from other particle methods [26, 27], and enforce smoothness to fields produced by particle as well as fields in particles; fields in particle are requested to vanish near the boundary of the particle. Enforcing smoothness is surely attractive in solving a differential equation. However, it is contradicting to the consequence of the local polynomial expansion, i.e., a smooth function allows polynomial expansion but the expanded polynomials cannot be smoothly connected to each other.

Author is not denying the usefulness of the well-established particle methods. Instead, trying to point out the consequence of local polynomial expansion, and there could be a room to improve the particle methods. A function discretized by PDS has discontinuities

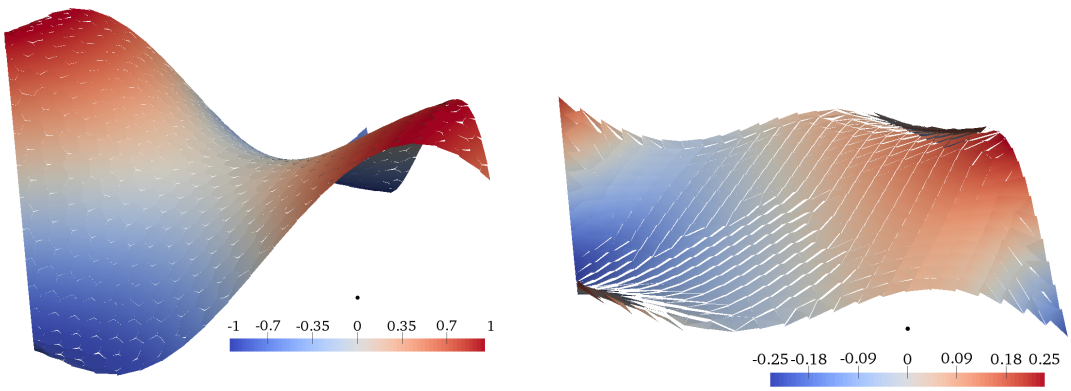

(a) $f(x, y)$ with formulation-A

(b) $\frac{\partial f(x,y)}{\partial x}$ with formulation-A

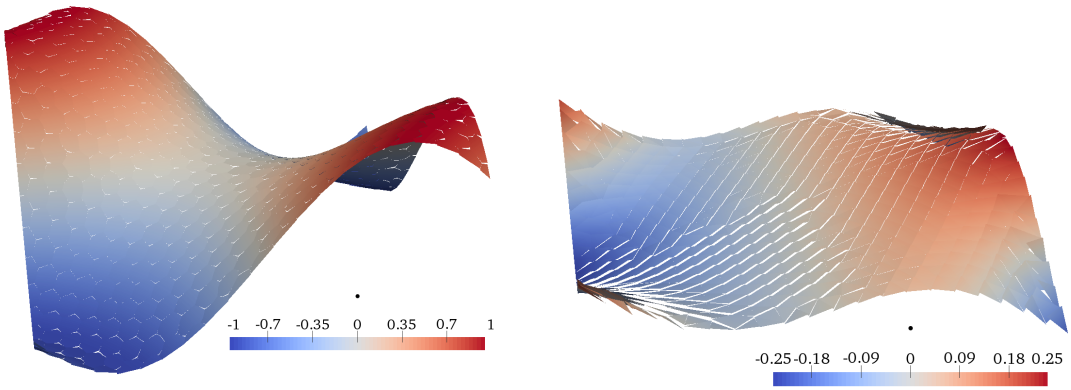

(c) $f(x, y)$ with formulation-B

(d) $\frac{\partial f(x,y)}{\partial x}$ with formulation-B

Figure 3.6: Plots of 1st-order PDS approximation of function $f(x, y) = \sin(xy/40)$ and the derivative $\frac{\partial f(x,y)}{\partial x}$

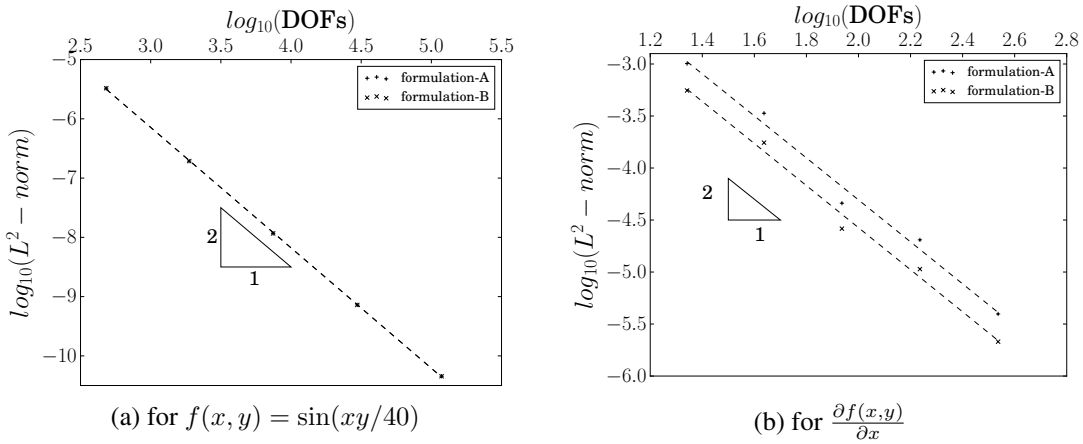

(a) for $f(x, y) = \sin(xy/40)$ (b) for $\frac{\partial f(x,y)}{\partial x}$

Figure 3.7: Comparison of convergence rates with *formulation-A* and *B*

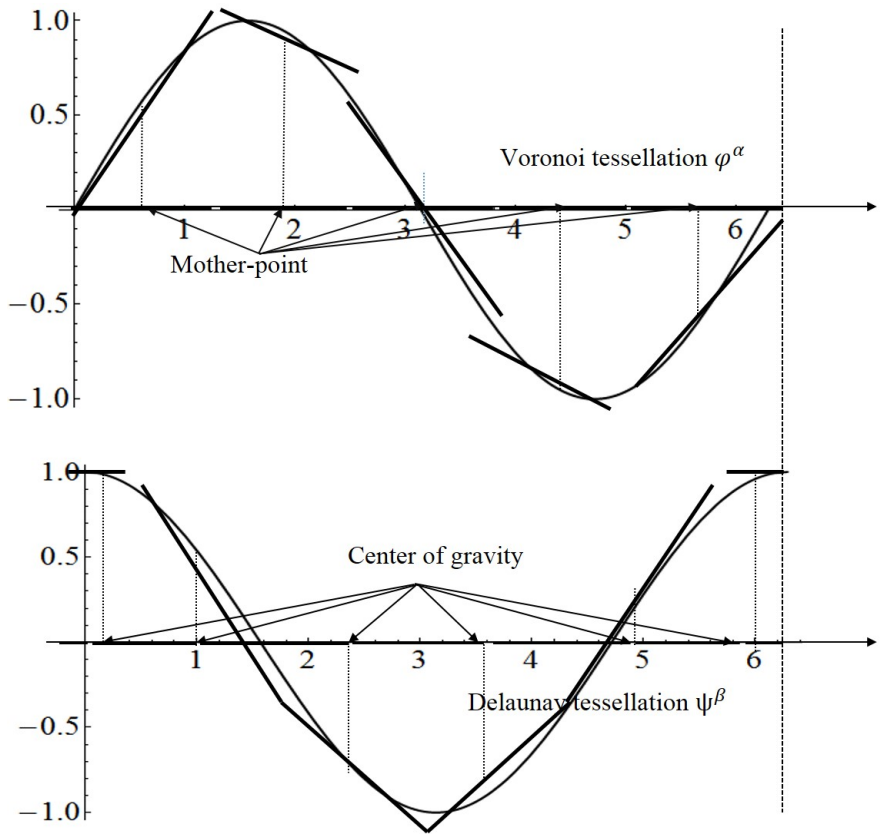

Figure 3.8: Explanation of function and derivative approximation

everywhere, which is a draw back in the viewpoint of the particle method. A further study is needed to investigate discontinuities of a discretized function.

3.5 Comparison with Taylor series expansion

While f^d and g_i^d of Eqs. (3.2) and (3.3) are computed by minimizing E^f and E^g, respectively, we can regard them as a union of Taylor series expansions for f and $f_{,i}$, respectively. The summed term, is of the same form as the Taylor series expansion of f or $f_{,i}$ at $\boldsymbol{y}^\alpha$ or $\boldsymbol{z}^\beta$, if the expansion domain is chosen as Φ^α or Ψ^β; see following for more detailed discussion in regarding higher order PDS as a union of Taylor series expansion.

When higher order PDS is regarded as a union of local Taylor series expansion, the accuracy could be examined by checking the coefficients of the expansion. For instance, the following errors could be useful:

$$
\begin{aligned}
E^{f*} &= \sum_{\alpha}^{N^\alpha} \sum_{n}^{|P^\alpha|} \int \left(\left(f_{,n} \left(\boldsymbol{y}^\alpha \right) - f^{\alpha n} \right) P^{\alpha n} \right)^2 dv, \\
E^{g*} &= \sum_{\beta}^{N^\beta} \sum_{m}^{\left|Q^\beta\right|} \sum_{j} \int \left(\left(\left(f_{,mj} \left(\boldsymbol{z}^\beta \right) - g_j^{\beta m} \right) Q^{\beta m} \right)^2 dv.
\end{aligned}
$$

Here, j is the dimensional setting of problem. Note that E^f and E^g should be used to check the convergence rate of PDS discretized function; E^{f*} and E^{g*} are for the Taylor series expansion coefficients. The coefficients $f_{,n}$ and $f_{,mn}$ are values at specific points $\boldsymbol{y}^\alpha$ and $\boldsymbol{z}^\beta$, respectively. Whereas, coefficients, $f^{\alpha n}$ and $g_j^{\beta m}$ are the average value over the support domain. Above mentioned error can be zero only if $N^\alpha \to \infty$ and $N^\beta \to \infty$. Though, proposed higher order PDS uses the same basis function as Taylor series expansion; current scheme should not be interpreted as extension or modification of Taylor series expansion.

Chapter 4

Implementation of PDS in FEM framework

In this chapter, implementations of both the of higher order extensions of PDS(i.e. formulation-A and B presented in the last chapter) in FEM framework are presented. Infinitesimal deformation of linear elastic continuum is set as the target Boundary Value Problem (BVP). Further, treatments for modeling brittle cracks in linear elastic continuum are presented. As it is explain in the latter part of this chapter, the proposed crack treatments are numerically as efficient as 0th-order PDS-FEM.

We use 2 or 3 dimensional Cartesian coordinates system with axes x_i, and comma subscript to denote partial derivatives (i.e. $u_{i,j} = {}^{\partial u_i}/_{\partial x_j}$). Further, Einstein summation convention is subscripts; i.e. repeated subscripts denotes summation. Note that summation with respect to superscripts are explicitly expressed; repeated superscripts does not denote Einstein summation.

4.1 Target boundary value problem: infinitesimal deformation of linear elastic continuum

As the target boundary value problem, we consider the infinitesimal deformation of linear elastic continuum, which occupies the domain Ω, subjected to prescribed displacement $\bar{\boldsymbol{u}}$ along the boundary $\partial\Omega$. The domain considered can either be 2D or 3D. Consider $\boldsymbol{c}(\boldsymbol{x})$ to be the fourth order tensor defining the distribution of elastic properties of the body, and $\boldsymbol{b}(\boldsymbol{x})$ to be the body force. Let's denote the unknown deformation at $\boldsymbol{x} \in \Omega$ to be $\boldsymbol{u}(\boldsymbol{x})$. For simplicity we consider static deformation and all the displacement boundary conditions to be specified over the whole boundary. It is straight forward to extend the discussion to dynamic problems and include Neumman boundary conditions.

We follow the Hamilton's principle of stationary action and obtain the governing equations which should be satisfied by our unknown variable $\boldsymbol{u}$. The standard Lagrangian for the above mentioned BVP can be written as

$$\mathcal{L}[\boldsymbol{u}] = \int_{\Omega} \frac{1}{2}\boldsymbol{\epsilon} : \boldsymbol{c} : \boldsymbol{\epsilon} + \boldsymbol{b}.\boldsymbol{u} dv, \tag{4.1}$$

where the strain tensor $\boldsymbol{\epsilon} = sym(\boldsymbol{\nabla u})$. Employing the Hamilton's principle of least action ($\delta S = 0$), it is straightforward to obtain the governing partial differential equations for the above BVP. The action integral (i.e. $S = \int \mathcal{L} dt$) for our system is equal to Lagrangian itself, since we are considering static problems. Therefore, setting the first variation $\delta\mathcal{L} = 0$, we can obtain the familiar set of equations given below.

$$\begin{aligned} (c_{ijkl}(\boldsymbol{x})u_{k,l}(\boldsymbol{x}))_{,i} - b_j(\boldsymbol{x}) &= 0 \text{ in } \Omega \\ u_i(\boldsymbol{x}) &= \overline{u}_i(\boldsymbol{x}) \text{ on } \partial\Omega \end{aligned} \tag{4.2}$$

Here onwards, the body force $\boldsymbol{b}(\boldsymbol{x})$ is assumed to be zero for the sake of simplicity; it is straightforward to consider it.

4.2 Formulation of higher order PDS-FEM

In higher order PDS-FEM, we approximate the field variables in Eq. 4.1 with higher order PDS, and obtain the governing linear set of equations by employing the Hamilton's principal. In this subsection, implementation of PDS-FEM with both the higher order extensions of PDS, proposed in the previous section, are presented.

4.2.1 *Higher order PDS-FEM with the formulation-A*

The unknown displacement field $\boldsymbol{u}$ and the body force field $\boldsymbol{b}$ are approximated using Voronoi tessellation, Φ^{α}, as

$$\begin{aligned} u_i &\approx u_i^d = \sum_{\alpha}^{N^{\alpha}} \sum_{n}^{|P^{\alpha}|} u_i^{\alpha n} P^{\alpha n} \\ b_i &\approx b_i^d = \sum_{\alpha}^{N^{\alpha}} \sum_{n}^{|P^{\alpha}|} b_i^{\alpha n} P^{\alpha n}, \end{aligned} \tag{4.3}$$

where $P^{\alpha n} \in P^{\alpha}$(see Eq. 3.4). P^{α} is the set of polynomial bases used with compact support over Φ^{α} defined by Eq.3.1. On the other hand, the derivative of $u_{i,j}$ is approximated

using Delaunay tessellations as $u_{i,j} \approx \sum_\beta \bar{u}_{ij}^{\beta m} Q^{\beta m}$. Based on the Eq. 3.7, the derivative coefficients $\bar{u}_{ij}^{\beta m}$ can be expressed as

$$\begin{aligned}\bar{u}_{ij}^{\beta m} &= \sum_{m'}^{|Q^\beta|} w^{\beta m m'} \sum_\alpha \sum_n^{|P^\alpha|} u_i^{\alpha n} \int_{\Psi^\beta} Q^{\beta m'} P_{,j}^{\alpha n}\, dv \\ &= \sum_{m'}^{|Q^\beta|} w^{\beta m m'} \sum_\alpha \sum_n^{|P^\alpha|} h_j^{\beta \alpha m' n} u_i^{\alpha n}. \end{aligned} \tag{4.4}$$

Strain tensor $\epsilon_{ij}^{\beta m} = \frac{1}{2}(\bar{u}_{ij}^{\beta m} + \bar{u}_{ji}^{\beta m})$, which can be approximated as

$$\epsilon_{ij} \approx \sum_\beta^{N^\beta} \sum_m^{|Q^\beta|} \epsilon_{ij}^{\beta m} Q^{\beta m},$$

can be re-phrased using Eq. 4.4 in following manner

$$\epsilon_{ij}^{\beta m} = \sum_{m'}^{|Q^\beta|} w^{\beta m m'} \sum_\alpha \sum_n^{|P^\alpha|} \frac{1}{2} \left(h_j^{\beta \alpha m' n} u_i^{\alpha n} + h_i^{\beta \alpha m' n} u_j^{\alpha n} \right). \tag{4.5}$$

Similarly, the stress tensor $\boldsymbol{\sigma}$ are also approximated over Delaunay tessellation as

$$\sigma_{ij} \approx \sum_\beta^{N^\beta} \sum_m^{|Q^\beta|} \sigma_{ij}^{\beta m} Q^{\beta m},$$

while the elasticity tensor is approximated with the characteristic functions of the Delaunay tessellation as

$$c_{ijkl} \simeq \sum_\beta^{N^\beta} c_{ijkl}^\beta \psi^\beta(\boldsymbol{x}).$$

It is straight forward to obtain that

$$\sigma_{ij}^{\beta n} = c_{ijkl}^\beta \epsilon_{kl}^{\beta n}.$$

For the sake of brevity, lets express the Eq. 4.5 in the following tensor form,

$$\boldsymbol{\epsilon}^{\beta m} = sym\left(\boldsymbol{B}^{\beta m \alpha n} \otimes \boldsymbol{u}^{\alpha n}\right), \text{ where, } B_i^{\beta m \alpha n} = \sum_{m'}^{|Q^\beta|} w^{\beta m m'} h_i^{\beta \alpha m' n}. \tag{4.6}$$

Substituting Eq. 4.6 to the the Lagrangian in Eq. 4.1 and setting the first variation with respect to the unknown coefficients $u_i^{\alpha n}$ zero, the following governing linear set of equations can be obtained.

$$\sum_{\alpha', n, n', m'} \boldsymbol{w}^{\beta n n'} \cdot (\boldsymbol{B}^{\beta n \alpha m} \cdot \boldsymbol{c}^\beta \cdot \boldsymbol{B}^{\beta n \alpha' m'}) \cdot \boldsymbol{u}^{\alpha' m'} = \boldsymbol{0}, \tag{4.7}$$

This linear set of equations is the PDS-FEM equivalent of global stiffness matrix in FEM. Indeed,

$$\boldsymbol{k}^\beta = \boldsymbol{w}^\beta \cdot \boldsymbol{B}^{\beta n \alpha m} \cdot \boldsymbol{c} \cdot \boldsymbol{B}^{\beta n \alpha' m'} \quad \text{or} \quad \sum_{i,k} w^{\beta n m} B_i^{\beta n \alpha m} c_{ijkl} B_k^{\beta n \alpha' m'} \tag{4.8}$$

can be considered as the element stiffness matrix of higher order PDS-FEM (i.e. governing linear set of equations for a Delaunay element). Explicit expressions and matrix appearances of above mentioned equations are given in Appendix A and B.

4.2.2 *Higher order PDS-FEM with the formulation*-B; with $\boldsymbol{\nabla} \times \boldsymbol{\nabla}(u_i^d) = 0$

As mentioned in the section 3.2.2, the only difference between the formulation-A and B is how the gradient approximated. Both these formulations of PDS have the same approximations for functions. Therefore, in PDS-FEM with formulation-A and B have exactly the same approximations for $\boldsymbol{u}$ and $\boldsymbol{b}$ (see Eq. 4.3).

Following the formulation in subsection 3.2.2, a curl free approximation for the derivative $u_{i,j}$ can be defined as $u_i^\psi{}_{,j} = \sum_\beta \tilde{u}_i^\beta{}_{,j}$, where

$$\tilde{u}_i^\beta{}_{,j} = \sum_\alpha \sum_m^{|\bar{Q}^\beta|} \sum_n^{|P^\alpha|} A^{\beta m \alpha n} u_i^{\alpha n} \bar{Q}_{,j}^{\beta m}. \tag{4.9}$$

With the above definitions, implementation of curl-free PDS in FEM framework is straightforward. Using Eq. 4.9, $\boldsymbol{\epsilon}$ can be approximated as $\epsilon_{ij}^\psi = \sum_\beta \epsilon_{ij}^\beta$, where

$$\epsilon_{ij}^\beta = \frac{1}{2}\left(\tilde{u}_i^\beta{}_{,j} + \tilde{u}_j^\beta{}_{,i}\right). \tag{4.10}$$

For the sake of brevity, Eq. 4.10 can be written in the following vector form

$$\boldsymbol{\epsilon}^{\beta} = sym\left(\bar{\boldsymbol{B}}^{\beta\alpha n} \otimes \boldsymbol{u}^{\alpha n}\right), \tag{4.11}$$

where sym stands for symmetric part of the second order tensor, and the vector $\bar{\boldsymbol{B}}^{\beta\alpha n} = \left[\sum_{m}^{|Q^{\beta}|} A^{\beta m\alpha n}\bar{Q}_{,j}^{\beta m}\right]$. It is straight forward to define an approximation of $\boldsymbol{\sigma}$ as $\boldsymbol{\sigma}^{\beta} = \boldsymbol{c}^{\beta} : \boldsymbol{\epsilon}^{\beta}$.

Substituting Eq. 4.11 into 4.1 and setting the first variation $\delta\mathcal{L} = 0$, we can obtain the following governing linear set of equations.

$$\sum_{\alpha',n'}(\bar{\boldsymbol{B}}^{\beta\alpha n} \cdot \boldsymbol{c}^{\beta} \cdot \bar{\boldsymbol{B}}^{\beta\alpha' n'}) \cdot \boldsymbol{u}^{\alpha' n'} = \boldsymbol{0} \tag{4.12}$$

The element stiffness matrix can be readily recognized as

$$\bar{\boldsymbol{k}}^{\beta} \quad = \quad \bar{\boldsymbol{B}}^{\beta\alpha n} \cdot \boldsymbol{c}^{\beta} \cdot \bar{\boldsymbol{B}}^{\beta\alpha' n'}, \tag{4.13}$$

where $\boldsymbol{k}^{\beta}$ is a matrix of size $(6\,|P^{\alpha}|) \times (6\,|P^{\alpha}|)$ or $(12\,|P^{\alpha}|) \times (12\,|P^{\alpha}|)$ with triangular element in 2D or tetrahedral elements in 3D, respectively.

In numerical point of view, evaluation of the element stiffness matrix of formulation-A (Eq. 4.8) require more floating point operations that that with formulation-B (Eq. 4.13). The multiplication with $w^{\beta nn'}$in Eq. 4.8 significantly increases the number of floating point operations involved in calculating element stiffness matrix of formulation-A, though it can be reduced making use of symmetry of $\boldsymbol{k}^{\beta}$ and with suitable coordinate transformations. Further, when it comes to implementation of higher order PDS-FEM in an existing FEM software, that with formulation-B requires lesser modifications to the existing software. However, the decision of which formulations to be used must be based on their performance in solving the target boundary value problem, not the ease of implementation.

4.3 Modeling crack in PDS-FEM

As mentioned in the section 1, a major advantage of PDS-FEM is the simple and numerically efficient treatment for modeling discontinuities. The displacement field approximated with PDS inherent discontinuities along each edge of Voronoi elements Φ^{α}. Close inspection of Eq. 4.3 clearly indicates this; the support of each polynomial base $P^{\alpha n}$ is limited to the domain of the corresponding tessellation element Φ^{α} creating discontinuities along it's boundary $\partial\Phi^{\alpha}$. Figure 4.1(a) shows an exaggerated illustration of a displacement component approximated with PDS over a Delaunay tessellation. As explained below, PDS-FEM utilizes these existing discontinuities along $\partial\Phi^{\alpha}$'s to model discontinuities in BVPs.

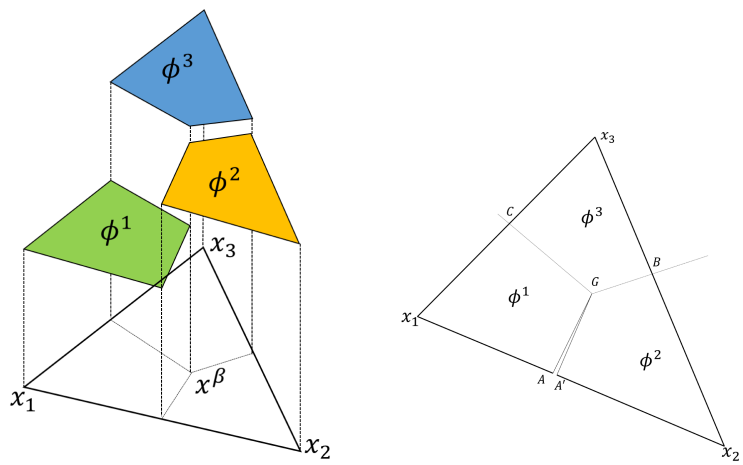

(a) (b)

Figure 4.1: Modeling a crack passing through a Delaunay element; (a) existing discontinuities in the displacement field approximated with PDS, (b) modeling a crack by dropping contribution from infinitesimally thin neighborhood of Voronoi boundary to be broken.

4.3.1 In *formulation-A*

As mentioned, the contribution from $\phi^\alpha(\boldsymbol{x})$ to relevant strain components, along the Voronoi boundary to be broken, are dropped to model discontinuities. This is equivalent to creation of a discontinuity by eliminating relevant contributions to strain tensor, from an infinitesimally thin neighborhood of the Voronoi block boundary.

According to the definition, $P^{\alpha n}$ can be written as $P^{\alpha n} = F^{\alpha n}\,\phi^\alpha(\boldsymbol{x})$, which allows to express $B_j^{\beta n \alpha m}$ in Eq. 4.5 as

$$\begin{aligned} B_j^{\beta n \alpha m} &= \sum_{n'}^{|Q^\beta|} I^{\beta n n'} \int_{\Psi^\beta} Q^{\beta n'} \left(F_{,j}^{\alpha m}\,\phi^\alpha + F^{\alpha m} \phi_{,j}^{\alpha} \right) dv \\ &= \sum_{n'}^{|Q^\beta|} I^{\beta n n'} \left(\int_{\Psi^\beta} Q^{\beta n'} F_{,j}^{\alpha m}\,\phi^\alpha dv + \int_{\partial\Phi^\alpha} Q^{\beta n'} F^{\alpha m} n_j ds \right), \end{aligned} \tag{4.14}$$

where, n_j^α is the unit outward normal along $\partial\Phi^\alpha$. In Eq. 4.14, the term $\int_{\partial\Phi^\alpha} Q^{\beta n'} F^{\alpha m} n_j ds$ is responsible for including the contribution to ϵ_{ij}^β from the discontinuities along $\partial\Phi^\alpha$ in the approximated displacement field.

What is required to model a brittle crack along a segment of Voronoi boundary, $\partial\Phi^\alpha$, is dropping this contribution $\int_{\partial\Phi^\alpha} Q^{\beta n'} F^{\alpha m} n_j ds$ which is generated by an infinitesimally thin neighborhood of the segment of $\partial\Phi^\alpha$, when evaluating $\boldsymbol{B}^{\beta n \alpha m}$. As an example, to

model a crack along the boundary AG creating a crack surfaces AG and GA′ in Fig. 4.1(b), all it needs is to exclude the contributions $\int_{AG} Q^{\beta n'} F^{\alpha_1 m} n_j^{\mathrm{AG}} dl$ and $\int_{\mathrm{A'G}} Q^{\beta n'} F^{\alpha_2 m} n_j^{\mathrm{A'G}} dl$, when evaluating $\boldsymbol{b}^{\beta n \alpha m}$, and recalculate the element stiffness matrix of corresponding Delaunay element. The integration $\int_{\partial\Phi^\alpha} Q^{\beta n'} F^{\alpha m} n_j ds$ can easily be evaluated with numerical integration over lines/planes in 2D/3D settings, respectively.

4.3.2 In *formulation-B*

Just as in the formulation-A, writing $P^{\alpha n} = F^{\alpha n}\, \phi^\alpha(\boldsymbol{x})$, $A^{\beta m \alpha n}$ from Eq. 3.10 can be expressed as

$$A^{\beta m \alpha n} = \left[J^{\beta r m}\right]^{-1} \Big[\sum_j^{2\mathrm{or}3} \int Q,_j^{\beta r} \left(F,_j^{\alpha n}\, \phi^\alpha + F^{\alpha n} \phi,_j^{\alpha}\right) dv\Big]. \tag{4.15}$$

The term $\int_{\psi^\beta \cap \phi^\alpha} Q,_j^{\beta r}\, F^{\alpha n} \phi,_j^{\alpha}\, dv$ represent the contribution to the derivatives $u_i^\beta,_j$ or ϵ_{ij}^β from an infinitesimal thin neighborhood along the boundary $\partial\Phi^\alpha$. Using Gauss theorem, the term$\int_{\psi^\beta \cap \phi^\alpha} Q,_j^{\beta r}\, F^{\alpha n} \phi,_j^{\alpha}\, dv$ can be re-expressed as $\int_{\partial\Phi^\alpha} Q,_j^{\beta r}\, F^{\alpha n} n_j^\alpha ds$, where n_j^α is the outward normal to the corresponding Voronoi boundary.

What is required to model a crack along a Voronoi boundary, $\partial\Phi^\alpha$, is dropping this contribution $\int_{\partial\Phi^\alpha} Q,_j^{\beta r}\, F^{\alpha n} n_j^\alpha ds$ along the corresponding boundary when evaluating $A^{\beta m \alpha n}$. As an example, to model a crack along the boundary AG creating a crack surfaces AG and GA' in Fig. 4.1(b), all it needs is to exclude the contributions $\int_{AG} Q,_j^{\beta r}\, F^{\alpha n} n_j^{AG} ds$ and $\int_{GA'} Q,_j^{\beta r}\, F^{\alpha n} n_j^{GA'} ds$ in evaluating $A^{\beta m \alpha n}$ for the corresponding Delaunay element Ψ^β and recalculate the element stiffness matrix. These contributions can be easily evaluated with numerical integration over lines or planner surfaces in 2D or 3D settings, respectively.

Important thing to note is that displacement field is discontinuous along the Voronoi extremes as polynomials with local support are used in approximating. Such discontinuities are utilized in modeling the cracks and are explained in previous section. In the curl-free formulation the mapping of f^ϕ to f^ψ (i.e.Eq. 3.2 and 3.9) can be interpreted as the way to smoothly connect the discontinuous u_i^ϕ's defined over Voronoi elements, and define bounded derivatives over the Delaunay elements (i.e. Eq. 4.9). Need of conjugate domain can also be justified to fulfill the requirement of bounded derivative, which satisfies the given governing equation.

Unlike the treatments used in other methods to model propagating cracks, this treatment is simple and numerically efficient. Most of the existing numerical methods requires hefty numerical treatments like introduction of new nodes, enrichment involving complex integration,tracking the crack surface and crack front etc., while above PDS-FEM treatment require only recalculation of an element stiffness matrix. Especially, in simulating large scale problems utilizing high performance computing, this simple crack treatment has a clear advantage over the existing methods.

Chapter 5

Imposing essential boundary conditions

In this chapter, problems associated with imposing essential boundary conditions are discussed. Obstacles in enforcing the Dirichlet/Neumann boundary conditions are studied. Several treatments to address the issue have been explored. This chapter presents comparative discussion on accuracy, feasibility and performance of some of those ad-hoc technique. Only 1D Helmholtz equation is used for this scrutiny, in this chapter.. However, latter in this thesis, similar investigations are conducted with boundary value problem of 2D elasticity. Furthermore, *P-version* convergence rate of higher order PDS-FEM with different combination of basis function is presented by analyzing 1-dimensional Helmholtz equation.

5.1 Introduction

A generalized variational principle assuming displacement $\boldsymbol{u}$, an independent variable field, and with essential boundary conditions i.e. $\boldsymbol{u} = \bar{\boldsymbol{u}}$ on Γ_u and traction boundary conditions i.e. $\boldsymbol{t} = \bar{\boldsymbol{t}}$ on Γ_t is as follows; $\boldsymbol{\lambda}_1$ and $\boldsymbol{\lambda}_2$ are the Lagrange multipliers satisfying the given governing equation

$$\mathcal{L} = \int_\Omega \frac{1}{2}\boldsymbol{\epsilon} : \boldsymbol{c} : \boldsymbol{\epsilon} - \boldsymbol{b}.\boldsymbol{u} d\Omega - \int_{\Gamma t} (\boldsymbol{t} - \bar{\boldsymbol{t}}).\boldsymbol{\lambda}_2 d\Gamma - \int_{\Gamma u} (\boldsymbol{u} - \bar{\boldsymbol{u}}) .\boldsymbol{\lambda}_1 d\Gamma \tag{5.1}$$

The first variation of Lagrange for elasticity problem (See Eq. 5.1) is expressed as:

$$\begin{aligned}
\delta\mathcal{L} \;=\; & \int_\Omega -\delta\boldsymbol{u}(\boldsymbol{\nabla}.\boldsymbol{c} : \boldsymbol{\epsilon} - \boldsymbol{b}) d\Omega - \int_\Gamma \boldsymbol{n}. \left(\delta\boldsymbol{u}.\boldsymbol{c} : \boldsymbol{\epsilon}\right) d\Gamma \\
& - \int_{\Gamma_t} (\boldsymbol{t} - \bar{\boldsymbol{t}}).\delta\boldsymbol{\lambda}_2 d\Gamma - \int_{\Gamma_u} (\boldsymbol{u} - \bar{\boldsymbol{u}}).\delta\boldsymbol{\lambda}_1 d\Gamma \\
& - \int_{\Gamma_u} \delta\boldsymbol{u}.\boldsymbol{\lambda}_1 d\Gamma - \int_{\Gamma_t} \delta\boldsymbol{t}.\boldsymbol{\lambda}_2 d\Gamma.
\end{aligned}$$

$\boldsymbol{n}$ is the unit outward normal to the boundary. .

After rearranging and setting the first variation equal to zero, we get

$$\int_{\Gamma} \delta \boldsymbol{u}. \left(\boldsymbol{n}.\boldsymbol{c} : \boldsymbol{\epsilon} - \boldsymbol{\lambda_1}\right) = 0 \tag{5.2}$$

and

$$\int_{\Gamma_u} \delta \boldsymbol{\lambda}_1. \left(\boldsymbol{u} - \bar{\boldsymbol{u}}\right) d\Gamma = 0. \tag{5.3}$$

Eq. 5.2 provides the following relationship between stress and $\boldsymbol{\lambda}_1$.

$$\boldsymbol{\sigma}.\boldsymbol{n} = \boldsymbol{\lambda}_1 \tag{5.4}$$

One would readily recognize that $\boldsymbol{\lambda}_1$ traction vector in mechanics. Substituting the strain approximation $\boldsymbol{\sigma}^d = \sum_{\beta,m} \boldsymbol{\sigma}^{\beta m} Q^{\beta m}$, the variation of $\boldsymbol{\lambda}_1^d \approx \boldsymbol{\lambda}_1$can be expressed as

$$\sum_{\beta} \delta \boldsymbol{\lambda}_1^d = \sum_{\beta,m} \delta \boldsymbol{\sigma}^{\beta m}.\boldsymbol{n} Q^{\beta m}. \tag{5.5}$$

Eq. 5.3 exhibits the required boundary constraint. Further, substituting the approximation of displacement:$\sum_{\alpha,n} \boldsymbol{u}^{\alpha n} P^{\alpha n}$ and first variation of Lagrange (see Eq. 5.5), leads to constraint;

$$\sum_{\beta} \int_{\Gamma_u \cap \partial\Psi^{\beta}} \delta \boldsymbol{\sigma}^{\beta m} : \left(\boldsymbol{n} Q^{\beta m} \left(\sum_{\alpha,n} \boldsymbol{u}^{\alpha n} P^{\alpha n} - \bar{\boldsymbol{u}}\right)\right) d\Gamma = \boldsymbol{0} \tag{5.6}$$

and subsequently, acquired condition is simplified in following manner

$$\sum_{\alpha,n} \boldsymbol{u}^{\alpha n} \boldsymbol{n}^{\alpha} \int_{\Gamma_u \cap \partial\Psi^{\beta}} Q^{\beta m} P^{\alpha n} d\Gamma = \sum_{\alpha} \int_{\Gamma_u \cap \partial\Psi^{\beta}} \boldsymbol{n}^{\alpha} \bar{\boldsymbol{u}} Q^{\beta m} d\Gamma \tag{5.7}$$

Thus, each boundary condition problem must satisfy the above restriction.

On contrary, system of equation as seen in Eq. 5.7 doesn't not ensure the distinctive solution of $\boldsymbol{u}^{\alpha n}$s'. For example, 1-Dimensional problems, the required constraint turns into a ill-conditioned system of equations. Further, in higher dimensions, $\boldsymbol{u}^{\alpha n}$ along boundary edges/surfaces parallel to the axis, (see Fig.5.1) can not be determined uniquely. Basically, the integrals which have term $(\boldsymbol{x} - \boldsymbol{x}^{\alpha})^r$ (here, $r = Z_+$), equate to the value of zero and subsequently results into inconsistent system.

Further, the approximation scheme of PDS and Eq. 5.7 say that the coefficients $\boldsymbol{u}^{\alpha n}$ are not the point values of function and its derivatives. Rather, these are averaged values, in some sense. Determination of these coefficients requires prior-knowledge of explicit

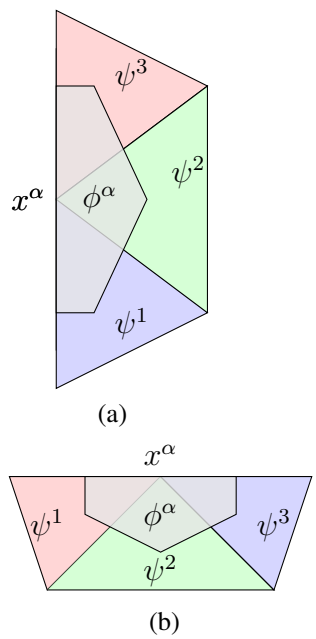

Figure 5.1: Boundary Voronoi and its Delaunay, with boundary edge is parallel to (a) vertical axis (b) horizontal axis}

expressions of solution, but unavailability of such information compel this into list of challenging tasks.

Therefore, system request some additional conditions, so that Eq. 5.7 inconsistency of system can be easily eliminated.

Moreover, $\boldsymbol{f}^{\alpha n}$'s; the counter-part of $\boldsymbol{u}^{\alpha n}$ shall be specified accurately. Otherwise, It will become a simple case of "garbage in, garbage out". Numerical experiments exhibit that by setting all the $u^{\alpha n}$'s, for $n = 1, 2$, to zero produces a solutions, which are significantly deviated from the analytic solutions.

Similarly, Neumann boundary conditions also require that all coefficients of local polynomial along the prescribed boundary should be specified. Here, these coefficients are multiplied with an additional factor, $\int_{\partial\phi} P^{\alpha n} d\Gamma$. The counter vector to applied external force, which is displacement vector, appears as additional unknown in global matrix system. Hence, it is important that coefficients associated with higher order of polynomial must be specified accurately, while enforcing the essential boundary conditions.

Prior-knowledge of higher order terms of polynomial, is not easy to obtain for real and complex problems and therefore it raises a valid question on the feasibility of newly proposed scheme. Thus, it is required to identify the alternative procedures to impose essential boundary conditions. Next section discuss the ad-hoc treatments of boundary conditions in higher order PDS-FEM.

5.2 Problem statement

1-dimensional Helmholtz equation is considered as model problem to demonstrate the various techniques to enforce the essential boundary conditions.

$$\begin{aligned} \nabla^2 u(x) + k^2 u(x) &= 0 \quad \text{in} \quad 0 < x < 1 && (5.8) \\ u(0) &= 0 \quad \text{on} \quad x = 0. && (5.9) \\ u(1) &= 1 \quad \text{on} \quad x = 1. \end{aligned}$$

Here, k is a constant with value of 1 for simplicity.

PDS-FEM uses the following functional to obtain an equivalent variational problem.

$$\mathcal{L}(u, \nabla u, k) = \int \frac{1}{2} \nabla u \, \nabla v - k^2 u \, v \, dx \tag{5.10}$$

where, u , ∇u are solution function and its derivative respectively.

5.2.1 Weak formulation

The solution function: u and it's derivative: $\nabla u \equiv g$ is approximated as union of local polynomial expansion about the mother point of Voronoi tessellation and center of gravity of Delaunay tessellation respectively. Here, concept of *formulation-A* has been considered in formulation.

$$\begin{aligned} u_i &= \sum_{\alpha} u_i^{\alpha n} P^{\alpha n} \\ g_i &= \sum_{\beta} g_i^{\beta n} Q^{\beta n} \end{aligned}$$

First variation of functional Eq. 5.10

$$\delta \mathcal{L} = \delta u. \left(- \int \nabla . \nabla u + k^2 \, u \, dx \right) \tag{5.11}$$

Equating the first variation of Lagrange Eq. 5.10 with respect to the displacement and setting it equal to zero, leads to the matrix form as follows,

$$-\boldsymbol{K} u + \boldsymbol{M} u = 0 \tag{5.12}$$

Where, $\boldsymbol{M} = \left\{ M^{\alpha m m'} \right\} = \int_{\psi^\beta} P^{\alpha m} P^{\alpha m'} \, dx$ and $\boldsymbol{K} = \left\{ K^{\alpha \alpha'} \right\} = \sum_{\beta, m, m'} W^{\beta m m'} \boldsymbol{B}^{\beta n \, \alpha m} . \boldsymbol{B}^{\beta n \, \alpha' m'} \, dx$

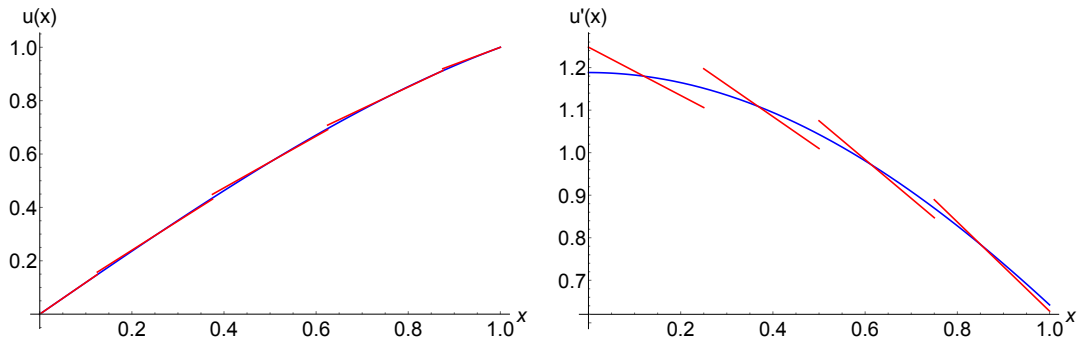

Figure 5.2: Solution function and its derivative by specifying all the terms of polynomial along boundary. Here, Analytical solution is shown in blue color, while red color curve denotes the solution from higher order PDS-FEM.

Here, $\boldsymbol{B}^{\beta n\, \alpha m}$ is defined as

$$\boldsymbol{B}^{\beta n\, \alpha m} = \sum_k W^{\beta nk} \int_{\psi^\beta} Q^{\beta k} \boldsymbol{\nabla}(P^{\alpha m}) dx$$

and $W^{\beta nk}$ is the inverse of the matrix of $I^{\beta nk} = \int_{\psi^\beta} Q^{\beta n} Q^{\beta k} dx$.

5.3 Treatment to enforce essential boundary conditions

One dimension Helmholtz equation with prescribed boundary condition mentioned in Eq. 5.8 is solved with basis $P^\alpha = \{1, (x - x^\alpha)\}\phi^\alpha(x)$ and $Q^\beta = \{1, (x - x^\beta)\}\psi^\beta(x)$ for function and it's derivative approximation, respectively. Various approaches to enforce boundary conditions are discussed here. A comparative study is also performed.

5.3.1 Specifying the all coefficients of approximation on boundary

In the previous section, it is concluded that all the terms of polynomial along the boundary must be specified. With the simple 1D Helmholtz problem, we numerically verify that an accurate solution can be obtained when all the coefficients of approximation are specified on boundary Voronoi. As shown in Fig. 5.2, the numerically obtained solution and its derivative are in good agreement with those of analytic solution.

Imposing essential boundary condition by specifying higher terms of polynomial $u^{\alpha n}$s'$(n = 1, 2, ..)$ along with constant terms $u^{\alpha 0}$s' may sound trivial in 1-D problem. Further, In 2-Dimensional simple problems, apart from the boundary segments parallel to the coordinate axes, all the derivatives of $\bar{\boldsymbol{u}}$ can be specified based on $\bar{\boldsymbol{u}}$. However, along boundary segments which are parallel to coordinate axes, derivatives of $\bar{\boldsymbol{u}}$ normal to the

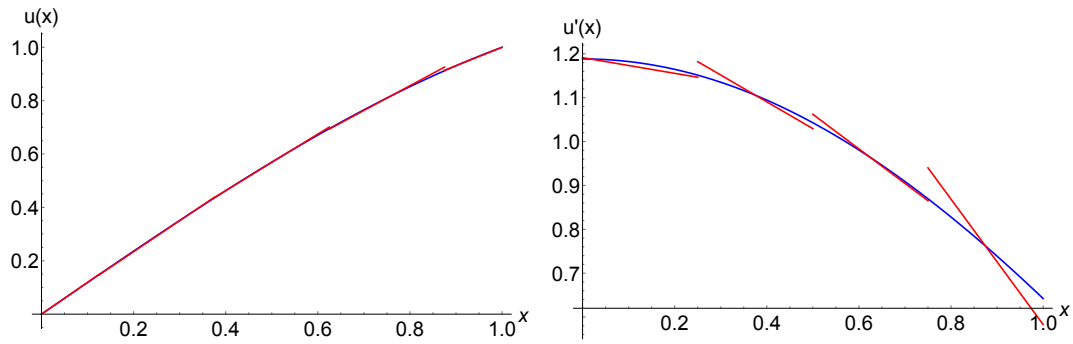

Figure 5.3: Solution function and its derivative with consistency equation (see Eq. 5.13) . Here, Analytical solution is shown in blue color, while red color curve denotes the solution from higher order PDS-FEM.

boundary cannot be evaluated. But, In case of complex problem, where priori knowledge about the solution space is not known, imposing essential boundary condition would be most challenging task. Subsequently leading the global linear system to be ill-posed. Therefore, a simple solution is needed to address this issue.

5.3.2 Consistency condition

Specifying the terms along boundary is not distinctive technique applicable to all sort of problems. Even, stationalization of functional of governing equation does not ensure the uniqueness of higher order coefficients unknown set, $\{u^{\alpha n}\}$ where, $n = \{1, 2, ..\}$. Hence, some additional condition is needed to resolve the issue of imposing boundary conditions.

Unlike Voronoi blocks inside the analysis domain, a Voronoi block on the boundary is covered by a unique Delaunay block. Hence, we may request derivatives of a function discretized in this Voronoi block to coincide with those of the unique Delaunay block. It might be more natural to use flux rather than derivative if we use this request as a sort of consistency for the boundary conditions as follows,

$$n.(\nabla u^d - \epsilon) = 0 \qquad \text{on} \quad \partial\Omega \tag{5.13}$$

here, n is outward unit normal on $\partial\Omega$.

1D Helmholtz equation is solved with basis set $P^\alpha = \{1, (x - x^\alpha)\}\phi^\alpha(x)$ and $Q^\beta = \{1, (x - x^\beta)\}\psi^\beta(x)$. Essential boundary conditions are enforced using reduced matrix methods. Consistency conditions are included by re-arranging the stiffness matrix into augmented form. System of linear equation is then solved and results are shown in Fig

5.3 . As is seen, though the function approximation is in good agreement, the derivative approximation has large deviations even within boundary Delaunays.

Inclusion of consistency condition into the regular stiffness matrix forces it to loose many of it's important properties such as positive definite determinant and symmetricity, which is vital for numerical schemes like Conjugate Gradient method.

5.3.3 Increasing the order of polynomial bases used for derivative approximation

While seeking the solution to problem of enforcing boundary condition, nature of stiffness matrix is explored. Important to note is that all components of stiffness matrix does not posses the same physical dimension and these terms can be interpreted as different physical quantities. Moreover, Order of magnitude of these terms also varies and often terms corresponding to gradient terms are very small compare to terms related to constant term of approximation scheme. And this lead to ill-conditioned system of equations. Therefore, it is prudent to strengthen the terms related to gradient terms.

Amplification of comparatively smaller components of stiffness matrix can also be achieved by adopting distinct set of basis used for approximating derivatives. As an initial motivation, 1-Dimensional bar problem is solved with bases set of $P^{\alpha} = \{1, (x - x^{\alpha})\}\phi^{\alpha}(x)$ and $Q^{\beta} = \{1, (x - x^{\beta}), (x - x^{\alpha})^2\}\psi^{\beta}(x)$ (see Appendix C). It is shown that opting one order higher polynomial for derivative approximation than that of function approximation leads to the unique solution. In this section, author is intended to further extend the motivation work discussed in Appendix C. Further, a criterion to select most suitable basis function set is defined. Convergence rate being a quantitative measurement of efficiency of numerical schemes, is chosen to deciding parameter. Analysis of Helmholtz equation is performed following these guidelines and convergence rate for function and derivative is calculated for different combination of basis. Figure 5.4 shows the solution and its derivative with basis $P^{\alpha n} = \{1, (x - x^{\alpha})\}$ and $Q^{\beta n} = \{1, (x - x^{\beta}), (x - x^{\beta})^2\}$. Rate of convergence with different set of bases function is tabulated in Table 5.1 .

Obtained results advocate the use of one order higher polynomial for derivative as compare to the function approximation i.e. $ord(Q^{\beta}) \geqslant ord(P^{\alpha}) + 1$ to secure the unique solution, even when higher order coefficients of approximation are not specified and corresponding right hand side components are set to zero. On the other hand, for case with $ord(Q^{\beta}) = ord(P^{\alpha})$, all the higher order coefficients on the boundary has to be specified, which require the knowledge of analytical solution. However, increasing the order of polynomial of bases for derivative approximation by two or more does not improve convergence rate any-more. Therefore, it is concluded that $ord(Q^{\beta}) \geqslant ord(P^{\alpha}) + 1$ is an acceptable solution for eliminating the need of specifying higher order coefficients of approximations as boundary conditions. Further, according to the numerical results, *p-version* convergence rate of proposed numerical scheme is well achieved by elevating the order of polynomial.

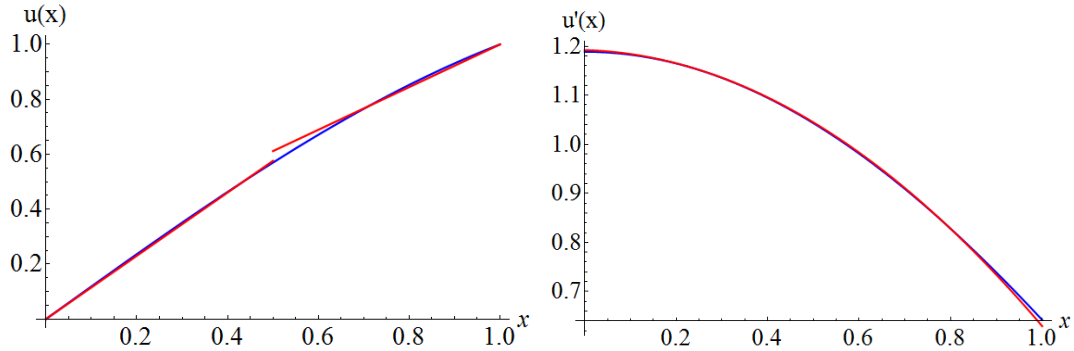

Figure 5.4: Solution function and its derivative with basis $P^{\alpha n} = \{1, (x - x^{\alpha})\}$ and $Q^{\beta n} = \{1, (x - x^{\beta}), (x - x^{\beta})^2\}$. Analytical solution is shown in blue color, while red color curve denotes the solution from higher order PDS-FEM.

	$ord(Q^{\beta})$				
		2	**3**	**4**	**5**
	2	(2,2)	(2, 3)	(2, 3)	(2, 3)
$ord(P^{\alpha})$	**3**		(3, 3)	(3, 3)	(3, 3)
	4			(4, 4)	(4, 4)

Table 5.1: Convergence rate of solution function and derivative with different combination of bases of approximation scheme. Here, $ord(P^{\alpha})$is highest order of polynomial bases for approximating the function while, $ord(Q^{\beta})$is same for derivative.

Similar numerical experiments are needed to performed to solve two-dimensional BVPs to strengthen the criterion. Numerical experiment is one way but, it is more important to identify the mathematical reasoning behind such improvement. It is essential to mention that increasing the order of basis for derivative will diminish the quality of stiffness matrix since the inertia tensor $I^{\beta mn} = \int_{\psi^{\beta}} Q^{\beta m} Q^{\beta n}\, dv$ results into non-invertible matrix. Therefore, a cautious approach shall be utilized in further investigations.

5.4 Conclusion

The approximation scheme of PDS-FEM does not possess the Kronecker delta property and, polynomial never decays at boundaries. Therefore, enforcing essential boundary condition by specifying prescribed value is not straightforward as in case of classical FEM.

There are several methods to impose essential boundary conditions available in the literature but It is difficult to implement them into current proposed scheme. In this chapter,

problems associated with enforcing the boundary conditions are discussed. Further, different techniques to address such issue is explored and investigated. It can be concluded that one order higher polynomial for derivative approximation in compare to that of function approximation is most suitable to solution found for the problem of boundary condition. Currently, this method can be classified as ad-hoc scheme to impose boundary condition. But, a robust and rigorous mathematical reasoning will provide sufficient support to make it substantial.

Non-dimensionalization of inertia tensor may improve the solution of problem. In absence of such technique it is suggested to use some pre-conditoner to enhance the stiffness matrix. However, it is not guaranteed but need exclusive investigations. It is recommended that Block-Jacobi preconditioning shall be used to improve the singular matrix.

Chapter 6

Linear elastic stress analysis of solid

In this chapter, some numerical results are presented to demonstrate the improvements in incorporating first order polynomials in PDS-FEM. Results of higher order PDS with the two different formulations presented in chapter 4 (i.e. formulation-A and B) are presented and compared with analytic solution.

Following polynomial base function sets are used for all the 2Dproblems; P^α and $\hat{P}^\beta$ for *formulation-A*, and P^α and Q^β for *formulation-B*.

$$
\begin{aligned}
P^\alpha &= \{1, (x - x^\alpha), (y - y^\alpha)\}\, \phi^\alpha(\boldsymbol{x}) \\
\hat{P}^\beta &= \left\{1, (x - x^\beta), (y - y^\beta), (x - x^\beta)^2, (y - y^\beta)^2, (x - x^\beta)(y - y^\beta)\right\} \psi^\beta(\boldsymbol{x}) \\
Q^\beta &= \left\{(x - x^\beta), (y - y^\beta), (x - x^\beta)^2, (y - y^\beta)^2, (x - x^\beta)(y - y^\beta),\right. \\
&\quad \left.(x - x^\beta)^3, (y - y^\beta)^3, (x - x^\beta)^2(y - y^\beta), (x - x^\beta)(y - y^\beta)^2\right\} \psi^\beta(\boldsymbol{x})
\end{aligned}
$$

Higher order -PDS-FEM with the above P^α and $\hat{P}^\beta$ are referred as 1st-order PDS-FEM-A, while that with P^α and Q^β are referred as 1st-order PDS-FEM-B. We used the prefix 1st-order since the highest order polynomial base included in P^α is one. *Formulation-A* with the base function sets are $P^\alpha = \{\phi^\alpha\}$ and $P^\beta = \left\{\psi^\beta\right\}$ are referred as 0th-order PDS-FEM; the original proposed by Hori *et. al.*[44]. These three formulations (0th-order and two 1st-order formulations) are compared with the aid of two benchmark problems. Specifically, the rate of convergence for displacement and stress are evaluated to demonstrate the improvements.

6.1 Infinite domain with circular cavity

A problem with weak stress singularity i.e. a standard plate of infinite extent with a circular hole subjected to far field tensile loading is considered as the 2D numerical example. Plane

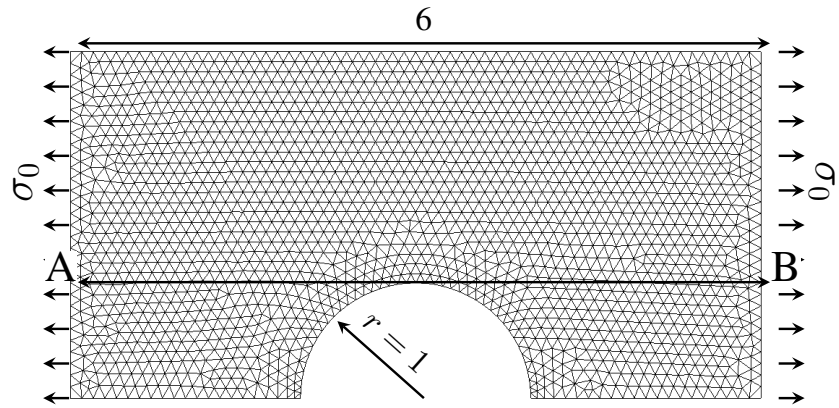

Figure 6.1: A plate with circular hole subjected to far field $\sigma_0 = 10$ MPa. Lower straight edge is subjected to symmetric boundary conditions.

stress conditions are assumed and the far field tensile stress in x-direction is assumed to be $\sigma_0 = 10$MPa. The Young's modulus and the Poison's ratio of the plate is assumed to be 1GPa and 0.33, respectively. The simulated domain shown in Fig. 6.1 has the dimension of 6m$\times$3m and the radius of the circular hole is set to 1 meter. The same figure shows a sample of the Delaunay tessellation used for approximating the derivative related fields (i.e. $\boldsymbol{\epsilon}$, $\boldsymbol{\sigma}$, etc.). Symmetric boundary conditions are set for the two straight edges at the bottom, while the displacement boundary conditions are set along the top and two vertical edges according to the analytical solution.

6.1.1 Setting boundary condition

Setting the correct boundary condition is essential in solving a boundary value problem. Different techniques to deal with problem of prescribing the essential boundary conditions are discussed in the chapter 5. In this chapter, boundary conditions are imposed in following ways

- Artificially set boundary conditions i.e. by specifying all terms of polynomial along the prescribed boundary. Hereafter, this technique will be refereed as *methodology-A*.
- Choosing one order higher polynomial for derivative approximation than that of function approximation. Hereafter, this naive technique will be referred as *methodology-B*.

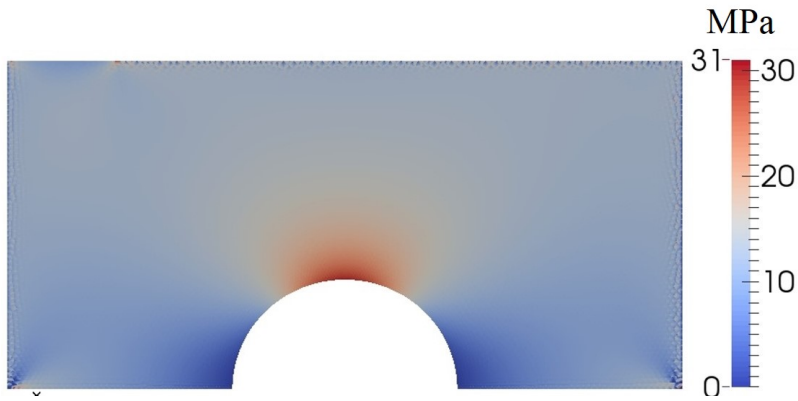

(a)

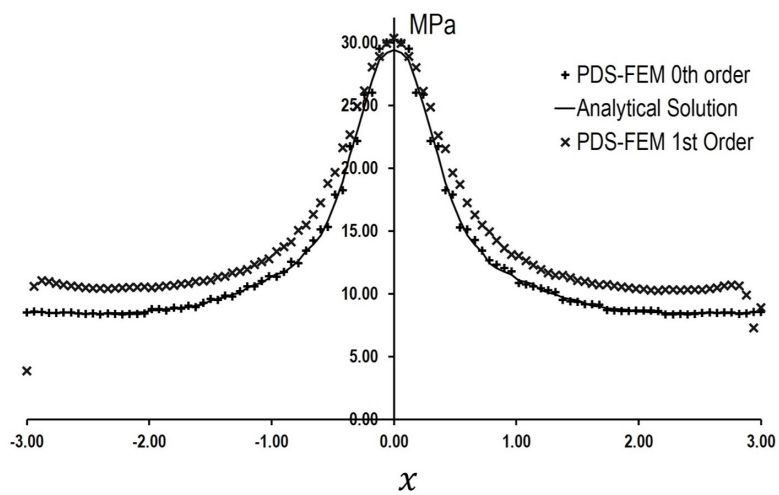

(b)

Figure 6.2: Result from PDS-FEM 1st order without any special treatment to boundary conditions (a) Stress σ_{xx} Distribution (b) Comparison of result with analytical solution along section AB

6.1.2 Results with artificially set boundary conditions

The plate with a hole problem is solved using both the 0th-order and 1st-order PDS-FEM, setting the prescribed boundary conditions. Figure 6.2a shows the results, when $u_j^{\alpha 0}$'s are specified and $u_j^{\alpha n}$'s $(n = 1, 2)$ are set to be zero. A high fluctuation along the boundaries can be easily observed. Further, procured result is plotted along the section-AB and compared with analytic solution (see in Fig. 6.2b). A significant deviation from analytic solution is noted. In order to improve the solution, boundary conditions are set with *methodology-A*. Figure 6.4(b) shows the results with boundary conditions by *methodology-A*. As it has been stated in chapter 3, the field variables are approximated as unions of local polynomial expansions. The obtained approximations are discontinuous since PDS-FEM does not enforce any conditions to smoothly connect polynomial expansions in neighboring Voronoi or Delaunay elements. These discontinuities are clearly visible in Fig. 6.3. A course mesh composed of 738 nodes and 1378 elements is used, so that the discontinuities in the approximated fields are visible. Figure 6.3(a) shows x component of displacement while 6.3(c) shows the stress component σ_{xx} , obtained with first order PDS-FEM. While the solution for displacement field consists of local patches of planes which are orderly arranged, there are discontinuities along the Voronoi boundaries. Figure 6.3(c) shows σ_{xx} estimated with the discontinuous displacement field shown in Fig. 6.3(a). As is seen, the stress field is also made of orderly arranged local patched of planes, which are discontinuous along Delaunay boundaries. Figure 6.3(b) and 6.3(d) shows the surface plot of displacement and stress with a fine mesh respectively. These figures advocate the smoothing of solution, even though no smoothing conditions are enforced along Voronoi or Delaunay boundaries.

It is of interest to examine the improvement in accuracy and smoothness of solution, which is accomplished by comparing the stress component σ_{xx} along the section A-B in Fig. 6.1. Figure 6.5 shows the analytical solutions and numerical solutions, which are calculated using 0th and 1st-order PDS-FEM formulation-A, of σ_{xx}. The comparison made in Fig. 6.5 indicates that the numerical results are in good agreement with analytical solution with artificial boundary condition, and the first order PDS-FEM has relatively smoother than zero-th order, which is clearly visible in the vicinity of the stress concentration in Fig. 6.4. A quick comparison of Fig. 6.2(b) and 6.5 indicates the significant improvement in the results along the boundary. Moreover, It is essential to investigate the *p-version* of higher order PDS-FEM. Table 5.1 is tabulated with the convergence rate value of displacement and strain with different combination of polynomial set for approximating function and the derivative.

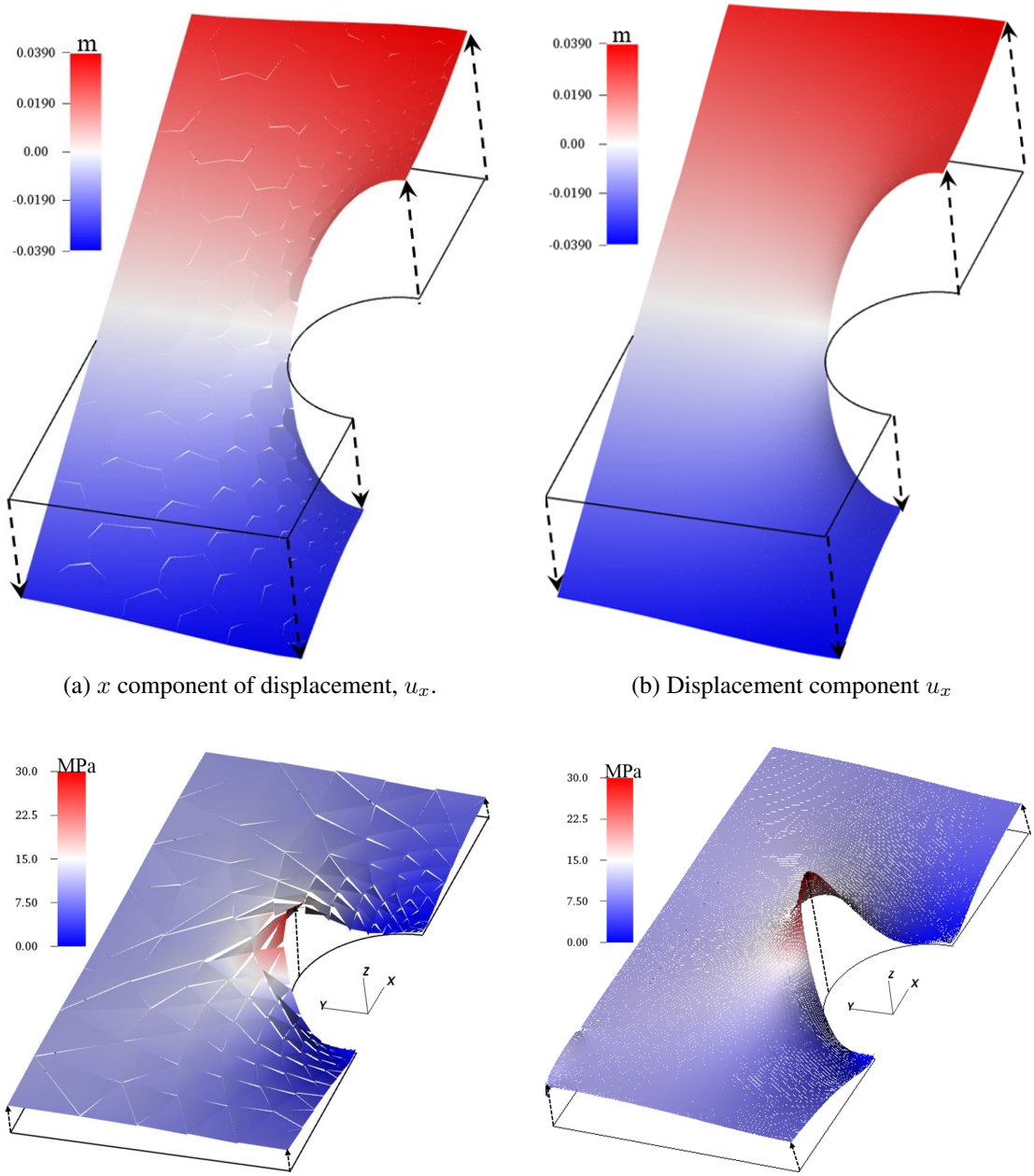

(a) x component of displacement, u_x.

(b) Displacement component u_x

(c) Stress component σ_{xx}

(d) Stress component σ_{xx}

Figure 6.3: Surface plot of displacement and stress fields obtained with first order PDS-FEM. The color indicates the scale of vertical axis.

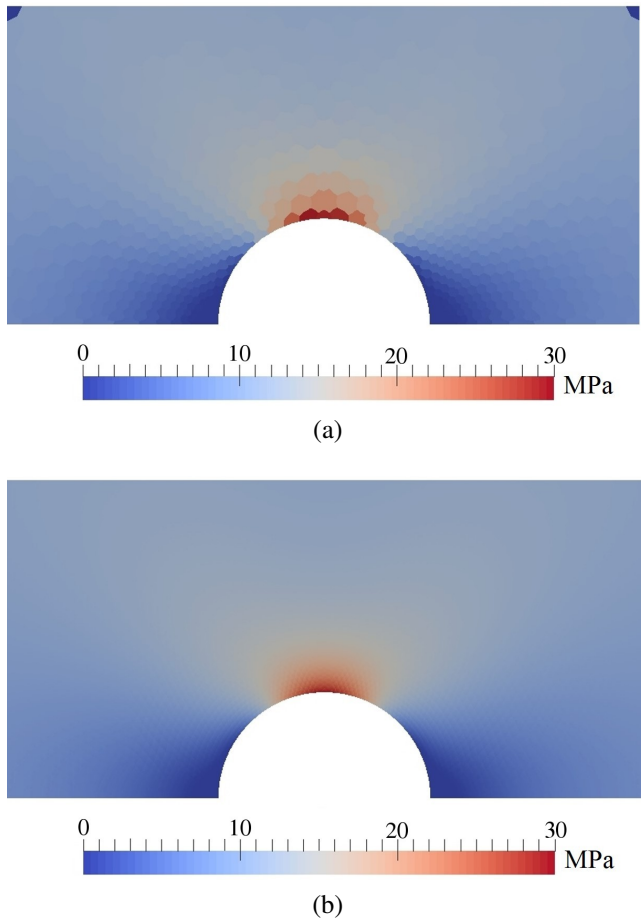

Figure 6.4: Comparison of stress in x-direction, σ_{xx} from (a) 0-th order PDS-FEM (b)1st order PDS-FEM

		$ord(Q^\beta)$			
		2	**3**	**4**	**5**
$ord(P^\alpha)$	**2**	(2,2)	(2, 3)	(2, 3)	(2, 3)
	3		(3, 3)	(3, 3)	(3, 3)
	4			(4, 4)	(4, 4)

Table 6.1: Convergence rate of solution function and derivative with different combination of bases of approximation scheme. Here, $ord(P^\alpha)$ is highest order of polynomial bases for approximating the function while, $ord(Q^\beta)$ is same for derivative.

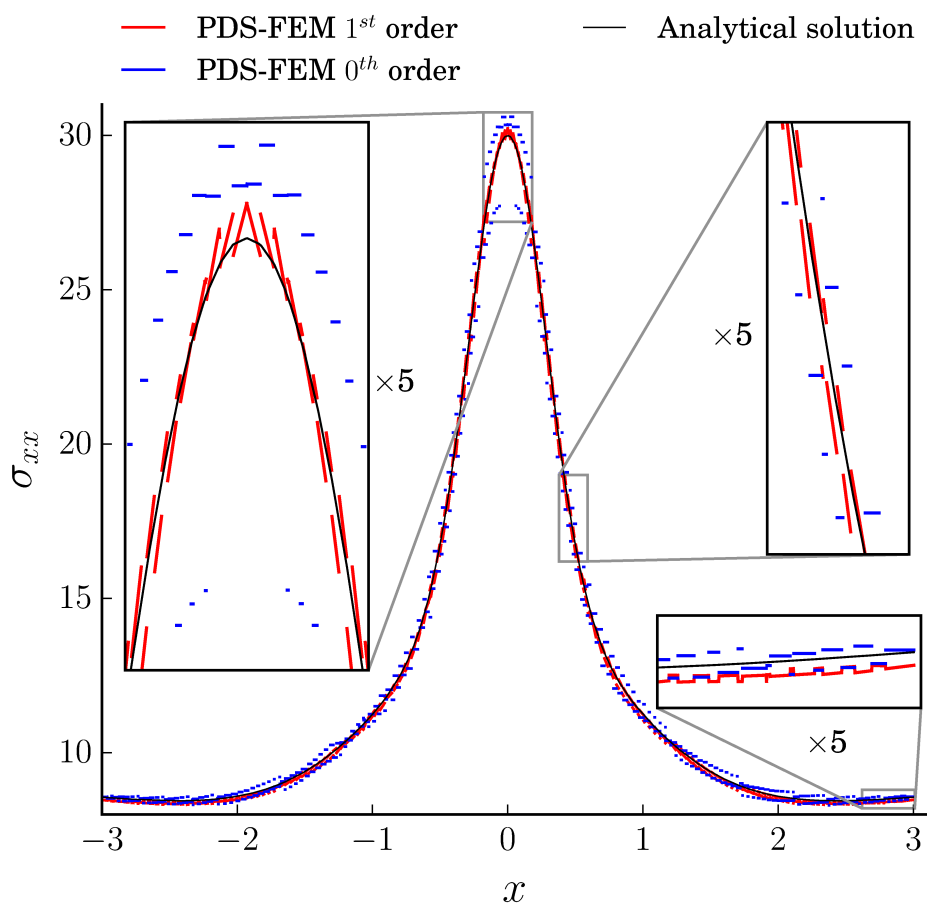

Figure 6.5: Comparison of stress, σ_{xx} with analytical solution along the width of plate (AB section)

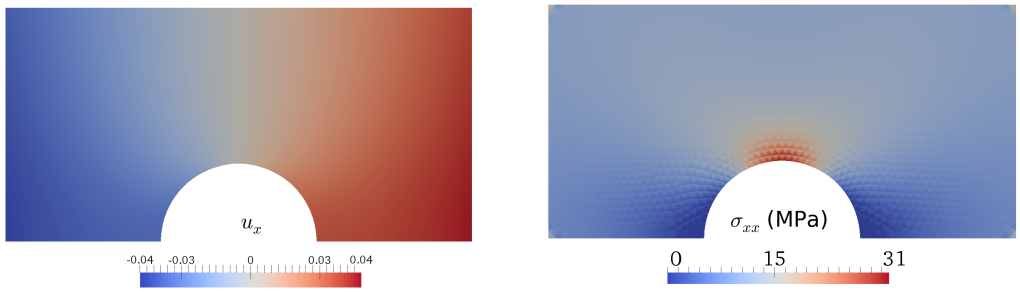

(a) u_x of curl-free 1st-order PDS-FEM (b) σ_{xx} of curl-free 1st-order PDS-FEM

Figure 6.6: Displacement and stress fields with 1st-order PDS-FEM with *formulation-B*.

6.1.3 Comparison of two formulations: weak stress concentration

Figure 6.6 shows the u_x and σ_{yy} obtained with the curl free 1st-order PDS-FEM presented in the section 3.2.1 and 3.2.2. Important thing to note is that displacement field is discontinuous along the Voronoi extremes as polynomials with local support are used in approximating. Such discontinuities are utilized in modeling the cracks and are explained in previous chapter. Presence of these discontinuities are not denied here. One may question continuity requirement of solution of continuum problems. Relation between the variables approximated over Delaunay and Voronoi tessellation, provides a continuity condition. Variable approximated over conjugate tessellation may be interpreted as bridging variable. It also justify the usage of conjugate tessellations.

The Figure 6.7 shows that the stress concentration on the circular boundary is correctly reproduced. Improvement in accuracy of solution and higher convergence rates are some salient features HO-PDS-FEM. Figure 6.8 demonstrate the difference of displacement fields, u_x and σ_{xx} obtained with the *formulation-A* and *B* of 1st-order PDS-FEM. Shown is the vicinity of the weak stress concentration on the circular boundary, where the difference is largest. As is seen, the difference both in $\boldsymbol{u}$ and σ_{xx} are negligibly small, which is of order 10^{-5}.

The negligible difference in results of *formulation-A* and *B* indicates that, curl-free implementation does not have any advantage over the *formulation-A* presented in section 3.2.1 and [48], which is not guaranteed to satisfy curl-free condition. However, the it is not surprising that *formulation-A* manages to find a solution with negligible difference from that of *formulation-B*. As shown in Fig. 3.2, solution space of *formulation-B* is a subset of that of *formulation-A* and the stationary solution found via variational approach makes both the formulations to find solutions of negligible differences.

Furthermore, convergence rate analysis is performed for *formulation-A* and *B*, setting the boundary conditions with *methodology-A* and *B*. Rate at which L^2-norm of higher order PDS-FEM vanishes is compared with 0th order PDS-FEM. Higher order PDS-FEM

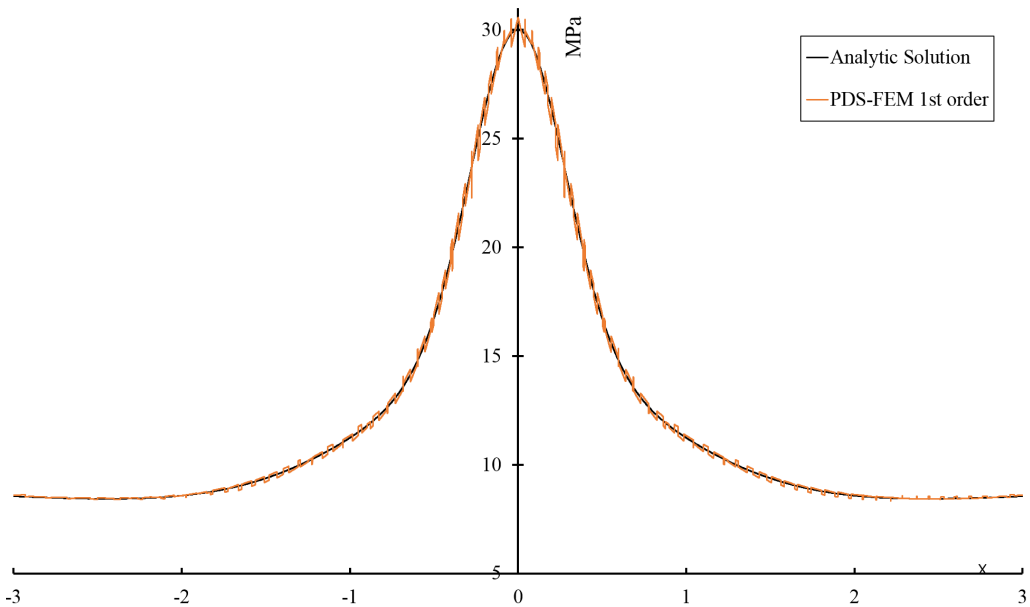

Figure 6.7: σ_{xx} obtained with curl-free HO-PDS-FEM, along the section A-B.

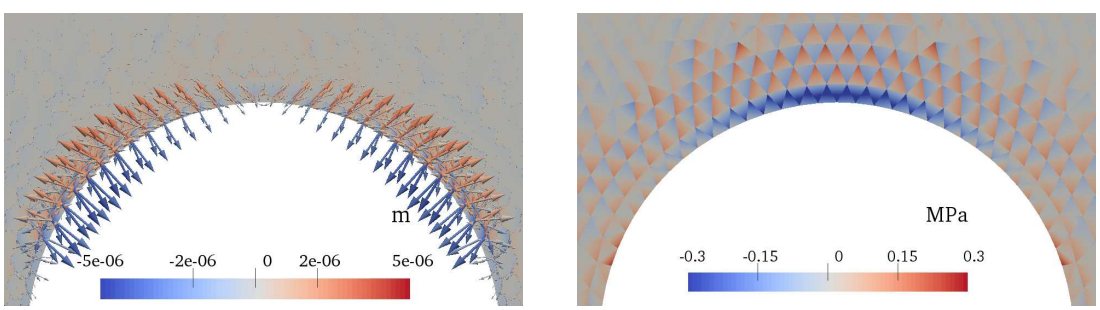

(a) $\boldsymbol{u}$ of curl-free 1st-order PDS-FEM (b) σ_{xx} of curl-free 1st-order PDS-FEM

Figure 6.8: Difference of $\boldsymbol{u}$ and σ_{xx} from 1st-order PDS-FEM *formulations A* and *B*, in the vicinity of the stress concentration.

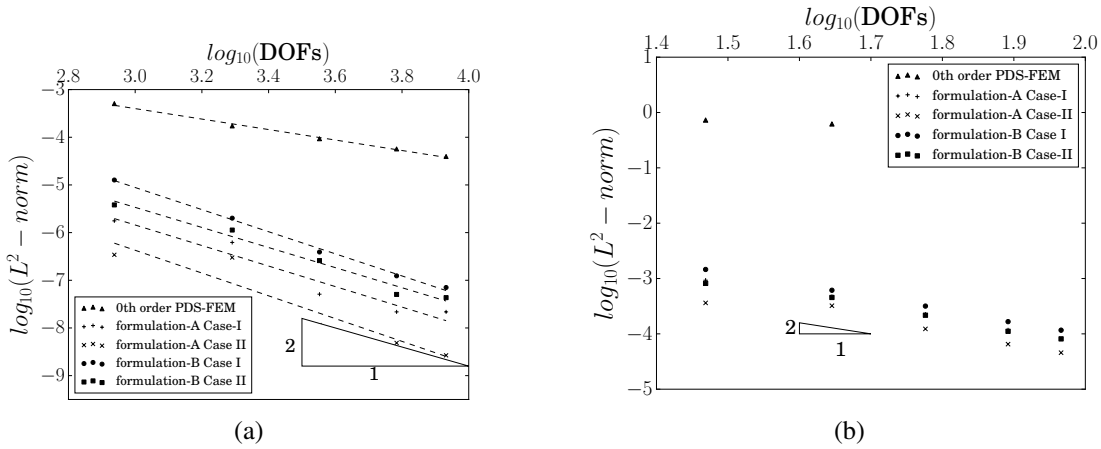

Figure 6.9: Rate of convergence (a) displacement (b) strain , setting the boundary conditions with *methodology-A and B*

inherent the properties of *p-version* convergence of numerical schemes. Increase in the rate of convergence to the solution is expected with increment in order of polynomial. Convergence rate reaches to the value of 2 with first order polynomial bases. However, order of accuracy is different for *formulation-A* and *B* by setting the boundary conditions with the help of *methodology-A* and *B* (see Fig. 6.9). Higher accuracy of solution obtained by specifying all terms of polynomials (i.e. *methodology-A*) is not surprising in both formulations, since, it is the demand of proposed numerical method. *Formulation-A* delivers slightly accurate strain field compared to curl-free formulation. It can be concluded that *formulation-A* is better in reproducing the stress singularity than *formulation-B*.

6.2 Uniformly pressured thick hollow cylinder

A thick cylinder subjected to internal and external pressure, which is a classical problem, is considered to verify the 3D implementation of formulation-A of PDS-FEM. The problem settings are illustrated in Fig. 6.10(a) and (b). The boundary conditions at the cylinder ends are set to reproduce plain strain conditions. The set of polynomial bases used are

$$
\begin{aligned}
P^{\alpha} &= \{1, (x - x^{\alpha}), (y - y^{\alpha}), (z - z^{\alpha})\} \\
Q^{\beta} &= \{1, (x - x^{\beta}), (y - y^{\beta}), (z - z^{\beta}), (x - x^{\beta})^2, (y - y^{\beta})^2, (z - z^{\beta})^2, (x - x^{\beta})(y - y^{\beta}), \\
&\quad (x - x^{\beta})(z - z^{\beta}), (y - y^{\beta})(z - z^{\beta})\}
\end{aligned}
$$

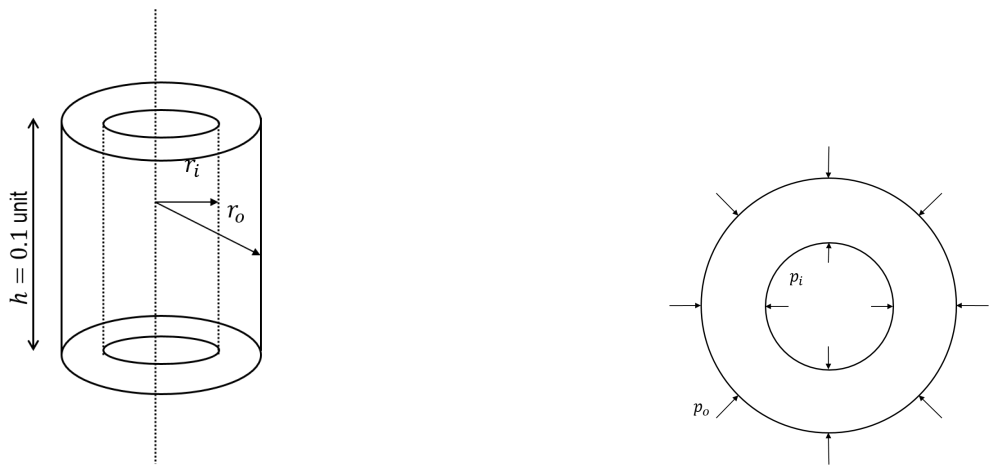

(a) (b)

Figure 6.10: Thick hollow cylinder applied with uniform internal and external pressure

6.2.1 Results and discussions

Figure 6.11 compares the analytic solutions and numerical results of radial displacement u_r and strain component ϵ_{rr}, along a radial line. A quick comparison advocates the improvement in solution with the mesh refinement, and that the numerical solutions are in good agreement with analytic solution. For this specific setting, u_r reaches its maximum at $r = 0.2$. Figure 6.12 shows the error of u_r and ϵ_{rr} at $r = 0.2$, for several tessellations with different element sizes. As is seen, the error diminishes at a second order rate with respect to the number of degrees of freedoms, which is the expected.

6.3 Conclusion

Numerical results of linear elasticity problem show that rate of convergence reaches to the value of 2 with first order of polynomial. As is demonstrated, elevating the order of polynomial bases for derivative approximation by one resolve the problem of imposing essential boundary conditions. The comparative analysis shows that *formulation-A* is superior than *formulation-B*.

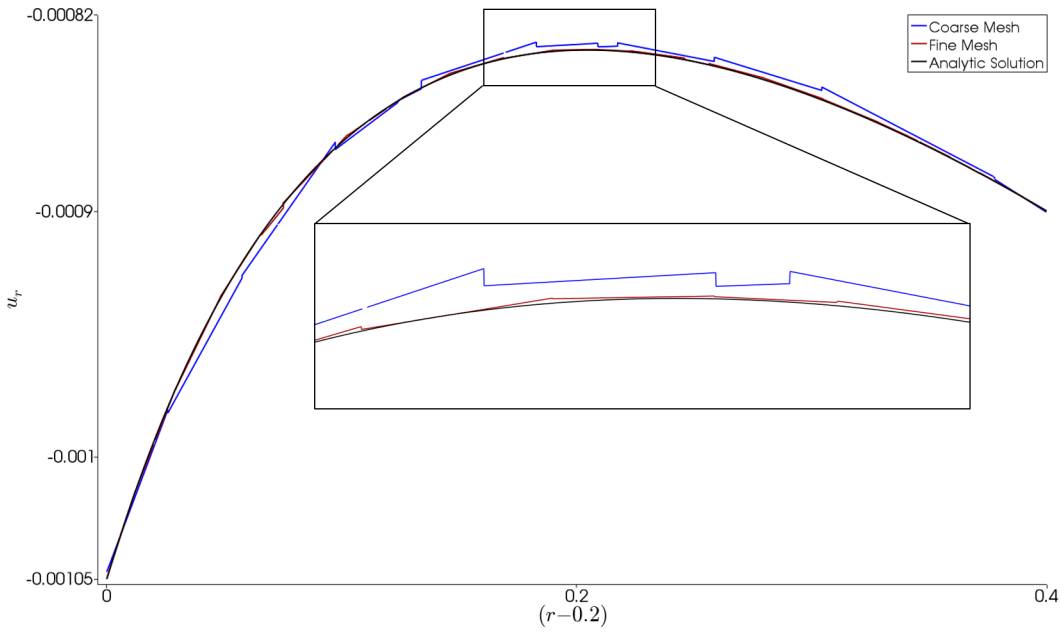

Figure 6.11: (a) Displacement, u_r in radial direction

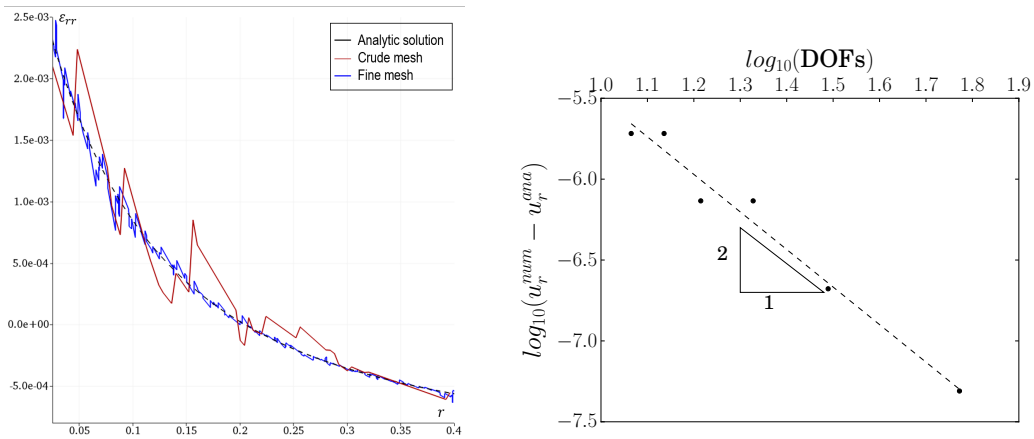

(a) (b)

Figure 6.12: (a) ϵ_{rr} (b) Convergence rate of displacement with 1st order PDS-FEM based on *formulation-A*

Chapter 7

Stress analysis of fracture mechanics

In this chapter, we present the numerical results to demonstrate the capabilities of higher order PDS implemented into FEM framework. Crack modeling techniques has been discussed in this section. Mode-I crack problem is analyzed and calculation of J-integral has been performed. Results have been discussed latter in this section. Further, the rate of convergence of displacement, strain and J-integral have been illustrated to ensure the enhancement. Further, crack with branching, arch-shaped crack (bending in crack) have been considered in chapter. Extension of current proposed work to 3-dimensional problem is also presented in this chapter.

7.1 Mode-I problem: Infinite domain with finite crack

A Mode-I center crack problem is considered to quantitatively evaluate the accuracy of cracks modeled with 0th-order PDS-FEM and the two formulations of 1st-order PDS-FEM. Specifically, the accuracy of following quantities are tested; crack tip stress singularity, traction free crack surface and J-Integral. Figure 7.1 shows the geometric configuration of the mode-I center crack considered. The boundary conditions on the circular boundary is set so as to simulate a mode-I center crack subjected to far field stress $\sigma_{yy} = 10$ MPa. Plane stress conditions are assumed with Young's modulus of 1GPa and the Poisson's ratio of 0.33, respectively.

7.2 shows σ_{yy} in the vicinity of the crack tip. As seen in Fig. 7.2 (a) and (b), both the *formulations-A* and *B* produces large negative stress, instead of the large tensile stress, in the crack tip elements (i.e. the element with the crack tip). Only the 0th order PDS produces a large tensile stress; the accuracy of 0th-order PDS in modeling crack tip singularity is discussed in [45]. Detailed analysis indicates that this error is localized to the crack tip neighborhood. Further, Fig. 7.3 also confirms this localization of the error. Stress components are found to be converging to the exact solution at the expected rate close to 2, at

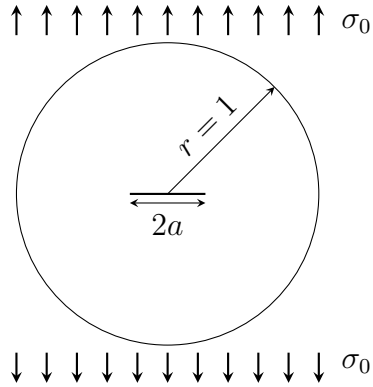

Figure 7.1: Setting of the mode-I problem. $a = 0.25$

points far from the crack tip (see Fig.7.4). whereas points in the vicinity of crack-tip have marginal deviation from analytic value.

It is not surprising that both the 1st-order formulations fail to reproduce the crack tip singularity, which is of the form $1/\sqrt{r}\cos\theta/2$. This singular field cannot be accurately approximated with polynomial bases which has their point of inflections located at the crack tip. Probably, the best approach would be to include the analytic solutions of $\boldsymbol{u}$ and $\boldsymbol{\sigma}$ as base functions for the tessellations in the neighborhood of the crack-tips.

It is of interest to investigate the effect of locating the point of inflections, $\boldsymbol{x}^{\beta_c}$, of base polynomial set P^{β_c}, where Ψ^{β_c} is the Delaunay element containing the crack-tip. As mentioned in the section 2, mother points (i.e. center of area $\boldsymbol{x}^g$) of Ψ^β's are used as $\boldsymbol{x}^\beta$ in P^β. Having the point of inflections of the polynomial bases within Ψ^{β_c} may have negative effects in approximating singular stress field. To investigate the effect of setting $\boldsymbol{x}^\beta$ of the crack tip element to be outside of Ψ^{β_c}, a set of simulations are conducted with setting $\boldsymbol{x}^{\beta_c} = \bar{\boldsymbol{x}}$, where $\bar{\boldsymbol{x}}$ is the mid of broken edge as shown in Fig. 7.5.

As seen in Fig. 7.6, when $\boldsymbol{x}^{\beta_c} = \bar{\boldsymbol{x}}$, brings a significant improvements. σ_{yy} of the crack tip element is restored to the expected high tensile range, in the case of both *formulation-A* and *B*. However, *formulation-A* outperform B, by producing smaller negative stress in the adjacent elements and producing near zero σ_{yy} along the crack surface (see Fig. 7.7). The same figure shows that the *formulation-B* produces higher negative stress in adjacent element of Ψ^{β_c} and σ_{yy} along the crack surface oscillates in a large range. One negative effect of setting $\boldsymbol{x}^{\beta_c} = \bar{\boldsymbol{x}}$ is the moving of crack tip singularity to $\bar{\boldsymbol{x}}$, from $\boldsymbol{x}^g$ which is its correct location. While this preliminary investigation indicates that crack tip solution can be improved by choosing a proper base polynomial set. Selection of a suitable base functions and choosing appropriate $\boldsymbol{x}^\beta$ for the crack tip element has to be further investigated. Especially, a mathematical proof should be sought.

In order to quantitatively estimate the accuracy of the crack tip singularity with $\boldsymbol{x}^{\beta_c} = \bar{\boldsymbol{x}}$, J-integral is calculated along several paths enclosing the right side crack tip, for many

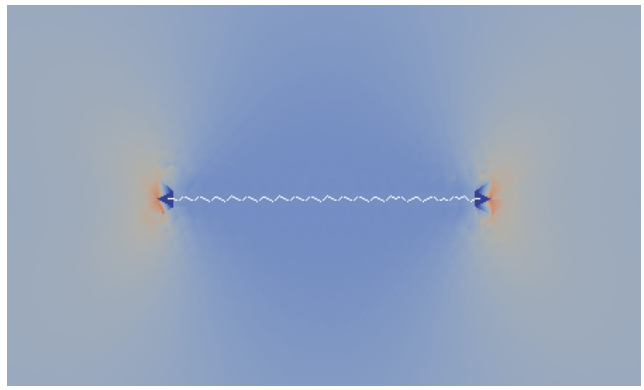

(a) 1st-order formulation-A

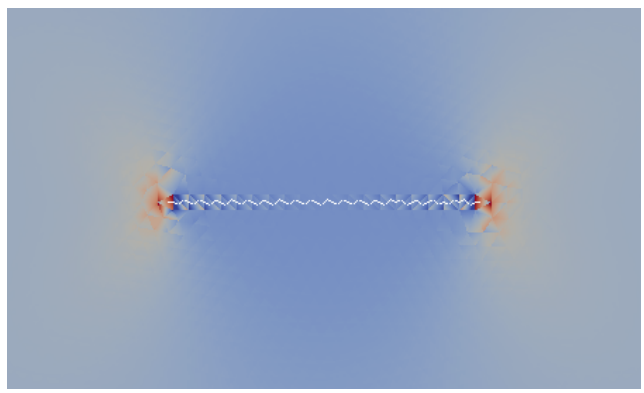

(b) 1st-order formulation-B

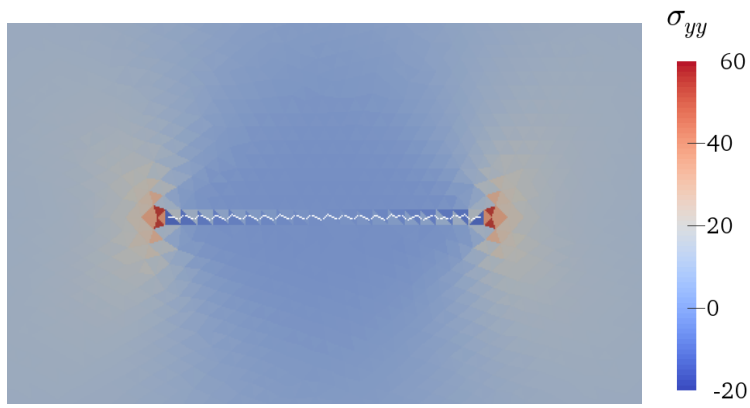

(c) 1st-order formulation-B

Figure 7.2: Distribution of σ_{yy} in the vicinity of the crack tip at the right end. Note that blue color indicates compression.

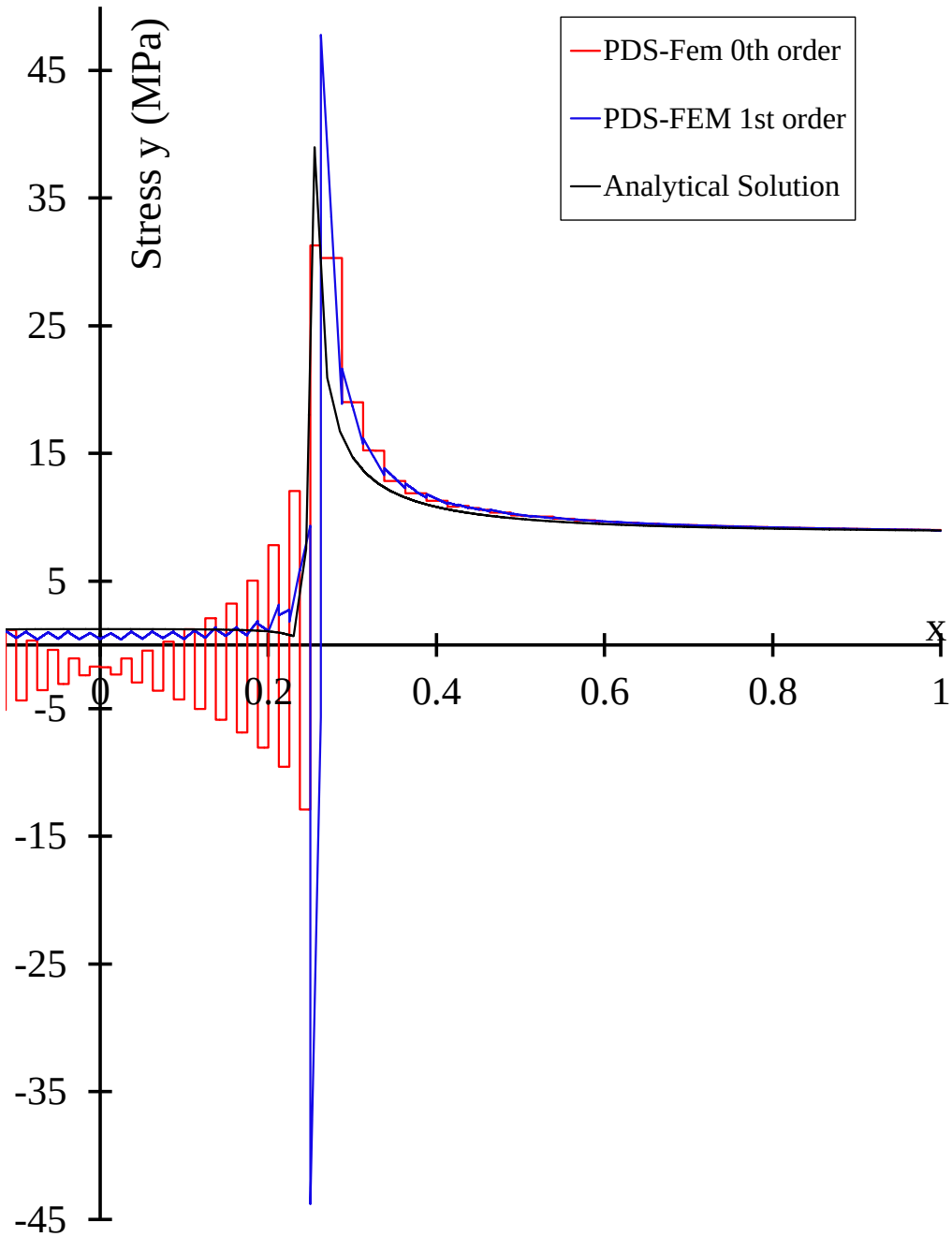

Figure 7.3: σ_{yy} along a section passing through the upper crack surface, in the right half of the crack.

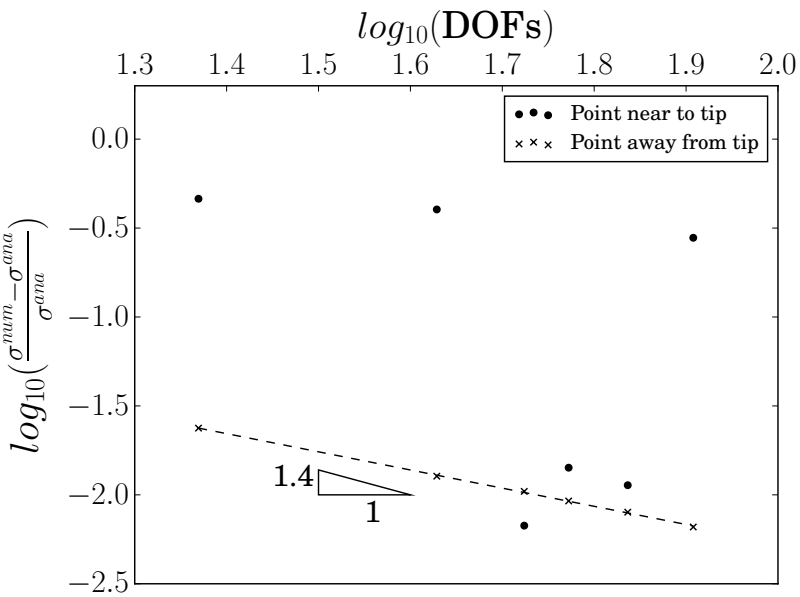

Figure 7.4: Point-wise convergence of stress σ_{yy} for mode-I crack problem

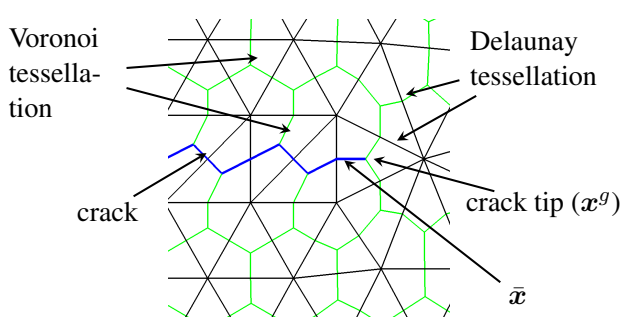

Figure 7.5: Crack tip element

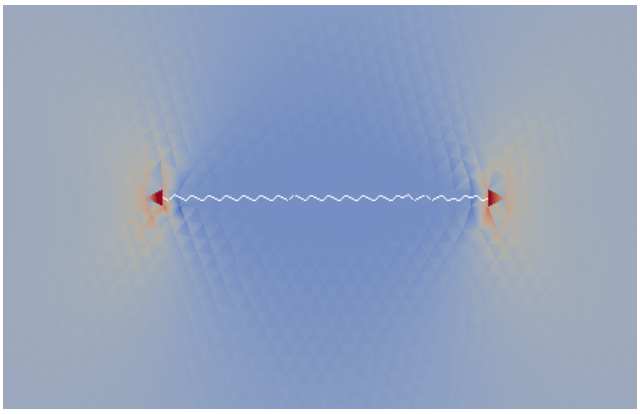

(a) 1st-order formulation-A

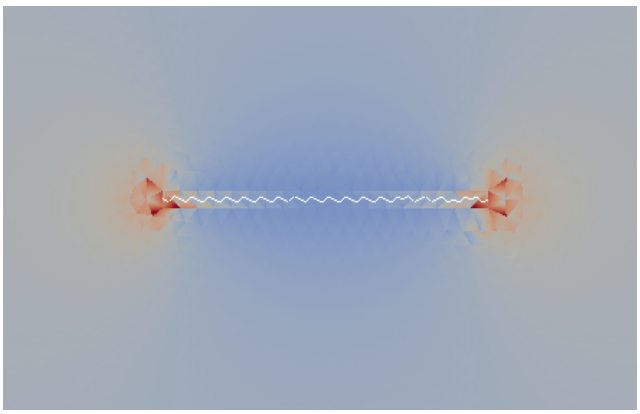

(b) 1st-order formulation-B

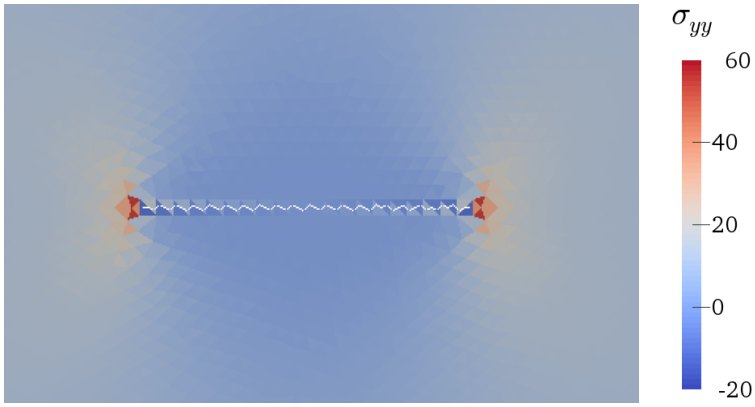

(c) 1st-order formulation-B

Figure 7.6: Distribution of σ_{yy} in the vicinity of the crack tip at the right end. blue color indicates compression.

Delaunay tessellations. Figure 7.8 shows the error of J-integral versus DOFs. As is seen, both *formulation-A* and *B* produces second order convergence for J-integral. However, the accuracy of the J-integral is still lower than the expected probably due to the shifting of the singularity from $\boldsymbol{x}^g$ to $\bar{\boldsymbol{x}}$.

One of the problem observed in 0th-order PDS-FEM is that crack surfaces have non-negligibly large traction normal to the crack surfaces. Figure 7.7 shows that 1st-order *formulation-A* rectify this problem producing negligibly small traction normal to the crack surfaces. This is clearly visible even in Fig. 7.2. Comparison of 7.7 (a) and (c) shows that σ_{yy} of 1st-order *formulation-B* is as bad as that of 0th-order PDS-FEM. However, *formulation-A* based 1st order PDS-FEM still does not reproduce very accurate result in the vicinity of crack-tip. It is interesting to find out if this minor non-performance has anything to do with curl-free requirement. Hence curl free formulation is proposed. Obtained results do not direct in expected direction. These observation leads to the conclusion that *formulation-A* is superior to *formulation-B*; A is better in both modeling singular stress filed at the crack tip and modeling traction free crack surfaces.

7.2 Branched crack problem

It is of interest to investigate and explore the capabilities of present methodology to simulate complex fracture problems such as branching. A finite domain of size 5×10 unit with static branched crack is considered as analysis domain . Crack surfaces are inclined with each other at the angle of $120°$. Bottom edge of rectangular plate is fixed, while a constant displacement, $u_y = 0.1$ unit is applied at the top edge. Material properties such as Young's modulus and Poison's ratio are assumed to be 1000 unit and 0.33, respectively. Problem setting for branched crack are shown in Fig. 7.9.

Numerical example is solved with 0th order PDS-FEM, *formulation-A* and *formulation-B*. Results from these numerical schemes are compared to comment on suitability different approaches to extend 0th order PDS-FEM. Figure 7.10 shows the stress, σ_{yy} calculated using different formulation of PDS-FEM. Tip stress is well reported with HO-PDS-FEM as current methodology inherent *p*-version properties like any other numerical scheme. The difference between the results of 0th order and 1st order are significant, while difference between *formulation-A* and curl free implementation is insignificant in the areas away from tip. A precise observation of difference is needed to draw some conclusion. Hence, stress variation along the crack line is plotted in Fig. 7.11. Ideally, crack surface is traction free surface and same shall be reproducible. 0th order PDS-FEM and curl free implementation do not reproduce the traction free surface. Moreover, stress distribution is oscillating in nature. While, *formulation-A* imitate nearly zero stress along the crack, which is a significant improvement over *formulation-B*. Before reaching to any concrete verdict on acceptability of two possible ways to extend the 0th order PDS, several other numerical examples are

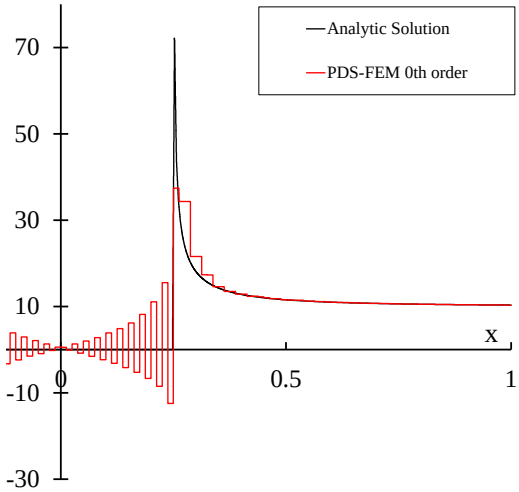

(a) 0th-order PDS-FEM

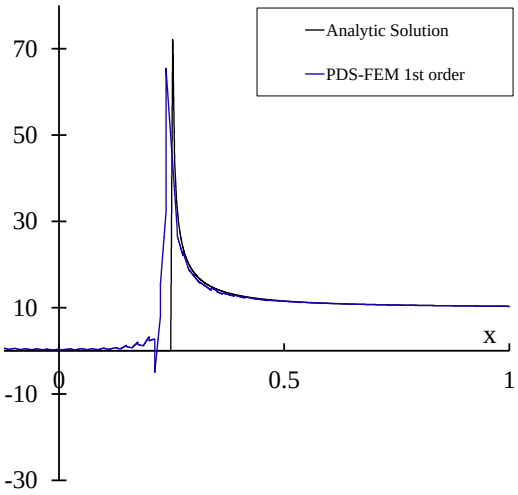

(b) Higher order formulation-A

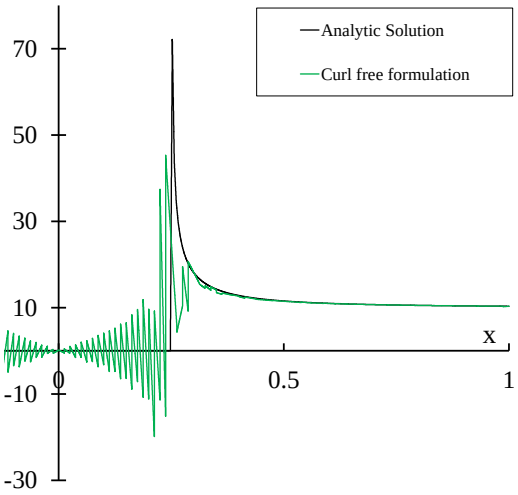

(c) Higher order formulation-B

Figure 7.7: Comaprison of σ_{yy} of analytic and PDS-FEM solutions, along right half of the crack length.

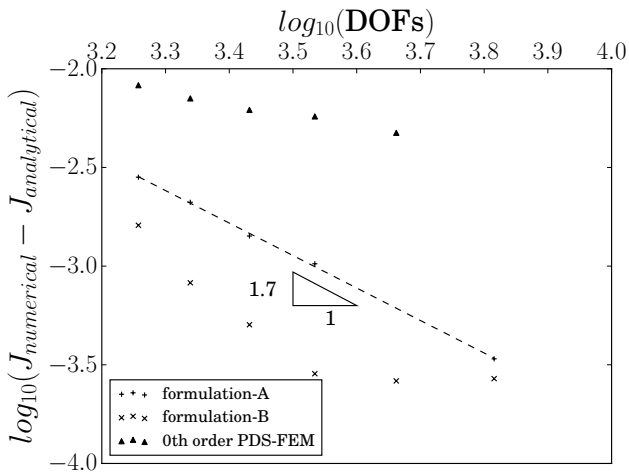

Figure 7.8: Convergence rates of J-integral for the mode-I crack problem.

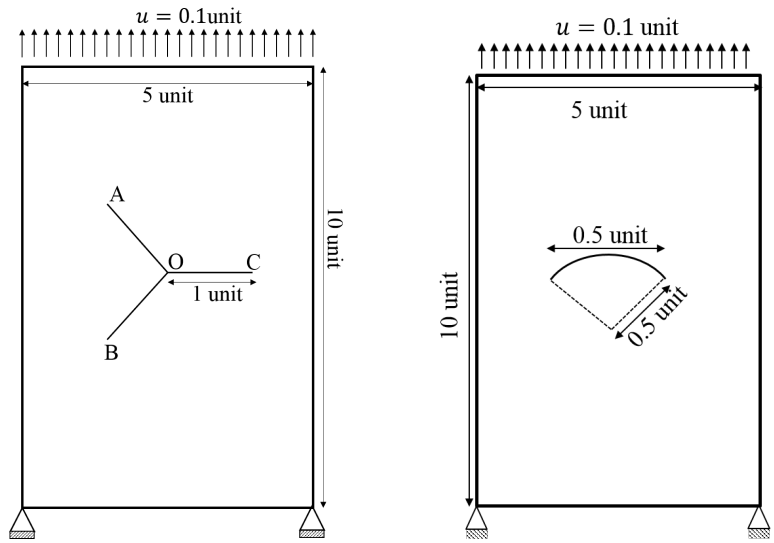

(a) Crack problem with branching (b) Crack problem with bending

Figure 7.9: Crack problems: A plate with dimensions 5×10 unit, fixed at bottom end and applied displacement at top edge

suggested to be solved and is work in progress. However, at this end, It can be stressed that *formulation-A* is superior to *formulation-B*.

7.3 Arch shape crack

Further, an arch shape crack in finite domain is considered to illustrate the capacity of higher order PDS-FEM to incorporate the bending of cracks. A finite domain of 2×2 unit with arch shape static crack is assumed as a numerical example. Bottom edge of plate is fixed and a constant displacement $u_y = 0.1$ unit is applied at the top edge. Vertical edges are modeled as free edges. Young's modulus and Poison's ratio are assumed to be 1000 unit and 0.33, respectively (see in Fig. 7.9(b)).

Presented numerical results are procured by solving the bending crack problem with 0th order PDS-FEM and 1st order PDS-FEM based on *formulation-A*. Stress analysis of solid suggests that curl *formulation-B* has lower accuracy than that of *formulation-A*. Moreover, *formulation-B* fails in reproducing the traction free surface along the cracked domain. Therefore, analysis with curl free higher order PDS-FEM i.e. *formulation-B* is aborted as it has no additional contribution in elevating the accuracy of results.

Figure 7.12 shows the stress, σ_{yy} obtained by solving the numerical example with 0th and 1st order PDS-FEM. Stress concentration ahead of crack-tip is well reproduced with both order of PDS-FEM. Results of 1st order are more accurate than that of 0th order, which is a natural phenomena. Further, traction along the cracked domain is calculated and illustrated in fig Reference. It can be easily seen that 1st order is capable of reproducing the traction free surface while former (0th order-PDS-FEM) fails to do so (see in Fig. 7.13).

7.4 Penny shaped crack in 3D

A rectangular prism of dimensions $4 \times 1.5 \times 1.5$m with a penny shape crack, is analyzed to verify the crack treatment in 3-dimension (see in Fig.7.14). The radius of penny shape crack is $2r = 0.25$m. Material properties such as Young's modulus and poison's ratio are set to the value of 1000 MPa and 0.25, respectively. A far field σ_0 of 10 MPa is applied at top end, while bottom end is fixed in vertical direction ($u_z = 0$). Delaunay tetrahedrons of given domain are generated and then domain is simulated with 0th order and 1st order of PDS-FEM. Stress σ_{zz}distribution plotted in Fig. 7.15. A smoother and more accurate stress concentration is obtained with 1st-order PDS-FEM in comparison of 0th-order PDS-FEM.

Reproducing nearly zero traction over the crack surface, is a major proposition of currently developed numerical method. Traction along and normal to the crack surface has

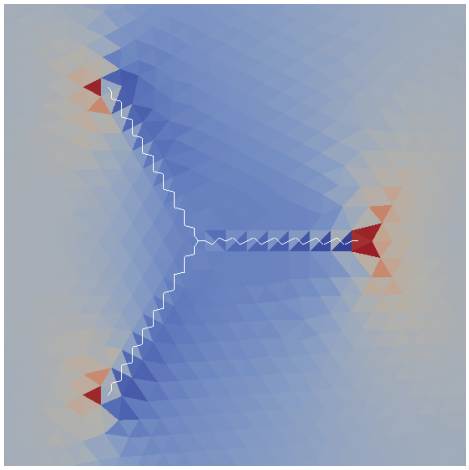

(a) 0th-order PDS-FEM

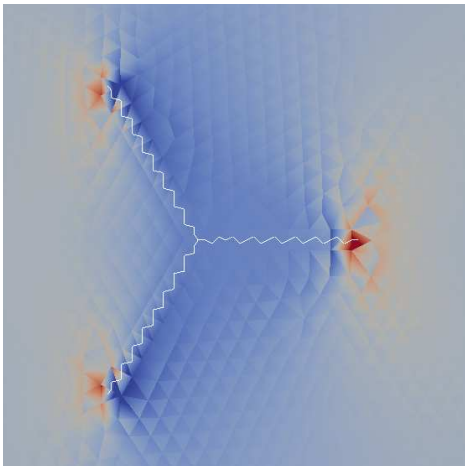

(b) 1st order PDS-FEM with formulation-A

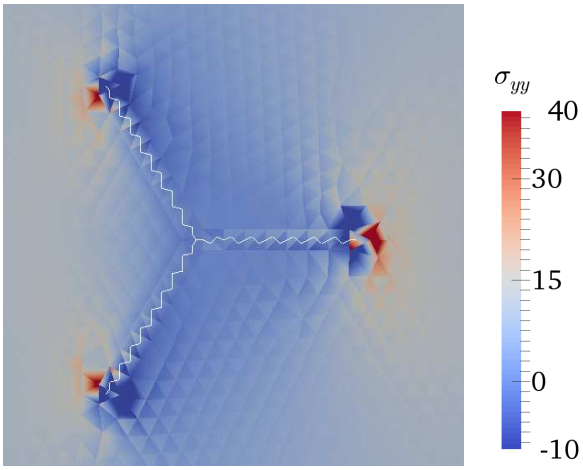

(c) 1st order PDS-FEM with formulation-B

Figure 7.10: Distribution of σ_{yy} in the vicinity of crack surfaces. 1st-order PDS-FEM with formulation-A perform better in modeling traction free crack surfaces.

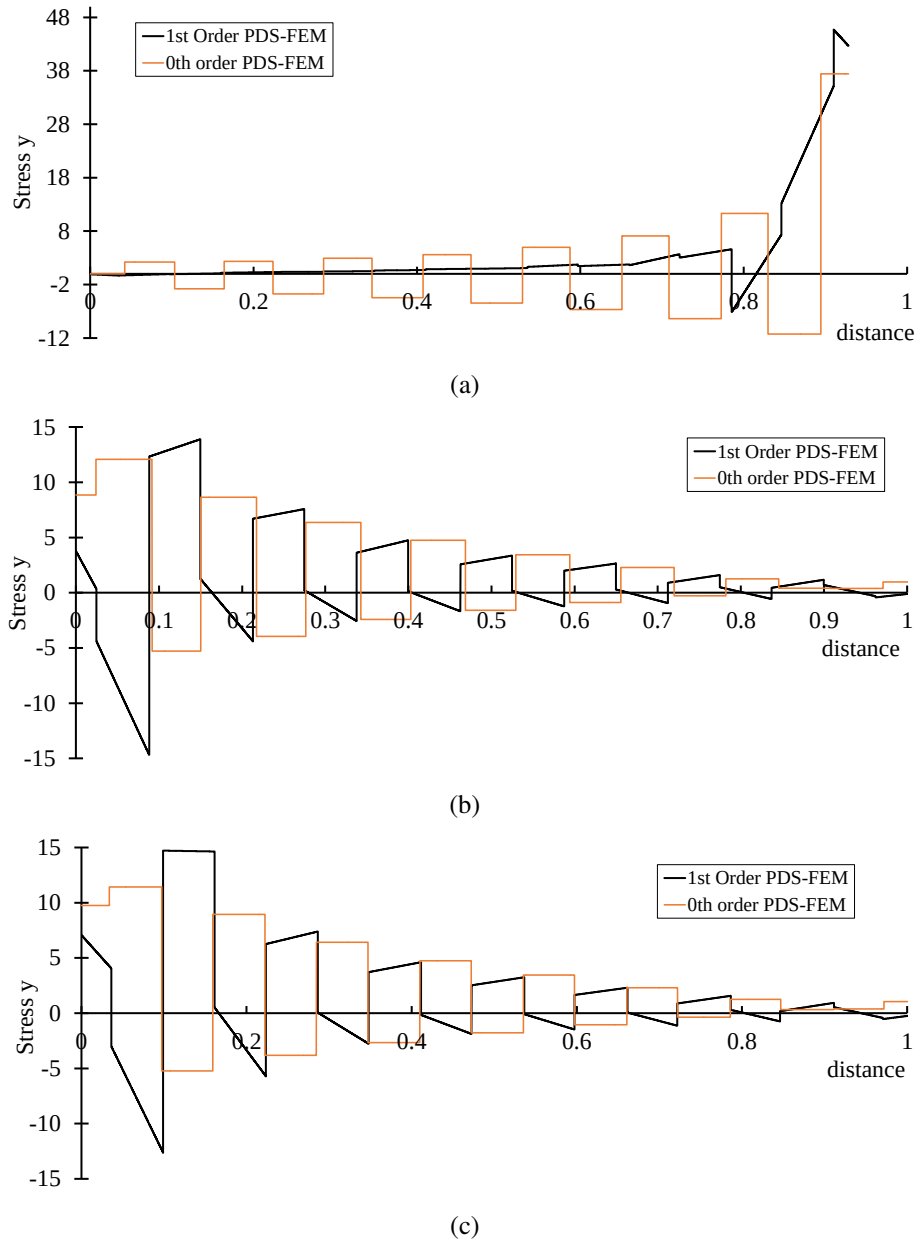

Figure 7.11: Comparison of stress obtained from 0th order PDS-FEM and 1st order PDS-FEM along OC

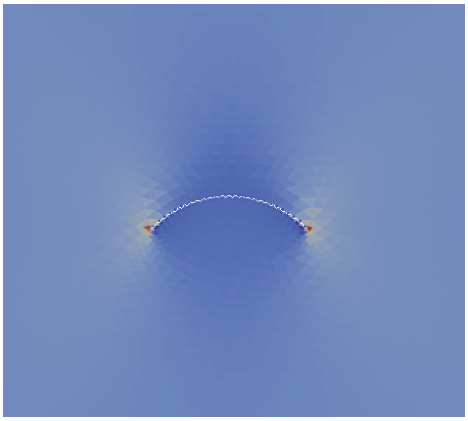

(a) 0th-order PDS-FEM

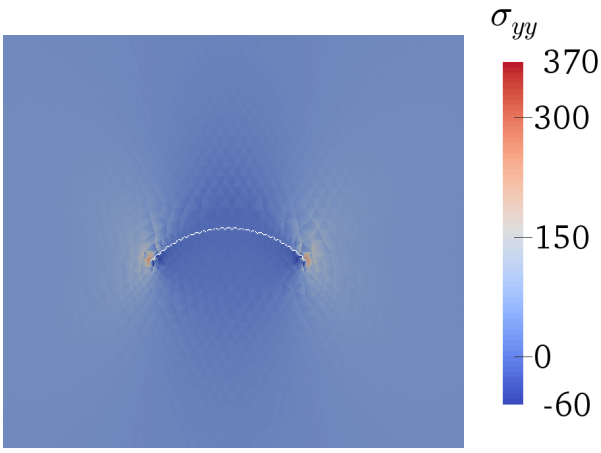

(b) 1st order PDS-FEM with formulation-A

Figure 7.12: Distribution of σ_{yy} in the vicinity of crack surfaces. 1st-order PDS-FEM with formulation-A perform better in modeling traction free crack surfaces.

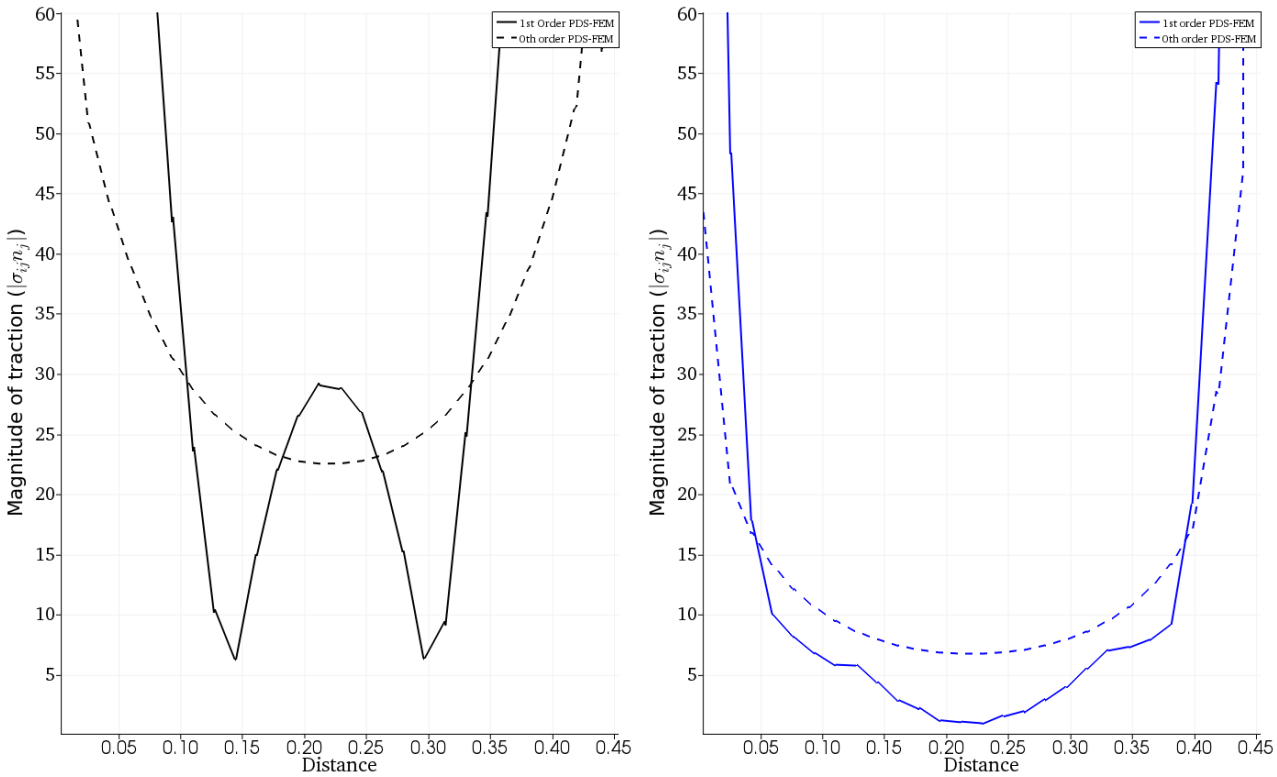

Figure 7.13: Comparison of calculated traction (a) Along the crack surface (b) Normal to the crack surface

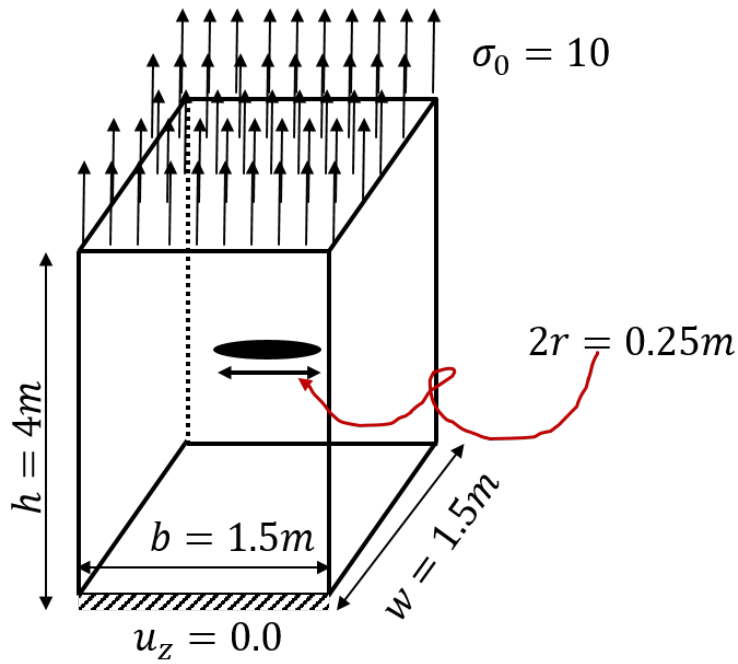

Figure 7.14: A penny shape crack problem

been calculated and results are presented here as vectors and streamlines. The normal component of traction is almost zero over complete crack-surface. Streamlines also don't penetrate the crack-surface. Rather, these streamlines diverge towards the stress concentration locations, which is very close to analytic pattern, as it can be seen in Fig. 7.16.

Traction component along the crack surface is oriented in the tangential direction of crack surface. Streamlines of tangential components are tangential to the cracking surface. These streamlines also get diverged towards the locations, where stress concentration is expected (See in Fig. 7.17).

7.5 Conclusion

While crack-tip singularity has higher accuracy, higher order PDS-FEM demonstrates the notable improvement in duplicating traction free crack surface, compared to the 0th-order PDS-FEM. Convergence analysis advocates that error in J-integral vanishes at the rate of $p + 1$ with pth order polynomial bases for function and $p + 1$th order polynomial bases for derivatives.

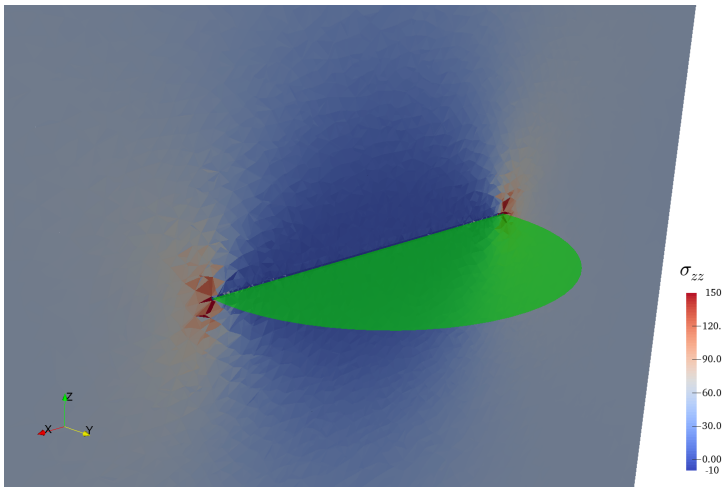

(a) 0th order PDS-FEM

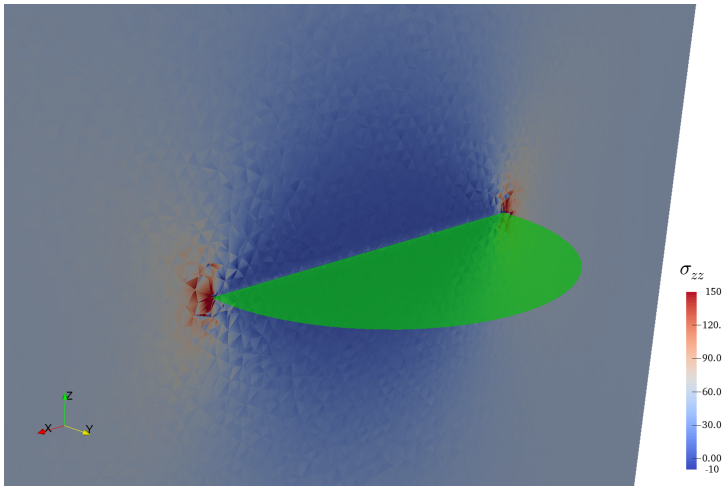

(b) 1st order PDS-FEM

Figure 7.15: Stress σ_{zz} distribution obtained with 0th and 1st order PDS-FEM.

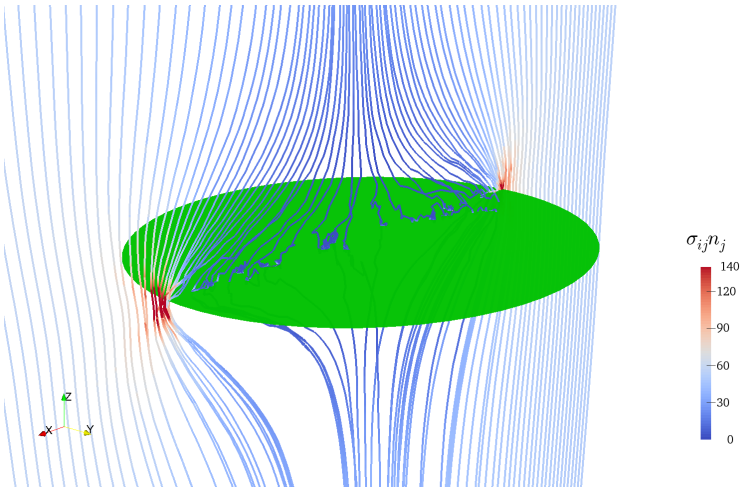

(a) Streamlines

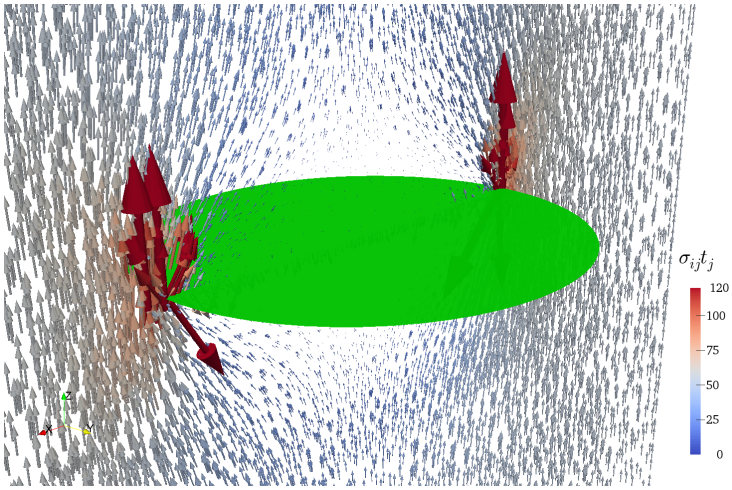

(b) Vector

Figure 7.16: Traction normal to the crack surface

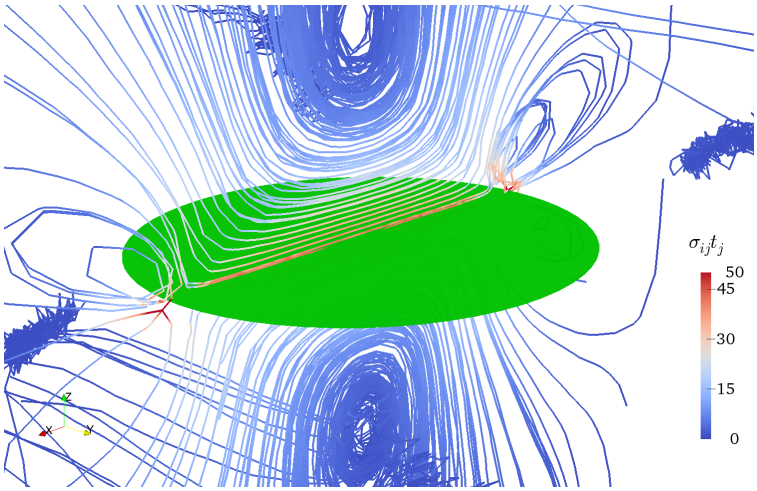

(a) Streamlines

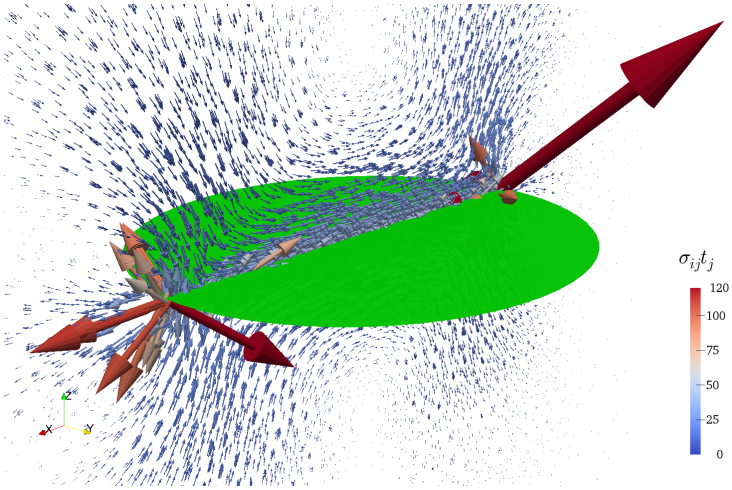

(b) Vector

Figure 7.17: Traction along the crack surface

Chapter 8

Concluding Remarks

8.1 Summary and conclusion

In this research, development of higher order Particle Discretization Scheme (PDS) by making use of localized polynomial expansions in naive sense, is presented. PDS, which approximate function and its derivatives utilizing conjugate domain tessellations, Voronoi and Delaunay, is extended by approximating the respective fields within each tessellation element with local polynomial expansion. Strictly speaking, the respective fields within each tessellation elements can be approximated with any suitable function expansion, though we use polynomial expansion in this work. The extended higher order PDS is implemented in FEM framework (PDS-FEM) to analyze boundary value problem, and further extended to simulate the cracking phenomena.

Two candidate extensions for higher order PDS are considered: *formulation-A* whose derivative approximation does not strictly satisfy the curl free condition; *formulation-B* whose derivative approximation does strictly satisfy the curl free condition. According to the benchmark tests, both the formulations perform almost equally in approximating functions and their derivatives; formulation-B perform slightly better in approximating derivatives. Both the formulations produced $(p+1)^{th}$-order rate of convergence for both function and its derivative, when p-th order polynomial bases are used for approximating both functions and derivatives.

Both these higher order extensions are implemented in FEM framework, verified using standard benchmark problems, and compared based on accuracy and convergence rates. Verification tests are conducted both in 2D and 3D: 2D test based on the standard plate with a circular hole problem, which has a weak stress singularity; 3D test based on hollow uniformly pressurized cylinder problem. Several methods are explored to deal with the problem of specifying coefficients related to higher order polynomial bases along boundaries parallel to coordinate axes, which arises in specifying essential boundary conditions.

It is found that the ad-hoc treatment of using a one order higher polynomial base set for approximating derivatives, compared to that for approximating function, solves this problem of specifying boundary conditions to certain extent. The results of benchmark test shows a significant improvement both in accuracy and convergence rate, compared to the 0th-order PDS-FEM. Both the formulations produced $(p+1)^{th}$ order of accuracy for displacement field, when using p^{th} and $(p+1)^{th}$ order polynomial bases for approximating functions and derivatives, respectively. While both the formulations produced same convergence rates, the formulation-A produced slightly higher accuracy.

One strong point of original PDS-FEM proposed by Hori *et. al.* is its simple and numerically efficient treatment for modeling cracks. It is shown that even the proposed higher order extensions of PDS-FEM can offer simple and numerically efficient crack treatment. The proposed crack treatment involves judicious selection of point of inflection to improve the crack tip stress field, and further research has to be conducted to find better crack treatment. However, the verification tests conducted with standard mode-I crack problem indicates even the present crack treatment has higher accuracy and convergence rate of J-integral, compared to those of 0th-order PDS-FEM. The comparisons shows that the formulation-A is superior in modeling cracks; formulation-A has higher and sustained convergence rate of J-integral. Further, crack surfaces produced by formulation-A are nearly traction free, while those with both formulation-B and 0th-order PDS-FEM have notable surface traction. Formulation-A is chosen as the higher order PDS-FEM, since it produces superior results in modeling cracks, which is the primary objective of PDS-FEM. When it comes to crack modeling, improved accuracy in crack tip stress field and surface traction are the main improvement in higher order PDS-FEM compared to 0th-order.

8.2 Future work

Though the developed numerical tool demonstrates the notable advancement and improvement in comparison to the 0th order PDS-FEM in modeling cracks, further efforts are required to bring it to a mature state for applications. Since, accuracy and acceptability of numerical results are largely defined by incorporating each and every minor details of problem. So the major future task, which shall be appended with immediate effect in near future, are mentioned in next few paragraphs.

Higher order PDS-FEM encounters difficulties in enforcing the essential boundary conditions and various ad-hoc techniques are implemented and examined. Though, applicability and accuracy are demonstrated with help of some numerical experiments, It demands for mathematical explanation; The rigorous mathematics, which support the proposed ad-hoc technique. Moreover, discovering a trivial and illustrative technique to apply essential boundary conditions could be another appealing research interest.

Reproducing the stress state in the vicinity of crack-tip is paramount aim of current research and it has been accomplished by judicial selection of inflection point for element, encapsulating the crack-tip. However, selection criterion to identify an appropriate inflection point is needed to be defined. Author is seeking to define a mathematical constrain, which allow to determine to suitable inflection point.

Furthermore, each and every boundary value problem request for appropriate set of basis function and therefore, it is important to use most suitable basis function, which satisfy that particular governing equation. Since, currently developed software is capable to include any set of functions as bases, author is keen to explore and extend the current scheme to use analytic stress functions in set of bases along with polynomials. Modeling strong discontinuities with such special set of basis would be an ideal problem to analyze.

The current work is limited to analysis of opening mode cracks. However, different crack configurations such as bending and branching are considered and illustrated. Though all of them depicts the remarkable improvement over the 0th order PDS-FEM. More numerical experiments are essentials to further explore and examine the performance of proposed scheme in the application to complex and large scale problems under static and dynamic loading conditions. Meanwhile, for the goal to efficiently model propagating crack in 3-dimensional domain, more efforts are still needed to amplify the performance of newly proposed numerical tool.

Appendix A

Explicit expressions

A.1 Strain displacement relations *(formulation-A)*

Matrix form of strain-displacement relationship; $\boldsymbol{\epsilon}^* = \boldsymbol{B}\boldsymbol{u}^*$ is procured by calculating the first variation of Lagrange with respect to the stress coefficients and setting it to zero.

$$
\begin{aligned}
\delta\mathcal{L}(\sigma_{ij}^{\beta m}) &= \sum_{\beta}^{N^\beta} \int_{\Psi^\beta} Q^{\beta m} \left(\epsilon_{ij}^{\beta n} Q^{\beta n} - u_i^{\alpha n'} \left(P^{\alpha n'} \right)_{,j} \right) \, dv = 0 \\
0 &= \sum_{\beta}^{N^\beta} \left(\sum_{n}^{|Q^\beta|} \epsilon_{ij}^{\beta n} \int_{\Psi^\beta} Q^{\beta m} Q^{\beta n} \, dv - \sum_{\alpha} \sum_{n'}^{|P^\alpha|} u_i^{\alpha n'} \int_{\Psi^\beta} Q^{\beta m} \left(P^{\alpha n'} \right)_{,j} \, dv \right) \\
\sum_{n}^{|Q^\beta|} I^{\beta mn} \epsilon_{ij}^{\beta n} &= \sum_{\alpha} \sum_{n'}^{|P^\alpha|} u_i^{\alpha n'} \int_{\Psi^\beta} Q^{\beta m} \left(P^{\alpha n'} \right)_{,j} \, dv \\
&= \sum_{\alpha} \sum_{n'}^{|P^\alpha|} u_i^{\alpha n'} \left(\int_{\Psi^\beta} Q^{\beta m} F^{\alpha n'}{}_{,j} \, \phi^\alpha(\boldsymbol{x}) \, dv + \int_{\Psi^\beta} Q^{\beta m} F^{\alpha n'} \phi^\alpha(\boldsymbol{x})_{,j} \, dv \right) \\
&= \sum_{\alpha} \sum_{n'}^{|P^\alpha|} u_i^{\alpha n'} \left(\int_{\Psi^\beta \cap \Phi^\alpha} Q^{\beta m} F^{\alpha n'}{}_{,j} \, dv + \int_{\Psi^\beta} Q^{\beta m} F^{\alpha n'} \phi^\alpha(\boldsymbol{x})_{,j} \, dv \right) \\
&= \sum_{\alpha} \sum_{n'}^{|P^\alpha|} h_j^{\beta \alpha m n'} u_i^{\alpha n'} \qquad \text{(A.1)}
\end{aligned}
$$

For sake of brevity, the above tensor equation can be expressed as

$$
\boldsymbol{\epsilon}^{\beta n} = sym \left(\boldsymbol{B}^{\beta n \alpha m} \otimes \boldsymbol{u}^{\alpha m} \right) \qquad \text{(A.2)}
$$

Equation A.1 can be expressed in the following matrix form:

$$\left[I^{\beta mn}\right]\left\{\ \epsilon_{ij}^{\beta n}\ \right\} = \left\{h_j^{\beta\alpha mn'}u_i^{\alpha n'}\right\}, \tag{A.3}$$

$$\left\{\ \epsilon_{ij}^{\beta n}\ \right\} = \left[W^{\beta nm}\right]\left\{h_j^{\beta\alpha mn'}u_i^{\alpha n'}\right\}, \tag{A.4}$$

For explicit expression of different integrations involve in calculation of $h_j^{\beta\alpha mn'}$, refer to the Appendix B.

A.1.1 Matrix form for $\epsilon_{ij}^{\beta n}$

For the ease of coding, we can write it in the following matrix form.

$$\begin{Bmatrix} \epsilon_{11}^{\beta n} \\ \epsilon_{22}^{\beta n} \\ \epsilon_{33}^{\beta n} \\ 2\epsilon_{12}^{\beta n} \\ 2\epsilon_{13}^{\beta n} \\ 2\epsilon_{23}^{\beta n} \end{Bmatrix} = \sum_m w^{\beta nm} \begin{bmatrix} h_1^{\alpha mn'} & 0 & 0 \\ 0 & h_2^{\alpha mn'} & 0 \\ 0 & 0 & h_3^{\alpha mn'} \\ h_2^{\alpha mn'} & h_1^{\alpha mn'} & 0 \\ h_3^{\alpha mn'} & 0 & h_1^{\alpha mn'} \\ 0 & h_3^{\alpha mn'} & h_2^{\alpha mn'} \end{bmatrix} \left\{\ u_i^{\alpha n'}\ \right\}$$

$$\sum_m w^{\beta nm} \left[\begin{array}{ccc|ccc|c} h_1^{\alpha_1 m1} & 0 & 0 & h_1^{\alpha_1 m2} & 0 & 0 & \\ 0 & h_2^{\alpha_1 m1} & 0 & 0 & h_2^{\alpha_1 m2} & 0 & \\ 0 & 0 & h_3^{\alpha_1 m1} & 0 & 0 & h_3^{\alpha_1 m2} & \cdots \\ h_2^{\alpha_1 m1} & h_1^{\alpha_1 m1} & 0 & h_2^{\alpha_1 m2} & h_1^{\alpha_1 m2} & 0 & \\ h_3^{\alpha_1 mn'} & 0 & h_1^{\alpha_1 m1} & h_3^{\alpha_1 m2} & 0 & h_1^{\alpha_1 m2} & \\ 0 & h_3^{\alpha_1 m1} & h_2^{\alpha_1 m1} & 0 & h_3^{\alpha_1 m2} & h_2^{\alpha_1 m2} & \end{array}\right] \begin{Bmatrix} u_1^{\alpha_1 1} \\ u_2^{\alpha_1 1} \\ u_3^{\alpha_1 1} \\ u_1^{\alpha_1 2} \\ u_2^{\alpha_1 2} \\ u_3^{\alpha_1 2} \\ \\ \vdots \end{Bmatrix}$$

$$\left\{\varepsilon_i^{\beta n}\right\} = \sum_m w^{\beta nm}\left[B^{m\alpha n'}\right]\left\{u^{\alpha n'}\right\}$$

$w^{\beta nm}$ is a $\left|Q^\beta\right|$-by-$\left|Q^\beta\right|$ matrix where, $\left|Q^\beta\right|$ length of basis used to approximate the derivative. Thus, $\boldsymbol{\epsilon}^{\beta n}$ and $\boldsymbol{\sigma}^{\beta n}$ are expressed in terms of in terms of $\boldsymbol{u}^{\alpha n}$,

A.2 Weak form of the equilibrium equation

We can derive the following equation from the stationalization of $\mathcal{L}$ of Eq. (4.1):

$$
\begin{aligned}
\delta\mathcal{L}(u_i^{\alpha n}) &= \sum_{\beta}^{N^\beta}\left(\sum_{m}^{|Q^\beta|}\sigma_{ij}^{\beta m}\int_{\Psi^\beta}Q^{\beta m}P^{\alpha n}{}_{,j}\ dv+\sum_{\alpha,}\sum_{n'}^{|P^\alpha|}b_i^{\alpha n'}\int_{\Psi^\beta\cap\Phi^\alpha}P^{\alpha n}P^{\alpha n'}\ dv\right)\\
&= \sum_{\beta}^{N^\beta}\left(\sum_{m}^{|Q^\beta|}c_{ijkl}^{\beta}\epsilon_{kl}^{\beta m}\int_{\Psi^\beta}Q^{\beta m}P^{\alpha n}{}_{,j}\ dv+\sum_{\alpha,}\sum_{n'}^{|P^\alpha|}b_i^{\alpha n'}\int_{\Psi^\beta\cap\Phi^\alpha}P^{\alpha n}P^{\alpha n'}\right)dv\\
&= \sum_{\beta}^{N^\beta}\left(\sum_{m}^{|Q^\beta|}\left(\int_{\Psi^\beta}Q^{\beta m}P^{\alpha n}{}_{,j}\ dv\right)c_{ijkl}^{\beta}\epsilon_{kl}^{\beta m}+\sum_{\alpha,}\sum_{n'}^{|P^\alpha|}I^{\alpha nn'}b_i^{\alpha n'}\right)\\
&= \sum_{\beta}^{N^\beta}\left(\sum_{m}^{|Q^\beta|}h_j^{\beta\alpha mn}c_{ijkl}^{\beta}\epsilon_{kl}^{\beta m}+\sum_{\alpha'}\sum_{n'}^{|P^\alpha|}I^{\alpha nn'}b_i^{\alpha n'}\right)\\
0 &= \sum_{\beta}^{N^\beta}\sum_{\alpha'}\left(\sum_{m}^{|Q^\beta|}w^{\beta mm'}h_j^{\beta\alpha mn}c_{ijkl}^{\beta}h_l^{\beta\alpha' m'n'}u_k^{\alpha' n'}+\sum_{n'}^{|P^\alpha|}I^{\alpha nn'}b_i^{\alpha n'}\right)
\end{aligned}
$$

Stationalization of Lagrange results into the linear set of equations and this matrix equation can be solved using any conventional solving techniques. All properties of classical FEM stiffness matrix such as positive definite, symmetricity, sparse and banded matrix are preserved in case of higher order PDS-FEM. However, physical dimension of each column of stiffness matrix is not same. Usage of pre-conditioner to non-dimensionalize the stiffness matrix could improve the results and computational efficiency.

A.2.1 Matrix form of the weak form of the equilibrium equation

For the ease of better understanding, precedent equations are re-written in matrix form as follows,

$$K_{ik}^{\alpha\alpha'}u_k^{\alpha'}-b_i^{\alpha}=0,$$

where

$$\left[K_{ik}^{\alpha\alpha'}\right] = \left[w^{\beta mm'}\right]\left[B^{m\alpha n}\right]^T\left[C\right]\left[B^{m'\alpha' n'}\right]$$

In absence of body force, matrix equations can be written as follows,

$$\sum_{\alpha',m'} (\boldsymbol{B}^{\beta n\,\alpha m} \cdot \boldsymbol{c} \cdot \boldsymbol{B}^{\beta n\,\alpha' m'}) \cdot \boldsymbol{u}^{\alpha' m'} = \boldsymbol{0}, \tag{A.5}$$

for α and m. This matrix equation is the equation that is solved by higher order PDS-FEM. Indeed,

$$\boldsymbol{B}^{\beta n\,\alpha m} \cdot \boldsymbol{c} \cdot \boldsymbol{B}^{\beta n\,\alpha' m'} \quad \text{or} \quad \sum_{i,k} B_i^{\beta n\,\alpha m} c_{ijkl} B_k^{\beta n\,\alpha' m'}$$

gives the element stiffness matrix of higher order PDS-FEM.

A.3 Strain displacement relations (*formulation-B*)

Strain displacement relationship in formulation-B is established by calculating the derivative of displacement. In order to simplify and standardize the expression, relation is phrased in matrix form as $\boldsymbol{\epsilon}^* = \bar{\boldsymbol{B}}.\boldsymbol{u}^*$. Here $\bar{\boldsymbol{B}}$ is called strain-displacement matrix consist of partial derivative of basis function. The explicit expression of strain-displacement relationship is obtained as follows
From the definition of derivative in PDS (see Eq. 4.9) and definition of strain, following expression can be written in following manner

$$\begin{aligned}
\epsilon_{ij}^{\beta} &= \frac{1}{2}\left(\tilde{u}_i^{\beta}{}_{,j} + \tilde{u}_j^{\beta}{}_{,i}\right) \\
&= \frac{1}{2}\left(\sum_{\alpha}\sum_{m}^{|Q^{\beta}|}\sum_{n}^{|P^{\alpha}|} A^{\beta m\alpha n} u_i^{\alpha n} Q_{,j}^{\beta m} + \sum_{\alpha}\sum_{m}^{|Q^{\beta}|}\sum_{n}^{|P^{\alpha}|} A^{\beta m\alpha n} u_j^{\alpha n} Q_{,i}^{\beta m}\right) \\
&= \sum_{\alpha}\sum_{m}^{|Q^{\beta}|}\sum_{n}^{|P^{\alpha}|} \bar{h_j}^{\beta\alpha mn} u_i^{\alpha n}
\end{aligned}$$

Here, $\bar{h_j}^{\beta\alpha mn} = A^{\beta m\alpha n} Q_{,j}^{\beta m}$.
For the sake of simplicity, the tensor of above expression is written as $\boldsymbol{\epsilon}^{\beta} = sym\left(\bar{\boldsymbol{B}}^{\boldsymbol{\beta\alpha n}} \otimes \bar{\boldsymbol{u}}^{\boldsymbol{\alpha n}}\right)$.

Appendix B

Integration Scheme

Characteristic function $\{\phi^a\}$ of a Voronoi element can be written as the union of a set of Heaviside functions, each Heaviside function defining an edge of the Voronoi element. Consider one Voronoi edge defined by the Following Heaviside function (see Fig. B.1).

$$\phi(x, y) = 1 - H(n_y(y - y_0) + n_x(x - x_0))$$

Directional derivatives of the Heaviside function $H(x, y) = H(n_y(y-y_0)+n_x(x-x_0))$ can be written as

$$\boldsymbol{\nabla} H.\boldsymbol{n} = H_{,x}\, n_x + H_{,y}\, n_y = \delta(n_y(y - y_0) + n_x(x - x_0)) \tag{B.1}$$

$$\boldsymbol{\nabla} H.\boldsymbol{m} = -H_{,x}\, n_y + H_{,y}\, n_x = 0 \tag{B.2}$$

Above pair of equations provides

$$\begin{aligned} H_{,x} &= n_x \delta(n_y(y - y_0) + n_x(x - x_0)) \\ H_{,y} &= n_y \delta(n_y(y - y_0) + n_x(x - x_0)) \end{aligned}$$

Therefore,

$$\begin{aligned} \phi(\boldsymbol{x})_{,x} &= -H_{,x} = -n_x \delta(n_y(y - y_0) + n_x(x - x_0)) \\ \phi(\boldsymbol{x})_{,y} &= -H_{,y} = -n_y \delta(n_y(y - y_0) + n_x(x - x_0)) \end{aligned}$$

Using the above results, contributions to B-matrix from each Voronoi edge can be found as follows. Only the relevant integrations are given here.

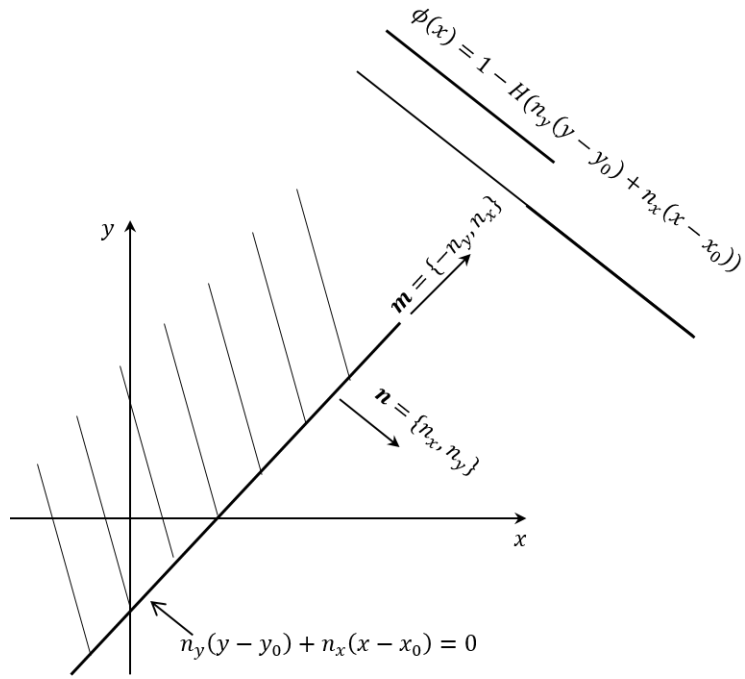

Figure B.1: $\phi(x, y) = 1 - H(n_y(y - y_0) + n_x(x - x_0))$

$$\begin{aligned}
\int_{\Psi} \phi(\boldsymbol{x})_{,j}\, ds &= \int_{\Delta\Psi} \phi(\boldsymbol{x})_{,j}\, ds \\
&= -n_j \int_{\Delta\Psi} \delta(n_y(y - y_0) + n_x(x - x_0)) ds \\
&= -n_j L
\end{aligned}$$

Where $\Delta\Psi$ is a infinitesimally thin neighbourhood around the line $n_y(y - y_0) + n_x(x - x_0) = 0$, and L is the length of the Voronoi boundary.

$$\begin{aligned}
\int_{\Psi} (x_p - x_p^{\alpha}) \phi(\boldsymbol{x})_{,j}\, ds &= \int_{\Delta\Psi} (x_p - x_p^{\alpha}) \phi(\boldsymbol{x})_{,j}\, ds \\
&= -n_j \int_{\Delta\Psi} (x_p - x_p^{\alpha}) \delta(n_y(y - y_0) + n_x(x - x_0)) ds \\
&= -n_j (\bar{x}_p - x_p^{\alpha}) L
\end{aligned}$$

Where $\bar{\boldsymbol{x}}$ is the center of gravity of the Voronoi boundary of length L.
Similarly,

$$
\begin{aligned}
\int_{\Psi} (x_p - x_p^{\alpha})^q \phi(\boldsymbol{x})_{,j}\, ds &= \int_{\Delta\Psi} (x_p - x_p^{\alpha})^q \phi(\boldsymbol{x})_{,j}\, ds \\
&= -n_j \int_{\Delta\Psi} (x_p - x_p^{\alpha})^q \delta(n_y(y - y_0) + n_x(x - x_0)) ds \\
&= -n_j M_q
\end{aligned}
$$

Where M_{pq} is the qth order moment of the Voronoi edge, about the axis x_p passing through the point $\boldsymbol{x}^{\alpha}$.

Appendix C

Motivation for 1O/2O PDS

Assume a second order partial differential equation in 1-Dimension as follows,

$$\begin{aligned} u'' = 0 \quad \text{in} \quad 0 < x < \\ u = \bar{u}^0, \bar{u}^1 \text{on} \quad x = 0, 1 \end{aligned} \tag{C.1}$$

Here, the proposal is the usage of first of polynomial for function: u and higher order for derivative: u'. In order to avoid any confusion in notation, v denotes derivative i.e. $v \equiv u'$. Therefore, approximations of function and derivative are as follows,

$$u = \sum_{\alpha=1} \left(u^{\alpha 0} + u^{\alpha 1} \left(x - x^{\alpha} \right) \right) \phi^{\alpha} \tag{C.2}$$

$$v = \sum_{\beta=1} \left(v^{\beta 0} + v^{\beta 1} \left(x - x^{\beta} \right) + v^{\beta 2} \left(x - x^{\beta} \right)^2 \right) \psi^{\beta} \tag{C.3}$$

One Delaunay and two Voronoi with mother points $x^{\beta} = 0.5$ and $x^{\alpha} = \{0, 1\}$ is used as domain tessellation for above mentioned problem setting. Squared error to evaluate coefficients is defined

$$E = \int_0^1 \frac{1}{2} \left(v - u' \right)^2 dx \tag{C.4}$$

and the minimization of E w.r.t $v^{\beta n}$ leads to,

$$\begin{aligned} \frac{\partial E}{\partial v^{10}} = \int \left(v - u' \right) \psi^1 dx \\ 0 = v^{10} + \frac{1}{12} v^{12} - \left(-u^{10} + u^{20} \right) \end{aligned} \tag{C.5}$$

$$\begin{aligned}
\frac{\partial E}{\partial v^{11}} &= \int (v - u') \left(x - \frac{1}{2}\right) \psi^1 dx \\
0 = \frac{1}{12} v^{11} &- \int u^{11} \left(x - \frac{1}{2}\right) \phi^1 + u^{21} \left(x - \frac{1}{2}\right) \phi^2 dx \\
0 &= \frac{1}{12} v^{11} - \left(-\frac{1}{8} u^{11} + \frac{1}{8} u^{21}\right)
\end{aligned} \tag{C.6}$$

$$\begin{aligned}
\frac{\partial E}{\partial v^{12}} &= \int (v - u') \left(x - \frac{1}{2}\right)^2 \psi^1 dx \\
0 = \frac{1}{12} v^{10} + \frac{1}{80} v^{12} &- \int u^{11} \left(x - \frac{1}{2}\right)^2 \phi^1 + u^{21} \left(x - \frac{1}{2}\right)^2 \phi^2 dx \\
0 &= \frac{1}{12} v^{10} + \frac{1}{80} v^{12} - \left(\frac{1}{24} u^{11} + \frac{1}{24} u^{21}\right)
\end{aligned} \tag{C.7}$$

On solving the Eqs. C.5, C.6, and C.7, we get

$$\left(v^{10}, v^{11}, v^{12}\right) = \left(\frac{9}{4}\left(-u^{10} + u^{20}\right) - \frac{5}{8}\left(u^{11} + u^{21}\right), -\frac{3}{2}\left(-u^{11} + u^{21}\right), -15\left(-u^{10} + u^{20}\right) + \frac{15}{2}\left(u^{11}\right.\right.$$

A Lagrange of Eq. C.1 for u is

$$\mathcal{L}[u] = \int_0^1 \frac{1}{2} (u')^2 \, dx \tag{C.8}$$

Substitution of v, leads to

$$\mathcal{L} = \frac{1}{2} \left\{ \left(v^{10}\right)^2 + \frac{1}{12} \left(v^{11}\right)^2 + \frac{1}{80} \left(v^{12}\right)^2 + \frac{1}{6} v^{10}.v^{12} \right\}$$

Minimization of $\mathcal{L}$ for (u^{11}, u^{21}) with $(u^{10}, u^{20}) = (\bar{u}^0, \bar{u}^1)$ leads to

$$u^{11} = u^{21} \tag{C.9}$$

and

$$\begin{aligned}
\mathcal{L} &= \frac{1}{2}\left(\frac{1}{16}\left(9\Delta\bar{u} - 5u^{11}\right)^2 + \frac{45}{16}\left(-\Delta\bar{u} + u^{11}\right)^2 + \frac{5}{8}\left(9\Delta\bar{u} - 5u^{11}\right)\left(-\Delta\bar{u} + u^{11}\right)\right) \\
\mathcal{L}' &= -\frac{5}{16}\left(9\Delta\bar{u} - 5u^{11}\right) + \frac{45}{16}\left(-\Delta\bar{u} + u^{11}\right) - \frac{25}{16}\left(-\Delta\bar{u} + u^{11}\right) + \frac{5}{16}\left(9\Delta\bar{u} - 5u^{11}\right) \\
0 &= \frac{5}{4}\left(-\Delta\bar{u} + u^{11}\right)
\end{aligned} \tag{C.10}$$

with $\Delta\bar{u} = -u^{10} + u^{20}$. Thus

$$u^{11} = \Delta\bar{u} \tag{C.11}$$

Thus, A unique solution space for system of equation customary by discretization of BVP with prescribed boundary condition is procured. It is interesting to see that choosing one order higher polynomial basis for derivative approximation than that of function approximation gives a unique solution. It is matter of investigation of general applicability of this observation. Moreover, a rigorous mathematical reasoning is also needed to avoid any speculation.

Appendix D

Patch test

D.1 Patch Test

Patch test establish that developed PDS-FEM code correctly solves the strong form of governing equations and approaches to unique solution for given boundary conditions. It is a tool to be used for mathematical verification of any proposed discretization schemes. It also serves as important tool for element design.

D.1.1 Patch test as verification tool

Code verification namely accomplished by solving two scenarios i.e. *Individual Element Verification* and *Mix-ability Verification*.

In *Individual Element Verification*, developed code is run to simulate a single element with prescribed boundary conditions at all the nodes and preliminary checks are being performed. These preliminary check mainly perform the verification of stress and strain calculation. This specific test doesn't ensure that it solves the correct problem.

In *Mix-ability Verification*, developed code is run to analyse a patch with prescribed boundary conditions. In addition to verify the code, it also quantifies the interaction between different elements.

D.1.2 Patches

The concept of element patch, or simply patch is the set of all elements connected to a given node. This node is called patch node indicated as i in the Fig D.1. Patch shown in this figure has only one type of element (Delaunay triangular element), but in general it may consist of different type of elements.

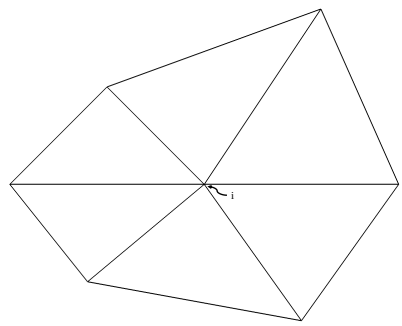

Figure D.1: An element patch attached to a patch node, herein labelled as i

The patch test has two form as follows

1. Rigid body mode patch test

   Translational rigid body motion

   Rotational rigid body motion

2. Constant strain mode patch test

Procedure to perform path test is as follows,

1. Pluck a patch of elements
2. Evaluate the displacement at each external nodes and apply evaluated displacement at each external node as boundary condition to system
3. Solve the patch domain with developed code to calculate displacement at patch node
4. Evaluate the stress and strain to verify the results. It must reproduce the expected value of strain/stress

D.1.2.1 Rigid body mode Patch test

In this test, constant displacement is applied to patch and then system is solved to reproduce zero strain in domain.

Rigid body motion in x-direction Following the procedure step by step with displacement field $u(x, y) = 0.1$ and $v(x, y) = 0.0$. This set of displacement gives the zero strain i.e. $\epsilon_{xx} = u(x, y)_{,x} = 0$, $\epsilon_{yy} = u(x, y)_{,y} = 0$. Developed code must reproduce zero strain state. Results shown in Fig. D.2 indicates the expected results.

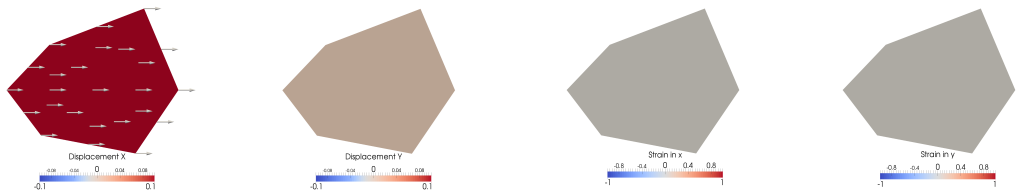

(a) u_x (b) u_y (c) ϵ_{xx} (d) ϵ_{yy}

Figure D.2: Procured results with displacement setting $u(x, y) = 0.1$ and $v(x, y) = 0$

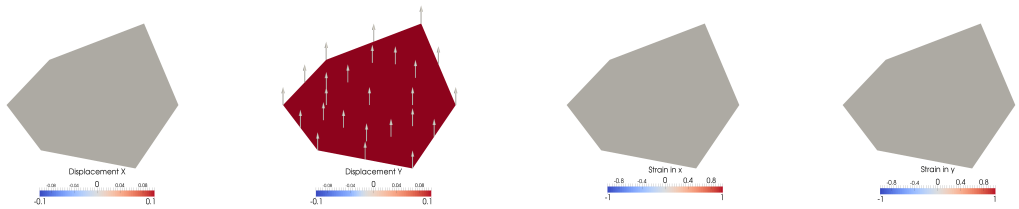

(a) u_x (b) u_y (c) $epsilon_{xx}$ (d) ϵ_{yy}

Figure D.3: Displacement and strain with BCs $u(x, y) = 0.0$ and $v(x, y) = 0.1$

Rigid body motion in y-direction Patch test is performed with displacement field $u(x, y) = 0.0$ and $v(x, y) = 0.1$. Displacement at boundary nodes is calculated and applied at each external node. System is solved to reproduce the zero strain i.e. $\epsilon_{xx} = u(x, y)_{,x} = 0$, $\epsilon_{yy} = u(x, y)_{,y} = 0$. Displacement vector is shown in Fig D.3 (a, b). Developed code reproduces zero strain state as seen in Fig. D.3 (c, d).

D.1.2.2 Constant strain mode Patch test

In this test, linear displacement boundary conditions are applied to patch and system is solved to reproduce exactly constant strain state in domain. All directions have been considered while performing this test.

Constant strain state in x-direction In order to recover the constant strain ϵ_{xx}, displacement field $u(x, y) = x$ and $v(x, y) = 0$ has to be applied. Figure D.4(a, b) illustrate the calculated displacement by the application of constant strain mode displacement. This gives strain $\epsilon_{xx} = 1$ and other strain field $\epsilon_{yy} = 0$ as it can be seen in Fig D.4 (c,d).

Constant strain state in y-direction Constant strain ϵ_{yy} is achieved with the displacement field $u(x, y) = 0$ and $v(x, y) = y$ which is shown in Fig D.5. Developed code reproduces the expected constant strain, ϵ_{yy} which is illustrated in FigD.5 (c, d).

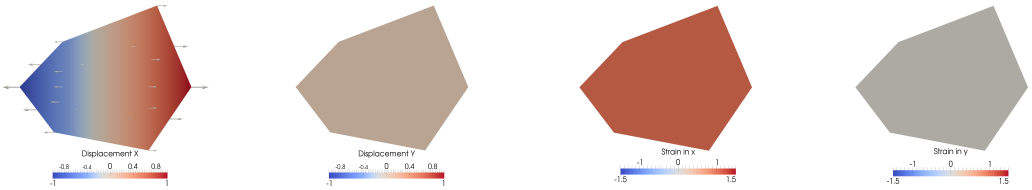

(a) u_x (b) u_y (c) ϵ_{xx} (d) ϵ_{yy}

Figure D.4: Displacement and strain results obtained by setting the BCs as $u(x, y) = x$ and $v(x, y) = 0.0$

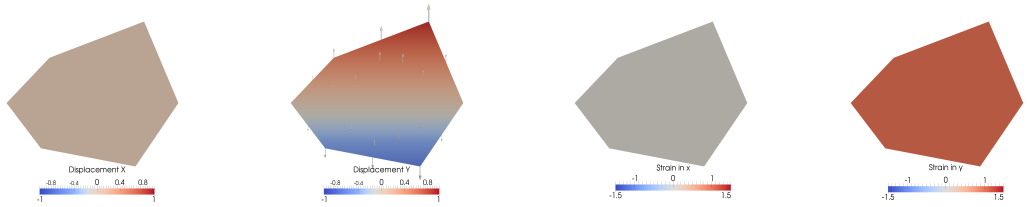

(a) u_x (b) u_y (c) ϵ_{xx} (d) ϵ_{yy}

Figure D.5: Displacement and strain with boundary condition setting $u(x, y) = 0.0$ and $v(x, y) = y$

D.2 Conclusion

Procured results are summarized and tabulated in Table D.1 and D.2. These results are accurate upto 13th decimal point, which advocate that proposed scheme passes the patch test. It denies the presence of inappropriate response in the patch. It provides the necessary condition for the convergence. However, this may not be sufficient condition to ensure the intend to achieve the unique solution.

Test mode	Displacement at external node		Displacement at patch node			
			Expected value		Obtained value	
	u_x	u_y	u_x	u_y	u_x	u_y
Rigid body mode	0.1	0.0	0.1	0.0	0.1	-3.22×10^{-16}
	0.0	0.1	0.0	0.1	6.13×10^{-17}	0.100000000000005
Constant strain mode	x	0.0	0.0	0.0	1.71×10^{-16}	2.17×10^{-16}
	0.0	y	0.0	0.0	6.82×10^{-16}	3.39×10^{-16}

Table D.1: Patch teat summary: Displacement value at patch node

Test mode	Displacement at external node		Strain at patch node					
			Expected value			Obtained value		
	u_x	u_y	ϵ_{xx}	ϵ_{yy}	ϵ_{xy}	ϵ_{xx}	ϵ_{yy}	ϵ_{xy}
Rigid body mode	0.1	0.0	0.0	0.0	0.0	1.43×10^{-17}	$-1.49 * 10^{-17}$	-9.30×10^{-17}
	0.0	0.1	0.0	0.0	0.0	1.57×10^{-167}	-9.11×10^{-17}	0.100000000000005
Constant strain mode	x	0.0	1.0	0.0	0.0	0.999999999998	-2.71×10^{-16}	2.17×10^{-16}
	0.0	y	0.0	1.0	0.0	-4.43×10^{-15}	1.00000000005	3.39×10^{-16}

Table D.2: Patch test summary: Strain value at patch node

Appendix E

Analytic expression for Mode-I crack

Kolosov and Muskhelishvili have proposed powerful and convenient complex potential function method to solve two-dimensional crack problem. In complex potential methods stress and displacement are written in terms of analytic function of complex variable. The unique solution for any boundary value problem can be obtained by imposing essential boundary conditions. A brief summary to get the analytic expression is presented here.

Complex potential function for Airy stress function For reference, potential function for Airy stress function is given here, which is as follows

$$\begin{aligned} \phi &= \Re\left\{\bar{z}\psi(z) + \chi(z)\right\} \\ 2\phi(x,y) &= \bar{z}\psi(z) + z\bar{\psi(z)} + \chi(z) + \bar{\chi(z)}. \end{aligned} \tag{E.1}$$

Here, $z = x + iy$, $\psi(z) = \frac{1}{4}\int f(z)dz = p + iq$ and $f(z) = P + iQ$ is an analytic complex function. p and q are the real numbers.

From the definition of Airy stress function,

$$\begin{aligned} \sigma_{xx} + i\sigma_{xy} &= \frac{\partial^2\phi}{\partial y^2} - i\frac{\partial^2\phi}{\partial x\partial y} = -i\frac{\partial}{\partial y}\left(\frac{\partial\phi}{\partial x} + i\frac{\partial\phi}{\partial y}\right) \\ \sigma_{xx} - i\sigma_{xy} &= \frac{\partial^2\phi}{\partial x^2} + i\frac{\partial^2\phi}{\partial x\partial y} = \frac{\partial}{\partial x}\left(\frac{\partial\phi}{\partial x} + i\frac{\partial\phi}{\partial y}\right) \end{aligned} \tag{E.2}$$

From the definition of complex potential function (Eq. E.1), we can get

$$\frac{\partial\phi}{\partial x} + i\frac{\partial\phi}{\partial y} = \psi(z) + z\overline{\psi'(z)} + \overline{\chi'(z)} \tag{E.3}$$

Substituting the Eq. E.3 into the Eq. E.2

$$\sigma_{xx} + i\sigma_{xy} = \psi'(z) + \overline{\psi'(z)} - z\overline{\psi''(z)} - \overline{\chi''(z)} \tag{E.4}$$

$$\sigma_{xx} - i\sigma_{xy} = \psi'(z) + \overline{\psi'(z)} + z\overline{\psi''(z)} + \overline{\chi''(z)} \tag{E.5}$$

Summation the Eq. E.4 and E.5

$$\sigma_{xx} + \sigma_{yy} = 2\left[\psi'(z) + \overline{\psi'(z)}\right] = 4\Re\left[\psi'(z)\right] \tag{E.6}$$

Subtraction the Eq. E.5 and E.4

$$\sigma_{xx} - \sigma_{yy} - 2i\sigma_{xy} = 2\left[z\overline{\psi''(z)} + \overline{\chi''(z)}\right] \tag{E.7}$$

Considering the conjugate of E.7 in both side, we can obtain

$$\sigma_{xx} - \sigma_{yy} + 2i\sigma_{xy} = 2\left[\bar{z}\psi''(z) + \chi''(z)\right] \tag{E.8}$$

Displacement function The definition of Airy stress function; $\sigma_{xx} = \frac{\partial^2\phi}{\partial y^2}$, $\sigma_{yy} = \frac{\partial^2\phi}{\partial x^2}$, $\sigma_{xy} = -\frac{\partial^2\phi}{\partial x\partial y}$, strain-displacement relationship and stress equations can be integrated to get the displacement field as follows

$$2\mu\left(u_x + iu_y\right) = \kappa\psi(z) - z\overline{\psi'(z)} - \overline{\chi'(z)} \tag{E.9}$$

Westergaard Function method The Kolosov-Muskhelishvili formulae hold for general plane elasticity problems, where the Westergaard function method is more convenient for discussing these basic crack problems. Hence, here Westergaard function method is considered to get the analytic solution.

Problem setting Consider an infinite domain with horizontal finite crack with applied external load at infinity. Preserving the symmetricity about horizontal axis i.e. x-direction,gives $\sigma_{xy} = 0$ along $y = 0$. And therefore,

$$\Im\left[\bar{z}\psi''(z) + \chi''(z)\right] = 0 \quad \text{at} \quad y = 0 \tag{E.10}$$

The above equation can be satisfied iff

$$\chi''(z) + z\psi''(z) + +A = 0 \tag{E.11}$$

Refer to fracture mechanics book [28] for detailed proof.

Substituting the constraint Eq. E.11 into Eq. E.6-E.9 and then solving the system leads to

$$\begin{aligned}
\sigma_{xx} &= 2\Re\left\{\psi'\right\} - 2y\Im\left\{\psi''\right\} + A \\
\sigma_{yy} &= 2\Re\left\{\psi'\right\} + 2y\Im\left\{\psi''\right\} - A \\
\sigma_{xy} &= -2y\Re\left\{\psi''\right\} \\
2\mu u_x &= (\kappa - 1)\Re\left\{\psi\right\} - 2y\Im\left\{\psi'\right\} + Ax \\
2\mu u_y &= (\kappa + 1)\Im\left\{\psi\right\} - 2y\Re\left\{\psi'\right\} - Ay
\end{aligned} \tag{E.12}$$

Define, $\psi' = \frac{1}{2}\left(Z_I + A\right)$, then $\psi = \frac{1}{2}\left(\hat{Z}_I + Az\right)$ and $\psi'' = \frac{1}{2}Z_I'$

Substituting the above definition in Eq. E.12

$$\begin{aligned}
\sigma_{xx} &= \Re\left\{Z_I\right\} - y\Im\left\{Z_I'\right\} + 2A \\
\sigma_{yy} &= \Re\left\{Z_I\right\} + y\Im\left\{Z_I'\right\} \\
\sigma_{xy} &= -2y\Re\left\{Z_I'\right\} \\
2\mu u_x &= \frac{(\kappa - 1)}{2}\Re\left\{\hat{Z}_I\right\} - y\Im\left\{Z_I\right\} + \frac{1}{2}(\kappa + 1)Ax \\
2\mu u_y &= \frac{(\kappa + 1)}{2}\Im\left\{\hat{Z}_I\right\} - y\Re\left\{Z_I\right\} + \frac{1}{2}(\kappa - 3)Ay
\end{aligned} \tag{E.13}$$

Here, Z_I is Westergaard function for Mode-I problem and it is defined [50] as

$$Z_I(z) = \frac{\sigma_0 z}{\sqrt{(z^2 - a^2)}} \tag{E.14}$$

Using the polar coordinate system

$$\begin{aligned}
z &= re^{i\theta} \\
z - a &= r_1 e^{i\theta_1} \\
z + a &= r_2 e^{i\theta_2}
\end{aligned} \tag{E.15}$$

The function, Z_I can be rewritten in polar coordinate system as follows,

$$Z_I = \frac{\sigma_0 z}{\sqrt{(z+a)}\sqrt{(z-a)}} \tag{E.16}$$

$$= \frac{\sigma_0 r}{\sqrt{(r_1 r_2)}} expi\left(\theta - \frac{1}{2}\theta_1 - \frac{1}{2}\theta_2\right) \tag{E.17}$$

Analytic expression need derivative and integration of complex potential function. Hence these quantities are calculated as follows, Derivative of function; Z_I'

$$Z_I' = \frac{\sigma_0}{\sqrt{(z+a)}\sqrt{(z-a)}} - \frac{\sigma_0 z^2}{(z^2-a^2)^{\frac{3}{2}}} = -\frac{\sigma_0 a^2}{(z^2-a^2)^{\frac{3}{2}}} \tag{E.18}$$

$$= \frac{\sigma_0 a^2}{(r_1 r_2)^{\frac{3}{2}}} exp\left(-i\left(\frac{3}{2}\theta_1 + \frac{3}{2}\theta_2\right)\right) \tag{E.19}$$

Integration of function; $\hat{Z}_I$

$$\hat{Z}_I = \sigma_0\left(\sqrt{z^2-a^2}\right) \tag{E.20}$$

$$= \sigma_0\sqrt{(r_1 r_2)} expi\left(\frac{1}{2}\theta_1 + \frac{1}{2}\theta_1\right) \tag{E.21}$$

Using these expressions, Eq. E.13 can be expressed as follows,

$$\sigma_{xx} = \frac{\sigma_0 r}{\sqrt{r_1 r_2}}\left[\cos\left(\theta - \frac{1}{2}\theta_1 - \frac{1}{2}\theta_2\right) - \frac{a^2}{r_1 r_2}\sin(\theta)\sin\frac{3}{2}(\theta_1+\theta_2)\right] \tag{E.22}$$

$$\sigma_{yy} = \frac{\sigma_0 r}{\sqrt{r_1 r_2}}\left[\cos\left(\theta - \frac{1}{2}\theta_1 - \frac{1}{2}\theta_2\right) + \frac{a^2}{r_1 r_2}\sin(\theta)\sin\frac{3}{2}(\theta_1+\theta_2)\right] \tag{E.23}$$

$$\sigma_{xy} = \frac{\sigma_0 r}{\sqrt{r_1 r_2}}\left[\frac{a^2}{r_1 r_2}\sin(\theta)\cos\frac{3}{2}(\theta_1+\theta_2)\right] \tag{E.24}$$

$$u_x = \frac{\sigma_0}{2\mu}\left[\frac{(\kappa-1)\sqrt{r_1 r_2}}{2}\cos(\frac{1}{2}\theta_1 + \frac{1}{2}\theta_2) - \frac{r^2}{\sqrt{r_1 r_2}}\sin\theta\sin(\theta - \frac{1}{2}\theta_1 - \frac{1}{2}\theta_2)\right] \tag{E.25}$$

$$u_y = \frac{\sigma_0}{2\mu}\left[\frac{(\kappa+1)\sqrt{r_1 r_2}}{2}\sin(\frac{1}{2}\theta_1 + \frac{1}{2}\theta_2) - \frac{r^2}{\sqrt{r_1 r_2}}\sin\theta\cos(\theta - \frac{1}{2}\theta_1 - \frac{1}{2}\theta_2)\right] \tag{E.26}$$

Thus, analytic expressions are obtained. By choosing the appropriate complex potential function, analytic solution of any crack problem can be derived. However, identifying the complex potential function is challenging task.

Bibliography

[1] D. H. McLain: Drawing contours from arbitrary data points, Comput. J., v. 17, pp. 318–324, 1974.

[2] W. J. Gordon, J. A. WrxoM: Shepard's method of 'metric interpolation' to bivariate and multivariate data, Math. Comp., v. 32, pp. 253–264, 1978.

[3] R. E. Barnhill: Representation and Approximation of Surfaces, Mathematical Software III, Academic Press, New York, pp. 69–120, 1977.

[4] P. Lancaster: Moving weighted least-squares methods, in Polynomial and Spline Approximation (B. N. Sahney, Ed.), NATO Advanced Study Institute SeriesC , Reidel, Dordrecht, pp. 103–120, 1979.

[5] P. Lancaster: Composite methods for generating surfaces," in Polynomial and Spline Approximation (B. N. Sahney, Ed.), NATO Advanced Study Institute Series C, Riedel, Dordrecht, pp. 91–102, 1979.

[6] P. Lancaster, K. Salkauskas: Surface generated by Moving Least Square Methods, Mathematics of computation, 35,155, pp. 141–158, 1981.

[7] K.M. Liew, Y.Q. Huang, J.N. Reddy: A hybrid moving least squares and differential quadrature (MLSDQ) meshfree method, Int. J. Comput. Engrg. Sci., 3, pp. 1–12, 2002.

[8] K.M. Liew, Y.Q. Huang, J.N. Reddy: Vibration analysis of symmetrically laminated plates based on FSDT using the moving least squares differential quadrature method, Int. J. Numer. Meth. Engrg., 56, pp. 2331–2351, 2003.

[9] Piotr Breitkopf , Alain Rassineux , Pierre Villon: An Introduction to Moving Least Squares Meshfree Methods, Revue Europeenne des Elements, 11:7-8, pp. 825–867, 2002

[10] R. Barrio: Sensitivity analysis of ODEs/DAEs using the Taylor series method, SIAM J. Sci. Comput., 27 (6) pp. 1929–1947, 2006.

[11] R. Barrio, M. Rodriguez, A. Abad, F. Blesa: Breaking the limits: the Taylor series method, Appl. Math. Comput. 217 pp. 7940–7954, 2011.

[12] H.R. Marzban, M. Razzaghi: Solution of multi-delay systems using hybrid of block-pulse functions and Taylor series, J. Sound Vib., 292 pp. 954–963, 2006.

[13] R.D. Neidinger: Directions for computing truncated multivariate Taylor series, Math. Comput., 74 (249) pp. 321–340, 2004.

[14] R.D. Neidinger: An efficient method for the numerical evaluation of partial derivatives of arbitrary order, ACM Trans. Math. Software 18 (2) pp. 159–173, 1992.

[15] M. Razzaghi, M. Razzaghi: Taylor series analysis of time-varying multi-delay systems, Internat. J. Control 50 (1) pp. 183–192, 1988.

[16] M. Razzaghi, M. Razzaghi,: Solution of linear two-point boundary value problems with time-varying coefficients via Taylor series, Int. J. Syst. Sci. 20 (11) pp. 2075–2084, 1989.

[17] G. Groza, N. Pop: Approximate solution of multipoint boundary value problems for linear differential equations by polynomial functions, J. Difference Equ. Appl. 14 (12) pp. 1289–1309, 2008.

[18] Tavarez FA, Plesha ME: Discrete element method for modelling solid and particulate materials, Int. J. Numer. Meth. Engrg., 70(4), pp. 379–404, 2006.

[19] Miehe C, Grses E: A robust algorithm for configurational-force-driven brittle crack propagation with R-adaptive mesh alignment, Int. J. Numer. Meth. Engrg., 72, pp. 127–155, 2007.

[20] Moes N, Dolbow J, Belytschko T: A finite element method for crack growth without remeshing. Int. J. Numer. Meth. Engrg., 46(1), pp. 131–150, 1999.

[21] Oliver J, Huespe AE, Sanchez PJ: A comparative study on finite elements for capturing strong discontinuities: E-FEM vs X-FEM, Computer Methods in Applied Mechanics and Engineering, 195, pp. 4732–4752, 2006.

[22] Hansbo A, Hansbo P: A finite element method for the simulation of strong and weak discontinuities in solid mechanics, Computer Methods in Applied Mechanics and Engineering, 193, pp. 3523–3540, 2004.

[23] Laborde P, Pommier J, Renard Y, Salaun M.: High-order extended finite element method for cracked domains, Int. J. Numer. Meth. Engrg., 64, pp. 354–381, 2005.

[24] Bechet E, Minnebo H, Moes N, Burgardt B.: Improved implementation and robustness study of the x-fem for stress analysis around cracks, Int. J. Numer. Meth. Engrg., 64, pp. 1033–1056, 2005.

[25] Moes N, Bechet E, Tourbier M.: Imposing Dirichlet boundary conditions in the extended finite element method, Int. J. Numer. Meth. Engrg., 67, pp. 1641–1669, 2006.

[26] Gingold RA, Monaghan JJ: Smoothed particle hydrodynamics: theory and application to non-spherical stars, Monthly Notices of the Royal Astronomical Society, 181, pp 375–389, 1977.

[27] Schlangen E, Garboczi EJ: Fracture simulations of concrete using lattice models: computational aspects, Engineering Fracture Mechanics, 57(2), pp 319–332, 1997.

[28] C.T. Sun, Z.H. Jin : Fracture mechanics,Academic press, 2012.

[29] S. Rahman, J.S. Kim: Probabilistic fracture mechanics for nonlinear structures, Int. J. of Pressure Vessels and Piping, 78, pp. 261-269, 2001.

[30] Morsaleen Shehzad Chowdhury, Chongmin Song, Wei Gao: Probabilistic fracture mechanics by using Monte Carlo simulation and the scaled boundary finite element method, Engineering fracture mechanics, 78, pp. 2369-2389, 2011.

[31] Belytschko T, Lu YY, and Gu L: Element free galerkin methods. Int. J. Numer. Methods Eng. 37, pp. 229-256, 1994.

[32] Liu WK, Adee J, and Jun S,: Reproducing kernel and wavelets particle methods for elastic and plastic problems, In: Advanced Computational Methods for Material Modeling, AMD 180/PVP 268 ASME, pp. 175-190, 1993.

[33] Babus.ka I and Melenk JM: The partition of unity method, Int. J. Numer. Meth. Engrg., 40, pp. 727-758, 1997 .

[34] Campbell P. M.: Some new algorithms for boundary value problems in smooth particle hydrodynamics. Technical Report DNA-TR-88-286, Mission Research Corporation, 1989.

[35] Takeda H., Miyama SM and Sekiya M: Numerical simulation of viscous flow by smooth particle hydrodynamics, Prog. Theor. Phys. 116, pp. 123–134, 1994.

[36] Morris JP, Fox PJ and Zhu Y: Modeling low Reynolds number incompressible flow using SPH, J. Comput. Phys, 82, pp. 214–226, 1994.

[37] Libersky, L.D., Petschek, A.G.: Smooth particle hydrodynamics with strength of materials. Advances in the Free Lagrange Method, Lecture Notes in Physics, 395, pp. 248-257, 1990.

[38] Libersky, L.D., Petschek, A.G., Carney, T.C., Hipp, J.R., Allahdadi, F.A.: High Strain Lagrangian Hydrodynamics: A Three-Dimensional SPH Code for Dynamic Material Response, Journal of Computational Physics, 109(1), November, pp. 67-75, 1993

[39] Randles P. W., Libersky L. D.: Smoothed particle hydrodynamics: Some recent improvements and applications. Computer methods in applied mechanics and engineering, 139, pp. 375-408, 1996.

[40] Randles, P. W., Libersky, L. D., Petschek, A. G.: On neighbors, derivatives, and viscosity in particle codes, in: Proceedings of ECCM Conference, Munich, Germany, 31 August 3 September, 1996.

[41] Idelsohn, S.R., Onate, E., Calvo, N. and del Pin, F.: The meshless finite element method, Int. J. Numer. Meth. Engrg., 58,6, pp. 893–912, 2003.

[42] Idelsohn, S.R., Onate, E. and Del Pin, F. : A lagrangian meshless finite element method applied to fluid-structure interaction problems. in Computer and Structures, 81: pp. 655–671, 2003.

[43] Onate, E.: Possibilities of finite calculus in computational mechanics,Int. J. Numer. Meth. Engrg., 60 (1), pp. 255–281, 2004.

[44] M.L.L. Wijerathne, Kenji Oguni, Muneo Hori: Numerical analysis of growing crack problem using particle discretization scheme, Int. J. Numer. Meth. Engrg., 80, pp 46–73, 2009.

[45] Muneo Hori, Kenji Oguni, Hide Sakaguchi: Proposal of FEM implemented with particle discretization scheme for analysis of failure phenomena, Journal of Mechanics and Physics of Solids, 53, pp 681–703, 2005.

[46] M.L.L. Wijerathne, Muneo Hori, Hide Sakaguchi and Kenji Oguni: 3D dynamic simulation of crack propagation in extra corporeal shock wave lithotripsy, IOP Conference Series: Materials Science and Engineering, 10(1),doi:10.1088/1757-899X/10/1/012120 , 2010.

[47] Chen Hao, Wijerathne Lalith, Hori, Muneo and Ichimura Tsuyoshi: Stability of dynamic growth of two anti-symmetric cracks using PDS-FEM, J. of Japan Society of Civil Engineering, Ser. A2 (AM) 68(1), pp 10–17, 2012.

[48] Mahendra Kumar Pal, Lalith Wijerathne, Muneo Hori, Tsyushi Ichimura, Seizo Tanaka: Implementation of Finite Element Method with higher order Particle Discretization Scheme, J. of Japan Society of Civil Engineers, Ser.A2 (Applied Mechanics(AM)),70(2), pp. 297-305, 2014.

[49] Mahendra Kumar Pal, Lalith Wijerathne, Muneo Hori, Tsyushi Ichimura: Simulation of cracks in linear elastic solids using higher order Particle Discretization Scheme-FEM, J. of Japan Society of Civil Engineers, Ser.A2 (Applied Mechanics(AM)) (Submitted)

[50] H.Tada, P.Paris, G. Irwin: The stress analysis of cracks handbook, Del research c, 3rd edition, 2000.